2014-09-23

Geophysical Characterization of an Undrained Oil Sands Tailings Pond Dyke Alberta, Canada

Booterbaugh, Aaron

UNIVERSITY OF CALGARY

Geophysical Characterization of an Undrained Oil Sands Tailings Pond Dyke Alberta, Canada

by

Aaron Booterbaugh

A THESIS SUBMITTED TO THE FACULTY OF GRADUATE STUDIES

IN PARTIAL FULFILLMENT OF THE REQUIREMENTS FOR THE

DEGREE OF MASTER OF SCIENCE

DEPARTMENT OF GEOSCIENCE

CALGARY, ALBERTA

SEPTEMBER, 2014

Abstract

Geophysical characterization of an undrained oil sands tailings pond dyke was conducted at Syncrude Canada's Southwest Sand Storage Facility (SWSS). Push tool conductivity (PTC), electromagnetic (EM), and electrical resistivity tomography (ERT) methods in conjunction with hydrogeological and chemistry measurements were used to investigate soil moisture, hydraulic head, and groundwater salinity distributions. Normalization and calibration procedures were conducted on EM data to build statistically consistent maps between survey years. An Archie's Law petrophysical model was utilized to relate measured bulk conductivity, from geophysical surveying, with measures of soil moisture and fluid electrical conductivity. It was found that a relatively strong relationship between bulk electrical conductivity and soil moisture exists, while weak to no correlation was observed between bulk and fluid electrical conductivity. ERT surveying was capable of clearly identifying the location of the water table within the dyke. This study provides a unique look into the application of geophysical techniques to investigate soil moisture, hydraulic head, and salt distribution in an active undrained tailings dam structure.

Acknowledgements

I would first like to thank Dr. Larry Bentley and Dr. Carl Mendoza for their unwavering support throughout my time at the University of Calgary, as well as with the project presented in this manuscript.

My project was made possible through data provided by Dr. Carl Mendoza, Syncrude Canada Ltd., and WorleyParsons Ltd. Specifically I would like to thank Mr. Paul Bauman and Dr. Carl Mendoza for locating and delivering geophysical and hydrogeological data, some of which collected over 10 years ago.

I would also like to thank my officemates for their help with navigating my degree and project; Mike Callaghan, Lei Zhi, Frank Head, Amir Niazi, Sasha Zheltikova.

Finally, thanks to the University of Calgary and the Department of Geoscience.

Table of Contents

List of Tables

List of Figures and Illustrations

Chapter 1: Introduction

1.1 Alberta Oil Sands

Exploration and development of Alberta's oil sand deposits first began in the early to mid-20th century following Karl Clark's (Clark 1929) experimental work on hot-water bitumen extraction. The term oil sands, also known as tar sands and bituminous sands, refers to sand beds variously saturated with viscous, carbon disulphide-soluble bitumen that cannot be produced using conventional petroleum methods (Berkowitz and Speight 1975). The first major commercial production of Albertan oil sands began in the 1960's however it wasn't until the 1970's, under tight world oil supplies, that the industry began to rapidly grow. Canadian government subsidies in the early 2000's have allowed the industry to further expand. Currently, the industry produces about 2.3 x 10^5 m^3 per day of crude bitumen from mining and in situ techniques and is expected to grow to 4.5 x 10^5 m^3 per day by 2022 (Alberta Energy Resources 2012).

The Athabasca Oil Sand deposit is the largest of three major oil sand deposits located in northern Alberta; Athabasca, Peace River, and Cold Lake. They cover approximately 141,000 km^2 (Masliyah et al. 2004). Figure 1.1 displays Alberta's oil sand deposits. Collectively Alberta's oil sand deposits hold a remaining estimated established reserve of about 20 x 10^9 m^3 (Alberta Energy Resources 2012). However, Alberta oil sands are estimated to hold some 200 x 10^9 m^3 to 300 x 10^9 m^3 of crude bitumen in total (Kasperski and Mikula 2011, Morgan 2001). A significant portion, about 10%, of the Athabasca oil sand deposit is located within the top 45 meters of the subsurface where open pit mining is the most economically viable extraction method (Berkowitz and Speight 1975). This portion of surface mineable oil sands is located in the northeast

portion of the Athabasca deposit centered on the town of Fort McMurray, Alberta, and contains approximately 4 x 10^9 m^3 of remaining established reserves of crude bitumen (Alberta's Energy Industry 2012). Open pit mining techniques result in large volumes of waste, referred to as tailings, which require long term storage in structures known as tailings ponds.

The oil sands operation, as a whole, consists of mining, extraction, upgrading operations, and waste management. Proper integration of these four operations is necessary for economically efficient bitumen recovery and for minimizing adverse environmental impact (Masliyah et al. 2004). Without delving into too much detail, the integrated open pit operation is as follows. Mined oil sand lumps are crushed and mixed with heated recycled process water. Current operation slurry temperatures range between 40 to 55 ºC (Masliyah et al. 2004). This oil sand and water slurry is then directed to hydrotransport pipelines or tumblers, where the oil sand lumps are sheared and lump size is reduced. While in the hydrotransport pipelines or tumblers, the oil sand slurry is treated with chemical additives to assist in bitumen liberation. The addition of sodium, namely in the form of sodium hydroxide (NaOH), has been shown to increase bitumen recovery rates (Sanford 1983). Air attaches to bitumen within the hydrotransport pipeline or tumbler causing bitumen to float to the surface. The aerated bitumen is then skimmed off the process slurry after reaching large gravity separation vessels. The subsequent bitumen froth normally contains about 60% bitumen, 30% water, and 10% solids. This froth is then diluted with a solvent which facilitates the removal of solids and water within a settling vessel. Bitumen which was not captured in the initial aeration and

settling process is recovered in small amounts separately in secondary process streams. Bitumen recovery rate is usually about 88 to 95% (Masliyah et al. 2004).

The remaining water and solids from both the initial slurry and the froth, referred to as tailings, are directed to tailings ponds for storage, treatment, and water/solids separation. Tailings which enter the pond are a mixture of about 55wt% solids, of which 82wt% is sand, 17wt% are fines smaller than 44 μm and 1wt% bitumen (Chalaturnyk et al. 2002, Kasperski and Mikula 2011). The tailings usually have elevated salinity from both natural and artificial sources in the bitumen extraction process. Salinity generally increases as process water is continually recycled (Renault et al 1998). Tailings dam dykes are constructed gradually, utilizing the coarser fraction (although still relatively fine for sand) of beached tailings which settles from the initial tailings slurry, to support ever increasing volumes of tailings. The underlying goal is that, following the closure of the oil sands operation, the site will be reclaimed. Geotechnical and environmental concerns present a need for effective and efficient monitoring techniques. The integrated geophysical characterization, presented in this study, provides insight into the applicability of geophysical methods towards geotechnical and environmental monitoring.

1.2 Study Site: Syncrude's Southwest Sand Storage Facility

The Syncrude Canada Ltd. Southwest Sand Storage Facility (SWSS) is located in the southwest corner of the Mildred Lake Oil Sands Mine, approximately 35 kilometers northwest of Fort McMurray, Alberta. The SWSS is a large tailings pond, covering an area of approximately 25 km^2, with the dyke measuring about 40 m high and up to 1 km wide. The dyke is referred to as undrained in this report because there is was artificial

drainage system internally during the time in which data was collected for this study. It contains nearly 300 million cubic meters of tailings (Price 2005). The facility was commissioned in 1991 with three coarse tailing systems and a fluid return system, providing coarse tailings sand storage and a small operating pond. The fluid return system returned water and fluid fine tailings from the SWSS operating pond to the Mildred Lake Settling Basin, a Syncrude operated tailings pond to the northeast of the SWSS (Syncrude 2010). Between its commission and 2009, the dyke was constructed using the upstream method. This method builds subsequent dykes upstream, towards the tailings pond, from the initial starter dyke (Hoare 1972). Following dyke construction, about an 80 cm thick layer of reclamation material was placed on the outside of the dyke, consisting of peat and clay till mixture (Naeth et al 2011). However, the SWSS presented reclamation challenges due to high water tables which resulted in process affected water seeping into reclamation materials (Naeth et al. 2011). In 2009, it was redesigned to support increase volumes of mature fine tailings (MFT) and fluid capacity. This design change required a shift to the centerline dyke construction method (Syncrude 2008). This method builds subsequent dykes which maintain the centerline of the starter dyke (Hoare 1972).

Figure 1.2 displays the general location and satellite image of the SWSS facility in Alberta. The SWSS dyke was constructed with a terraced slope including benches (backslopes). The portion of the dyke within the study area consists of four slopes and three benches, which collect and transfer water to a swale south of the study area. Slopes are in this area are 100 to 120 m wide and graded to 8 to 9%; benches are 70 to 90 m

wide and graded to approximately 1%. At the toe of the dyke a perimeter ditch collects runoff and groundwater discharge.

1.3 Parameters of Interest and Petrophysical Model

Efficient geotechnical and environmental monitoring of tailings sites is important to ensure dam safety and improve reclamation efforts. Such monitoring can be assisted by characterizing soil-moisture, water level, and salt distributions. Such a study was conducted previously at the SWSS facility using traditional hydrogeological sampling methods involving many well and piezometer installations (Price 2005). Following the hydrogeological characterization, Price took the study further by implementing a groundwater flow and transport model. In this study, hydrogeological data from Price and coincidental geophysical data was integrated to not only further characterize soil-moisture and salt distributions at the SWSS, but also explore the usefulness of geophysical surveying as a characterization method. Geophysical methods inherently provide a larger spatial extent, as well as being less expensive and relatively non-intrusive compared to traditional hydrogeological methods. However, the drawback of geophysical surveying is that petrophysical model and relationships must be constructed to convert geophysical parameters, collected through surveying, to desired parameters of interest, e.g. soil-moisture and salinity.

The geophysical methods used in this study provide estimates for bulk electrical conductivity (EC). To convert bulk EC measurements to parameters of interest, a petrophysical model is required. In 1942, Gus Archie empirically developed a model which relates bulk EC, fluid EC, and saturation within a porous medium (Archie 1942). This model has since become known as Archie's Law, equation 1.

$$\sigma_b = s_w^n \sigma_w \; F^{-1} \qquad \text{where,} \qquad F = (a/\phi^m) \tag{1}$$

and σ_b is bulk EC, s_w is water saturation, n is the saturation exponent, σ_w is fluid EC, φ is porosity, m is the cement factor, and a is the tortuosity factor. This expression is only applicable in cases of clean or clay-free materials. When clay minerals are present, the exchange of cations from the clay mineral surface with the pore electrolyte must be considered (Devarajan 2006). The behavior of these exchange cations within an electrical field has been described by an empirically derived model presented by Waxman and Smits (1968). Another interpretation is that these hydrated cations form a "double layer" close to the grain surface. This led to the development of Dual-Water (DW) empirical model describing the electrical behavior of a porous medium which contains clay minerals, presented by Clavier et al. (1984). These two models for shaly sands (clay minerals present) are the most commonly used, however many more exist. Furthermore, temperature has been shown to have a strong influence on EC (Waxman and Thomas 1974, Sen and Goode 1992).

In the case of the SWSS facility however, petrophysical models of shaly sands can be ignored due to the low clay content of the tailings material which forms the dyke. This leaves Archie's law as a suitable petrophysical model to interpret bulk EC measurements from geophysical surveying. Unfortunately, limited subsurface temperature data were recorded during this study and the complex temperature distribution could not be adequately modeled. The effects of temperature on bulk EC were therefore left unaccounted for. This inhibits the quantitative capabilities of this study, however many valuable qualitative interpretations can still be made, as well as empirical estimates for parameters within the Archie law petrophysical model.

1.4 Geophysical Methods

1.4.1 Push Tool Conductivity

Push tool conductivity (PTC), also called direct-push conductivity, is an electrical logging based method in which an EC probe is driven directly into the subsurface, usually by a small truck-mounted rig or hydraulic hammer. The EC probe used in the PTC method consists of four electrodes or contact rings in a set array with known geometry. Figure 1.3 displays a schematic of a typical PTC probe and a photograph of the rig used in this study. This design is similar to other electrical geophysical methods in that an apparent resistivity (and its inverse, conductivity) is calculated by applying a geometric factor to the ratio of measured induced potential to a known injected current. A variety of electrode array types are used on current EC probes; most commonly the Wenner array, but also Schlumbeger and Dipole-dipole arrays have been utilized (Beck 2000, Christy 1994, Schulmeister 2003). Figure 1.4 shows a schematic of common electrode arrays, as well as their respective geometric factors used to calculate apparent resistivity. The probe is usually advanced in small increments; for this study, a conductivity measurement was taken every 1.64 cm. This provides a high resolution EC profile of the subsurface. PTC probes also allow direct contact with subsurface materials, while the accuracy of traditional borehole based EC logging methods may be negatively influenced by irregular borehole diameter and drilling fluids (Shulmeister 2003). PTC data are often assumed to be the most accurate representation of subsurface conductivity, making it useful for comparison with other less direct geophysical techniques (Bentley and Gharibi 2004, Hayley et al. 2009).

There are, however, some limitations to the method. First, the probe requires careful calibration to prevent error in the measured EC. This is typically done by using a

factory supplied series of resistors and should be performed prior to each log test. Secondly, the measured EC may be affected by the rate of advancement of the tool, where negative and positive spikes in the measured EC may be a result of decrease or increase of the rate of advancement respectively (Harrinton and Hendry 2006). In addition, physical limitations exist where large rocks or heavily consolidated layers may halt the advancement of the PTC probe.

1.4.2 Electromagnetic Surveying

Electromagnetic (EM) surveying techniques include a broad range of data acquisition instruments and applications. In general, EM geophysical techniques refer to methods which record the EM response of the subsurface to either an artificially or naturally produced EM field. In active EM methods, a transmitter coil is used to generate an EM field, referred to as the primary EM field. If a conductive medium is present in the subsurface, the magnetic component of the incident EM wave induces eddy currents. Eddy currents generate their own secondary EM field which can be detected by a receiver. The secondary EM field will differ in both phase and amplitude to the known primary field. The degree in which these components differ reveals information about the electrical properties of the subsurface (Reynolds 2011).

In this study, EM surveying will be used to refer to ground conductivity surveying from dual-coil instrument, Geonics EM-38. This instrument contains two separate coils; one serves as a transmitter which generates the primary EM field, and one acts as a receiver. The inter-coil spacing is fixed at one meter for the EM-38 device, and the dual-coil system is moved along a study transect. The device records both quadrature and in-phase components of the secondary EM field. The quadrature component can be directly

translated to an apparent conductivity, which is reported in milli-Siemens per meter (mS/m). The in-phase component is measured in parts per thousand (ppt) and provides an estimate for soil magnetic susceptibility. To rapidly collect data across the SWSS site, the EM-38 was placed in a small plastic sled and connected to an all-terrain vehicle (ATV). Figure 1.5 contains photographs of the EM-38 device and the EM-38 survey via ATV.

Ground conductivity meters respond to the conductivity composition of the subsurface depending on the inter-coil spacing and magnetic dipole orientation. Typically, as is the case for the EM-38 instrument, there are two modes in which data can be collected; vertical magnetic dipole and horizontal magnetic dipole. The dipole orientations have different response functions, i.e. contribution to apparent conductivity with depth. Figure 1.6 displays the response functions or relative sensitivity with depth for the EM-38 for both vertical and horizontal dipole orientations. In the case of the vertical magnetic dipole, there is less contribution to measured apparent conductivity from the near subsurface than in the horizontal dipole configuration. The maximum response occurs below the near subsurface, depending on inter-coil separation. For the EM-38, this depth is about 0.4 meters. For the horizontal magnetic dipole, the maximum contribution or sensitivity occurs at the surface and decreases with increasing subsurface depth. Consequently, the horizontal dipole orientation is very sensitive to near subsurface changes in conductivity, while the vertical dipole orientation is less so. The total secondary EM field, translated to apparent conductivity and measured at the receiver coil, is the integral of the respective response function from zero to infinity, assuming a homogenous subsurface half space (McNeill 1980).

1.4.3 Electrical Resistivity Tomography

Electrical resistivity tomography (ERT) is a geophysical technique which images subsurface features from electrical resistivity measurements made at the surface and/or within boreholes. Generally in field electrical resistivity (ER) methods, a current is applied to the subsurface using two electrodes and the potential (voltage) is measured between two separate electrodes. By combining Ohm's Law with known electrode geometry, the ER of the subsurface can be calculated, assuming a homogenous and isotropic half-space. Realistically, the subsurface may consist of many electrically different layers or features, and thus the calculated resistivity is not a 'true' resistivity, but rather an apparent resistivity (Reynolds 2011). Distinct electrode arrays with known geometries were developed, such as Wenner, Schlumberger, or dipole-dipole arrays (Figure 1.4), which provided varying sensitivity to subsurface resistivity features. More recently, computerized inverse modeling techniques allow for irregular array geometries and data acquisition. However, classic array surveys are still frequently conducted by convention.

In two-dimensional ERT methods, strings of electrodes are laid out in a line and apparent ER data are collected automatically, controlled from a laptop or ER system, using a pre-defined sequence of electrode sampling locations. In the automated data acquisition sequence, sets of four electrodes (quadrupoles) are selected for the application of current and measuring of potential. Many positions and electrode geometries are sampled, including reciprocal measurements, as defined by the user. Resistivity information can be found at increasing depths by increasing electrode separation within the quadrupoles, at a cost of resolution (Reynolds 2011). Current ER systems typically consist of 72 (or more) channels, allowing for 72 separate electrode positions to be

sampled in one continuous survey. The ER system used in this study was the ABEM Terrameter SAS 300C (Figure 1.7). If a survey requires a longer study transect, the entire 72 electrode array is shifted, and the automated data acquisition software is run again. Once the entire survey has been completed, all sampled electrode positions and measured apparent resistivities may be combined to generate one image or pseudosection. Figure 1.8 shows a schematic of the ERT methodology using the Wenner array, and includes data point locations which would be used to develop the resulting pseudosection of apparent resistivity. These pseudosections yield a representation of subsurface resistivity. However they are highly dependent on not only true subsurface resistivity distribution, but also the electrode geometry and data acquisition sequencing (Loke and Barker 1996). Currently, in nearly all levels of academic and commercial ERT surveys, inverse modeling techniques are applied to generate models of the subsurface resistivity distribution.

Given a resistivity model of the subsurface and the physics of the ER problem, it is possible to calculate a set of apparent resistivity values which would be observed by an ERT survey, under specific acquisition geometry and array sequencing. This process is called forward modeling. Using an iterative least-squares approach, it is possible to find a parameterized model space of resistivity which minimizes the difference between forward-modeled resistances and observed resistances. In this study, RES2DINV was used, an inversion software based on a smoothness-constrained, least-squares inversion method (Loke and Barker 1996). Most often, the model space is overparameterized (more parameters than data) and needs regularization; a variety of regularizing techniques have been created under physical, mathematical, and empirical inspirations (Ellis and

Oldenburg 1994). Some examples of regularization schemes include classical Marquardt (1970), Tikhonov (1977), and truncated singular value decomposition (TSVD) which is outlined in Hansen (1987), as well as more recent methods including an Occam's razor approach which yields the most simple and smoothest model to prevent over-interpretation by the practitioner (Constable et al. 1987). ERT inversions are affected by both the sensitivity of the method and the effects of regularization. Final inverted tomograms or models are dependent on the true distribution of subsurface resistivity, method and quality of data acquisition, model parameterization, and the constraint criteria (Singha and Gorelick 2006). Consequently, the solution to the problem is non-unique and may contain artifacts, as well as a smoothed representation of subsurface features.

The question remains however, in what way can we deal with the non-uniqueness of the inverse problem, i.e., how do we know which model produced through inversion procedures best represents the true earth? Many approaches have been taken to this problem including a priori knowledge provided by geological or geotechnical surveys (Ellis and Oldenburg 1994, Yeh et al. 2002), characterizing an error model to weight measured data (Binley et al. 1995, Singha and Gorelick 2006), and matching inverse models to supplementary data (Hayley et al 2009). In this study the latter approach was taken, where final inverse models were chosen based on best agreement with coincidental PTC data. The limitation of this particular method is that relationships between inverted models and supplementary data may still be subject to variable model resolution and regularization criteria in the inversion, as discussed previously. Nonetheless, it provides a

reasonable method for determining which inverted model should be chosen which best represents the true resistivity distribution of the subsurface.

1.5 Hydrogeological Methods

1.5.1 Neutron Probe and Soil Moisture

The neutron soil moisture gauge, commonly referred to as the neutron probe, is designed to provide estimates of soil moisture. The device basically consists of a fast neutron source, a slow neutron detector, a pulse counter (ratescaler), a cable connecting the two, and a transport shield (Bell 1987). For most systems, the transport shield is fitted to a vertical aluminum access tube which slightly protrudes from the subsurface. Following, the probe is lowered from the transport shield through the access tube, recording successive measurements with depth to create a profile. The transport shield generally consists of a plastic neutron moderator which provides shielding from the fast neutron source (Bell 1987). The ratescaler remains at the surface. Figure 1.9 displays a schematic of a typical neutron probe.

The probe contains a radioactive source which emits fast neutrons into the surrounding subsurface. When the emitted fast neutrons collide with the nuclei of other atoms, predominately hydrogen nuclei, the neutrons scatter, slow down, and lose energy. It should be noted that although hydrogen nuclei, including bound water and organic materials, exerts the primary effect on the count rate, every element has some ability to scatter and slow fast neutrons (Bell 1987). This creates a ‘cloud’ of slow neutrons around the neutron source and the density of this cloud, which is mainly a function of soil moisture, is sampled through the detector. The mean count rate is subsequently displayed on the ratescaler and can be translated to soil moisture, namely volumetric moisture,

using an appropriate calibration curve. Count rates are usually expressed as a count ratio, the number of counts at a given depth relative to the counts in a standard moderator to eliminate error due to instrument drift (Vachaud 1977). The generation of specific field calibration curves is necessary to ensure accurate results, however calibration methods are difficult to perform and regression correlation coefficients between count ratio and soil moisture content are not extremely high, usually between 0.80 and 0.95 (Reichardt 1997, Vachaud et al 1977). Despite the difficulties in the calibration of neutron probes, they have been successfully employed in a variety of studies (Grant et al. 2004, Huo et al. 2008, Evett et al. 2009, Hu et al. 2009).

1.5.2 Groundwater Sampling

Traditional groundwater sampling techniques include the drilling of boreholes and the installation of wells or piezometers. Both the well size, in diameter, and the length of the well screen, the slotted area in which water can flow into the well, depends on the application. Small well diameters, given they are large enough for sampling equipment and probes, are preferred in groundwater sampling applications because they are less expensive, easier to install, and are smaller in volume. Large screen lengths will provide non-depth specific groundwater samples that are integrated over the length of the screen, with high permeability units contributing more water than low permeability units. Generally however, in groundwater sampling applications where detailed groundwater characterization is necessary, small screen lengths are utilized as they provide depth specific information (Appelo and Postma 2005). To acquire depth specific sampling at multiple depths, multi-level wells or piezometer nests are required. This study, and the previous hydrogeological characterization of the SWSS site conducted by Price (Price

2005), utilized a series of piezometer nests where each piezometer is placed in separate boreholes and clustered in close proximity to one another.

Drilling operations, including drilling fluids, gravel packs, or casing materials, often disturb the natural chemistry and flow conditions of a well. To return groundwater produced by the well to its natural conditions, the well is flushed by drawing water from the well until the parameters of interest stabilize. This may vary between 2 to 10 well volumes depending on the local hydrological conditions (Appelo and Postma 2005). Once well or piezometer installation and flushing is completed, water samples are acquired and measured for a variety of parameters, in both the field and laboratory.

To acquire water level information well screens must be placed solely in the desired unit, as different units may be of varying hydraulic potential and result in inaccurate water level measurements (Appelo and Postma 2005). In the case of the SWSS site, the tailings material which forms the dyke represents the uppermost aquifer and the unit of interest. Thus water level wells were installed with screened intervals across the water table within the tailings dyke. Furthermore, a large number of piezometer nests at varying depths were installed during for the groundwater sampling program.

1.6 Purpose and Scope

With the growing number of tailings sites as a result of surface mined oil sands, there is a need to develop methods to efficiently monitor soil moisture and salt transport for both geotechnical and environmental concerns. A previous groundwater modeling study at the SWSS facility evaluated flow and salt transport, calibrated with hydrogeological field data, under varying hydrological inputs, boundary condition, and physical properties (Price 2005). The research presented in this study, aimed to improve

the understanding of flow and salt transport within the SWSS dyke and other tailings dam structures by augmenting hydrogeological data with geophysical data. Overall, this work helps improve tailings site monitoring methods and facilitates future geotechnical and environmental management of the SWSS site and other tailings sites. The research presents benefits and limitations of using geophysical methods to monitor tailings sand dykes. Furthermore, the applicability of geophysical data to aid in the calibration and validation of future groundwater flow models were investigated.

1.7 Study Objectives

In this study, the applicability of combined geophysical methods and hydrogeological measurements to map and monitor soil moisture and salt distribution at oil sands tailings sites is investigated. Furthermore, the usefulness of geophysical methods to the calibration and validation of groundwater flow and transport models is explored. This was achieved by developing a geophysical characterization of the SWSS site, using both forward and inverse modeling techniques to aid in the calibration and imaging of site bulk electrical conductivity. Furthermore, the petrophysical relationships between geophysical and hydrogeological data were investigated; specifically the relationships between bulk electrical conductivity versus soil moisture and fluid electrical conductivity were explored.

1.8 Contribution of Authors

Chapter 2 of this thesis is presented as a stand-alone manuscript.

Booterbaugh, A.P, Bentley, L.R., Mendoza, C.A. (in prep.). Geophysical characterization of an undrained oil sands tailings pond Alberta, Canada. JEEG.

Geophysical data were collected by Komex International Ltd. in 2001 and 2004, and WorleyParsons Ltd. in 2008. Hydrogeological data were collected by C.A.M. at the University of Alberta. A.P.B. processed all of the geophysical and hydrogeological data used in this study. Additionally, A.P.B developed and utilized MATLAB codes contained in the Appendix section; A.P.B. developed the method for normalizing the EM maps and automated layer designation for PTC data. The interpretations of results were made by A.P.B. following extensive discussions with L.R.B. and C.A.M.. A.P.B. wrote the manuscript.

1.9 References

Alberta's Energy Industry. An Overview. 2012. Alberta Energy Resources Conservation Board.

Appelo, C. and Postma, D. 2005. Geochemistry, groundwater and pollution. 2nd Edition. A.A. Balkema Publishers, Leiden, The Netherlands a member of Taylor & Fancis Group plc.

Archie, G. 1942. The electrical resistivity log as an aid in determining some reservoir characteristics. T. Am. I. Min. Met. Eng., Vol. 146. 54 – 62.

Beck, F., Clark, P., Puls, R. 2000. Location and characterization of subsurface anomalies using a soil conductivity probe.

Bell, J. 1987. Neutron probe practice. 3rd edition. Inst. of Hydrol., Rep. 19. 1 – 63.

Bentley, L., Gharibi, M. 2004. Two- and three-dimensional electrical resistivity imaging at a heterogeneous remediation site. Geophysics. Vol. 69, No. 3. 674 – 680.

Berkowitz, N. and Speight, J. 1975. The oil sands of Alberta. Fuel. Vol. 54. 138 – 149.

Binley, A., Ramirez, A., Daily, W. 1995. Regularised image reconstruction on noisy electrical resistance tomography data: 4th Workshop of the European Concerted Action on Process Tomography, Proceedings. 401 – 410.

Clavier, C., Coates, G., Dumanoir, J. 1984. Theoretical and experimental bases for the Dual-Water model for interpretation of shaly sands. Soc Petrol Eng J. Vol. 24. No. 2. 153 – 168.

Chirsty, C., Christy, T., Witting, V. 1994. A percussion probing tool for direct sensing of soil conductivity. Proceedings of the 8th National Outdoor Action Conference. 381 – 394.

Constable, S., Parker, R., Constable, C. 1987. Occam's inversion: a practical algorithm for generating smooth models from EM sounding data. Geophysics. Vol. 52. 289 – 300.

Devarajan, S., Toumelin, E., Torres-Verdin, C. 2006. Pore-scale analysis of the Waxman-Smits shaly sand conductivity model. SPWLA 47th Annual Logging Symposium, Vera Cruz, Mexico. 1- 9.

Ellis, R. and Oldenburg, D. 1994. Applied geophysical inversion. Geophys. J. Int. Vol. 116. 5 – 11.

Evett, S., Schwartz, R., Tolk, J., Howell, T. 2009. Soil profile water content determination: Spatiotemporal variability of electromagnetic and neutron probe sensors in access tubes. Vadose Zone J. Vol. 8. 926 – 941.

Government of Alberta. 2013. Oil Sands Reclamation. www.oilsands.alberta.ca/reclamation. html.

Grant, L., Seyfried, M., McNamara, J. 2004. Spatial variation and temporal stability of soil water in a snow-dominated mountain catchment. Hydrol. Process. Vol. 18. 3493 – 3511.

Hansen, C. 1987. The truncated SVD as a method for regularization. BIT. Vol. 27. No. 4. 534 – 553.

Harrinton, G. and Hendry, M. 2006. Using direct-push EC logging to delineate heterogeneity in a clay-rich aquitard. Ground Water Monit. Rem. Vol. 26. No. 1. 92 – 100.

Hayley, K., Bentley, L., Gharibi, M. 2009. Time-lapse electrical resistivity monitoring of salt-affected soil and groundwater. Water. Resour. Res. Vol. 45. 1 – 14.

Hoare, B. 1972. The disposal of mine tailings material. (Doctoral dissertation). University of Waterloo. 1-210.

Hu, W., Shao, M., Wang, Q., Reichardt, K. 2009. Time stability of soil water storage measured by neutron probe and the effects of calibration procedures in a small watershed. Catena. Vol. 79. 72 – 82.

Huo, Z., Shao, M., Horton, R. 2008. Impact of gully on soil moisture of shrubland in wind-water erosion crisscross region of the Loess Plateau. Pedosphere. Vol. 18. No. 5. 674 – 680.

Komex International Ltd. 2001. C55100000: Geophysical characterization of the Southwest Sand Storage Facility. Syncrude Canada Ltd., Fort McMurray, Alberta.

Komex International Ltd. 2005. E00050405: 2004 Geophysical Investigation of Southwest Sand Storage Facility. Syncrude Canada Ltd., Fort McMurray, Alberta.

Loke, M., and Barker, R. 1996. Rapid least-squares inversion of apparent resistivity pseudosections by a quasi-Newton method. Geophys. Prospect. Vol. 44. 131-152.

Marquardt, D. 1970. Generalized inverses, ridge regression, biased linear estimation, and nonlinear estimation. Technometrics. Vol. 12. 591 – 612.

Masliyah, J., Zhou, Z., Xu, Z., Czarnecki, J., Hamza, H. 2004. Understanding water-based bitumen extraction from Athabasca Oil Sands. Can. J. Chem. Eng. Vol. 82. 628 – 654.

Morgan, G. 2001. An energy renaissance in oil sands development. World Energy. Vol.4, No. 2. 46 – 53.

McNeill, J. 1980. Electromagnetic terrain conductivity measurement at low induction numbers. Technical Note TN-6, Geonics Ltd., Mississauga, Ontario, Canada.

Naeth, M., Chanasyk, D., Burgers, T. 2011. Vegetation and soil water interactions on a tailings sand storage facility in the Athabasca oil sands region of Alberta Canada. Phys. Chem. Earth. Vol. 36. 19-30.

Price, A. 2005. Evaluation of groundwater flow and salt transport within an undrained tailings sand dam (Master's Thesis). University of Alberta, Department of Earth and Atmospheric Sciences.

Reichardt, K., Portezan, O., Bacchi, O., Oliveira, J., Douradoneto, D., Pilotto, J., Calvache, M. 1997. Neutron probe calibration correction by temporal stability parameters of soil water content probability distribution. Sci. Agric. Vol. 54. 17 – 21.

Renault, S., Lait, C., Zwiazek, J., MacKinnon, M. 1998. Effect of high salinity tailings waters produced from gypsum treatment of oil sands tailings on plants of the boreal forest. Environ. Pollut. Vol. 102. 177 – 184.

Reynolds, J. 2011. An introduction to applied and environmental geophysics – 2nd ed. Wiley – Blackwell. Chichester, UK.

Sanford, E. 1983. Processibility of Athabasca oil sand: Interrelationship between oil sand fine solids, process aids, mechanical energy and oil sand age after mining. Can. J. Chem. Eng. Vol 61. 554 – 567.

Sen, P. and Goode, P. 1992. Influence of temperature on electrical conductivity on shaly sands. Geophysics. Vol. 57. No. 1. 89 – 96.

Singha, K., Gorelick, S. 2006. Effects of spatially variable resolution on field-scale estimates of tracer concentration from electrical inversions using Archies's law. Geophysics. Vol. 71, No. 3. G83 – G91.

Schulmeister, M., Butler, J., Healey, J., Zheng, L., Wysocki, D., McCall, G. 2003. Direct-push electrical conductivity logging for high-resolution hydrostratigraphic characterization. Ground Water Monit. Rem. Vol. 23, No. 3. 52 – 62.

Syncrude Canada Ltd.. 2008. Public Disclosure Document: South west sand storage Conversion. Phys. Chem. Earth. Vol. 36. 19 – 30.

Syncrude Canada Ltd. 2010. Directive 074: Baseline Survey for Fluid Deposits Syncrude Mildred Lake and Aurora North. Alberta Energy Resources. 1 – 49.

Tikhonov, A. and Valette, B. 1977. Solutions of ill-posed problems. John-Wiley & Sons, New York.

Vachaud, G., Royer, J., Cooper, J. 1977. Comparison of methods of calibration of a neutron probe by gravimetry or neutron-capture model. J. Hydrol. Vol. 34. 343 – 356.

Waxman, M. and Smits, L. 1968. Electrical conductivities in oil-bearing shaly sands. Soc Petrol Eng J. Vol. 8. 107 – 122.

Waxman, M. and Thomas, E. Elecrical conductivities in shaly sands- I. The relation between hydrocarbon saturation and resistivity index; II. The temperature coefficient of electrical conductivity. J. Petrol. Technol. Vol. 26. No. 2. 213 – 225.

Yeh, T., Liu, S., Glass, R., Barker, K., Brainard, J., Alumbaugh, D., LaBrecque, D. 2002. A geostatistically based inverse model for electrical resistivbity surveys and its applications to vadose zone hydrology. Water Resour. Res. Vol. 38. No. 12. 1 – 13.

Figure 1.1. Alberta oil sand deposits. Taken from (Government of Alberta 2013).

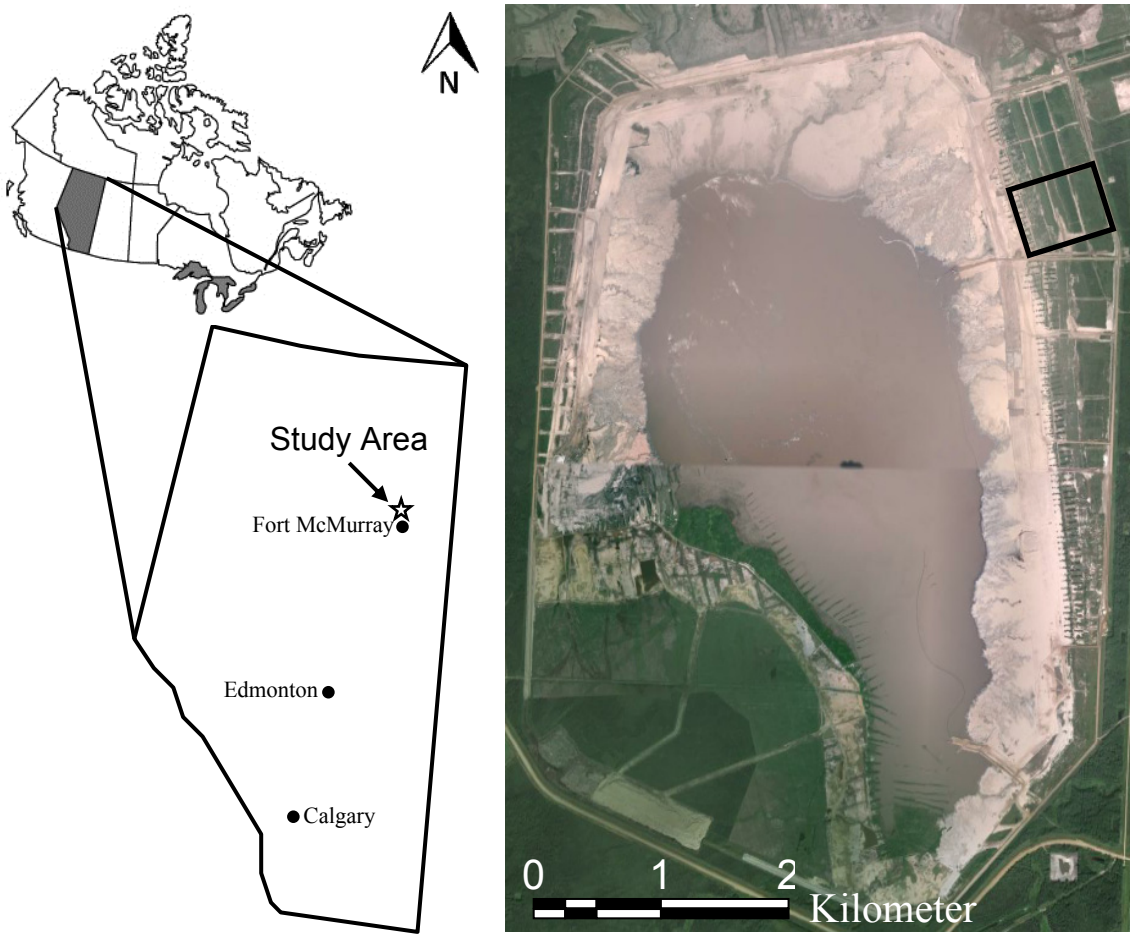

Figure 1.2.General location and satellite image of the SWSS facility. The study area is outlined in satellite image by the black rectangle.
Source: "Syncrude Southwest Sand Storage Facility." 56º58′24.89″ N and 111º45′35.73″ W. **Google Earth.** July 21, 2010 and August 31, 2009.

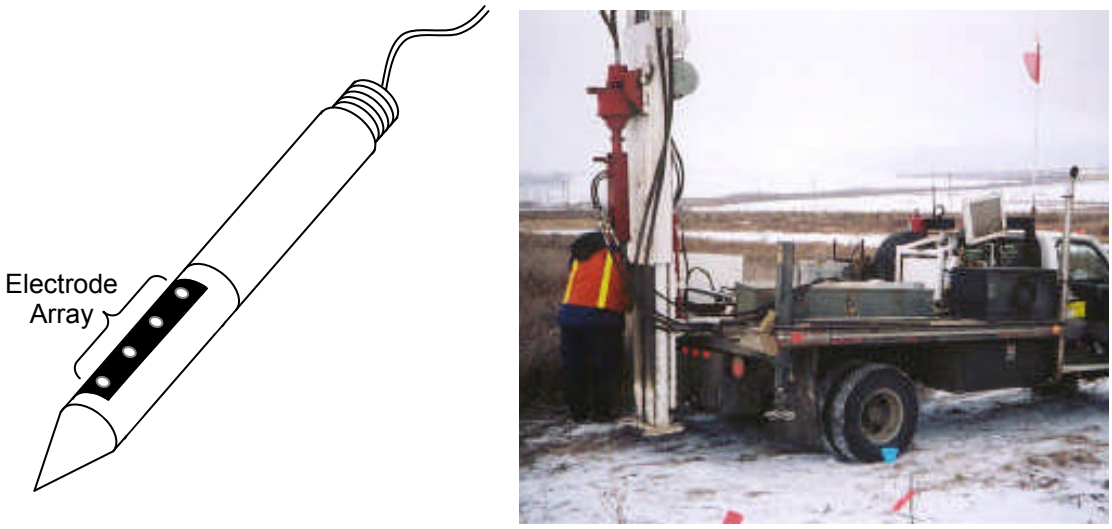

Figure 1.3. Schematic of PTC probe (left) and photograph of truck mounted rig for PTC implementation (right) at the SWSS facility. Schematic adapted from (Schulmeister 2003). Photograph from (Komex 2001).

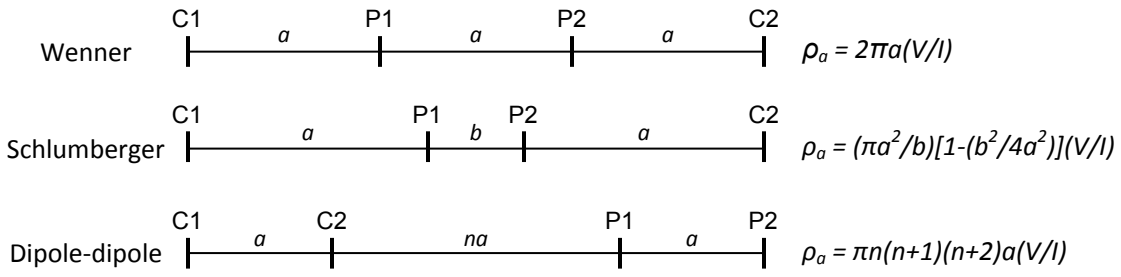

Figure 1.4. Common electrode arrays and geometric factors utilized in EC probes, as well as ER surveys. Adapted from (Reynolds 2011).

Figure 1.5. Photograph of the EM-38 device (top right) and photographs of EM-38 surveying with use of an ATV, conducted at the SWSS facility (Komex 2001).

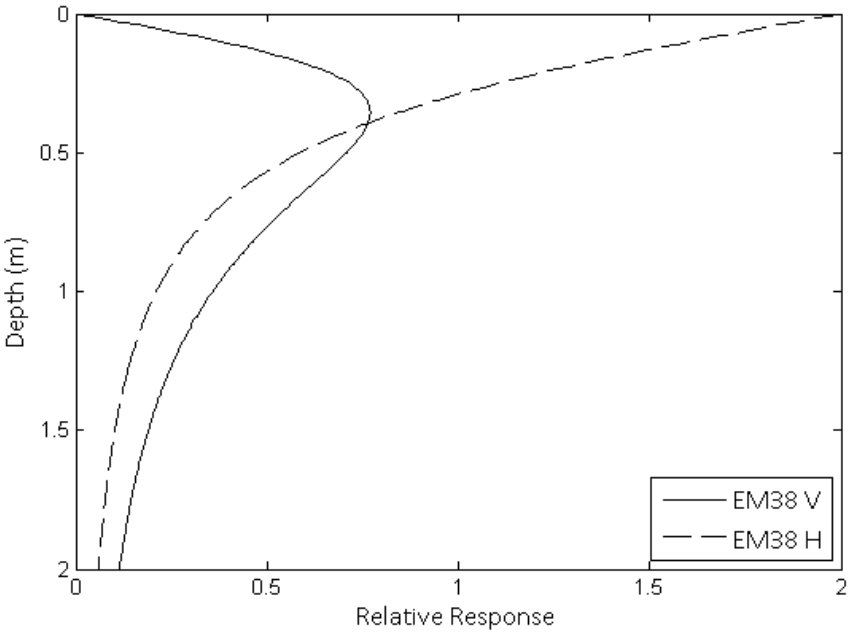

Figure 1.6. Response functions for EM-38 device for both vertical and horizontal dipole orientations. Adapted from (McNeill 1980).

Figure 1.7. Photograph of the ERT system used in this study, the ABEM Terrameter 300C (Komex 2005).

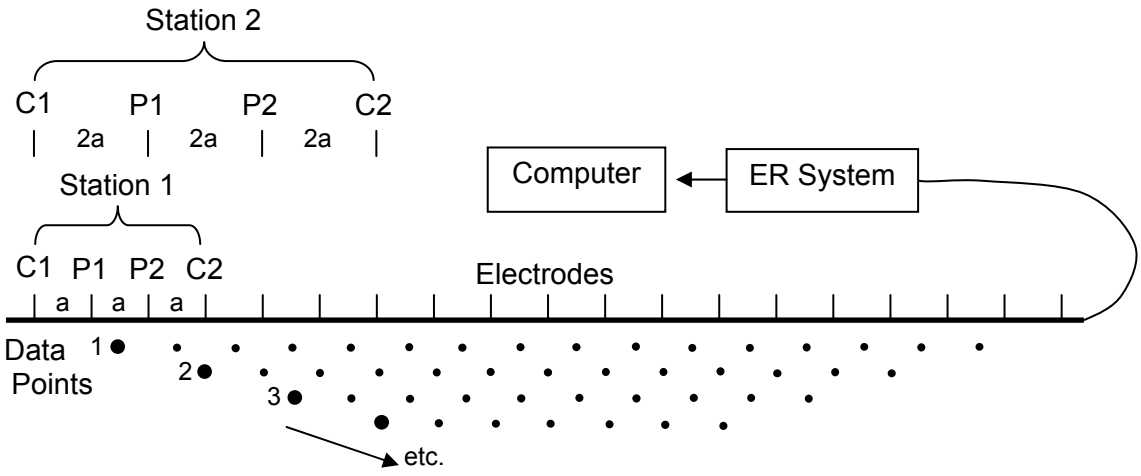

Figure 1.8. Sequence of measurements in a Wenner array ERT survey. Data points within the resulting apparent resistivity pseudosection are placed at the center of the quadrapole; depth depends on array type and geometry (electrode spacing 'a'). Adapted from (Loke and Barker 1996).

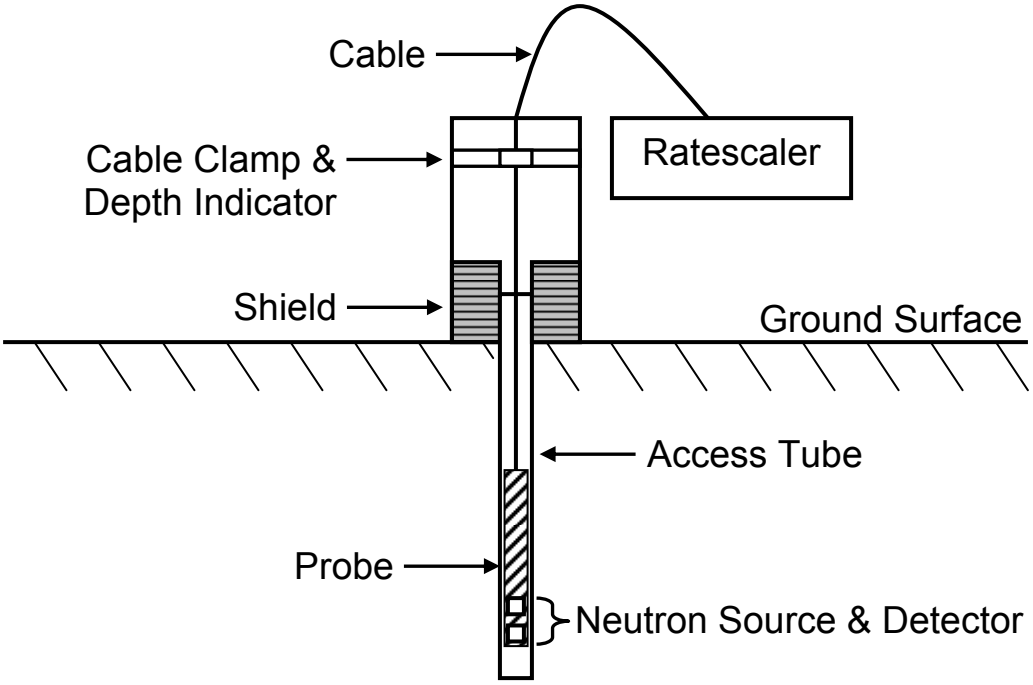

Figure 1.9. Schematic of a typical neutron probe system. Adapted from (Bell 1987).

Chapter 2: Geophysical characterization of an undrained dyke containing an oil-sands tailings pond, Alberta, Canada

Abstract

Geophysical characterization of an undrained oil sands tailings pond dyke was conducted at Syncrude Canada's Southwest Sand Storage Facility (SWSS). Push tool conductivity (PTC), electromagnetic (EM), and electrical resistivity tomography (ERT) methods in tangent with hydrogeological and chemistry measurements were used to investigate soil moisture, hydraulic heads, and groundwater salinity distributions. Geophysical data were collected from 2001 to 2008 and interpretations can further be used to validate studies of groundwater flow and salt transport within the structure. An Archie's Law petrophysical model was utilized to relate measured bulk conductivity, from geophysical surveying, with measures of soil moisture and fluid electrical conductivity. It was found that a relatively strong relationship between bulk electrical conductivity and soil moisture exists, while weak to no correlation was observed between bulk and fluid electrical conductivity. ERT surveying was capable of clearly identifying the location of the water table within the dyke. This study provides a unique look into the application of geophysical techniques to investigate soil moisture, hydraulic head, and salt distribution in an active undrained tailings dam structure. The methodology and insights gained from this study may be applied to similar undrained and drained oil sands tailings storage sites.

2.1 Introduction

The processing and production of the Athabasca Oil Sand deposit in northern Alberta, Canada has, in recent decades, grown into a large industry, producing about 2.3

x 10^5 m^3 per day and expected to grow to 4.5 x 10^5 m^3 per day by 2022 (Alberta Energy Resources 2012). The Athabasca is the largest of three major oil sand deposits in Alberta and collectively Alberta's oil sands constitute the world's largest bitumen reserve, containing an initial in-place resource of approximately 200 x 10^9 m^3, with an estimated established reserve of 20 x 10^9 barrels (Kasperski and Mikula 2011). About one tenth of the Athabasca oil sands deposit lies within the upper 45 meters of the subsurface where conventional open pit mining operations are most economically viable (Berkowitz and Speight 1975). Open pit mining operations of these near surface oil sand deposits results in large volumes of waste referred to as tailings. Bitumen is extracted using a water-based extraction process, a developed method that is similar in concept to the hot water extraction method first described by Clark (1929). This method involves a warm water slurry, typically 40 - 55ºC, and chemical additives, most notably NaOH, to assist in bitumen liberation (Masliyah et al. 2004).

Tailings are collectively made up of a combination of coarser-grained sediments, dispersed fines, process affected sodium-rich water, and residual bitumen. This slurry has about 55wt% solids, of which 82wt% is sand, 17wt% are fines smaller than 44 μm and 1wt% bitumen (Chalaturnyk et al. 2002, Kasperski and Mikula 2011). Tailings are directed to waste storage facilities referred to as tailings ponds (Dusseault and Scott, 1983). Tailings dam dykes are constructed gradually, utilizing the coarser fraction (although still relatively fine for sand) of beached tailings which settles from the initial tailings slurry, to support ever increasing volumes of tailings. The underlying goal is that, following closure of the oil sands production operation, the tailings pond sites will be reclaimed. However, there is often a need to investigate and monitor soil moisture and

salinity within tailings pond structures for both geotechnical and environmental concerns. Traditional hydrogeological monitoring techniques typically involve the installation of wells and only provide sparse point measurements. With the addition of geophysical techniques, sites may be mapped and monitored in a much more spatially extensive, rapid, and less expensive manner.

The bulk electrical conductivity (EC) of the subsurface is dependent on several parameters including soil type, soil moisture, fluid EC, and temperature. A petrophysical relationship for sand was described and empirically derived by Archie (1942) and has since become commonly known as Archie's Law. Tailings used for dyke construction provide an opportunity to build Archie's law relationships because of their relatively clay free properties. With available direct measures of soil moisture and fluid EC, as well as geophysical measures of bulk EC, site specific empirical relationships can be developed. Archie's Law and its use as a petrophysical model for this study is described in more detail later. Similar environmental and geotechnical geophysical investigations at mine tailings and other contaminated sites have been conducted in recent years (Hayley et al 2009, Martínez-Pagán et al 2009, Sjödahl et al 2005, Yuval and Oldenburg 1996).

In this study, the applicability of combined geophysical methods and hydrogeological measurements to map and monitor soil moisture and salt distribution at oil sands tailings sites is investigated. Furthermore, the usefulness of geophysical methods to the calibration and validation of groundwater flow and transport models is explored.

2.2 Study Site: Syncrude's Southwest Sand Storage Facility

The Southwest Sand Storage Facility (SWSS) is a large tailings pond located approximately 35 kilometers northwest of Fort McMurray, Alberta in the southwest corner the Syncrude Canada Ltd. Mildred Lake Oil Sands Lease. The SWSS dyke is up to 40 m high and 1 km wide and is referred to as undrained because there is no artificial drainage system internally. Figure 2.1 displays the approximate location and satellite image of the SWSS site, as well as a shaded relief map which includes sampling locations for a variety methods conducted in this study. It was commissioned in 1991 and designed to provide coarse tailings sand storage. It is 25 km^2 in area and approximately 40 m in height (Price 2005). Prior to 2009 and during the data acquisition for this study, the structure was without an internal drainage system and the dyke was constructed with the upstream method. The upstream construction method adds subsequent dykes upstream, towards the tailings pond, from the starter dyke (Hoare 1972). An approximately 80 cm thick layer of reclamation material, a peat and clay till mixture, was added following the placement of coarse tailings which form the dyke. However, the SWSS dyke presented reclamation challenges due to shallow water tables which, in some locations, resulted in process affected tailings water seeping to reclamation materials (Naeth et al. 2011).

The SWSS facility dyke was constructed with terraced slopes including benches (backslopes) creating a groundwater flow system conceptually similar to the classic small drainage basin flow under sinusoidal topography described by Tóth (1963). The study area in the northeast portion of the SWSS dyke consists of four slopes and three benches. As a result of high water tables and ponded water at the toes of slopes, benches began to function as a method of collecting and transferring runoff and seepage water to a swale south of the study area, eventually reaching a perimeter ditch at the toe of the dyke

(Naeth et al. 2011). Figure 2.2 displays a cross-section of the study area and conceptual groundwater flow with groundwater discharge and recharge areas in local topographic lows of the benches.

2.3 Petrophysical Model

The tailings sand which makes up the SWSS dyke is believed to be a relatively clay free sand. For this reason, as described previously, Archie's Law is a reasonable choice for the foundation of petrophysical relationships described in this study. Archie's description of the bulk EC of clay free porous medium is:

$$\sigma_b = s_w^n \sigma_w \ F^{-1} \qquad \text{where,} \qquad F = (a/\phi^m) \tag{1}$$

where σ_b is bulk EC, s_w is water saturation, n is the saturation exponent, σ_w is fluid EC, φ is porosity, m is the cement factor, and a is the tortuosity factor. F is known as the formation factor. In areas below the water table, where water saturation equals 1, cross-plots of coincidental bulk and fluid EC measurements should produce an estimate for F as the slope of linear regression with y-intercept equal to zero. This direct relationship and results which pertain from this study will be discussed later.

Additionally, Archie's Law can be transformed into a version which linearly relates bulk EC to saturation. Rearranging equation 1 with a logarithmic transform yields:

$$log\,(\sigma_b) = n \cdot log\,(s_w) + log(\sigma_w F^{-1}) \tag{2}$$

2.4 Materials and Methods

2.4.1 Data Acquisition

Geophysical methods for this study included push tool electrical conductivity (PTC), frequency domain electromagnetic (EM), and electrical resistivity tomography (ERT). Data for the three methods were collected in 2001 and 2004, with ERT also being

collected in 2008. Data were collected by Komex International Ltd. in 2001 and 2004, and WorleyParsons Ltd. in 2008. In 2001 data were acquired along study transects A and B (Figure 2.1), with EM taken over an extensive area of the northeast section of the SWSS dyke. In 2002, a total of sixty-seven piezometers and water table wells were installed along transect C to characterize hydraulic head and salt distribution. Hydrogeological and chemistry data collected during 2002 to 2003 were synthesized into a numerical model in order to evaluate groundwater flow and salt transport within the SWSS dyke (Price 2005). With the additional instrumentation along transect C, geophysical methods were refocused to transects A and C in 2004 and 2008, with the hypothesis that the integration of these data would provide a more spatially exhaustive image of hydraulic heads and salt distribution within the SWSS dyke.

2.4.2 Hydrogeological and Chemistry Methods

Hydrogeological and chemistry measurements were taken along Transect C between 2002 and 2008, including water level, fluid EC, fluid or porous medium temperature, total dissolved solids, pH, dissolved oxygen, and major anion and cation concentration measurements. Of most interest in this study were water level and fluid EC measurements which can be correlated directly with geophysical data. Figure 2.1 displays the locations of the various hydrogeological sampling used in this study. Water level measurements were taken from water table wells installed with 1 to 1.5 m screens across the water table. Piezometers, used for groundwater sampling, were installed with 0.3 m screens from 1 m below the water table to up to 9 m deep and spaced vertically by 2 m. Wells and piezometers were constructed of 0.025 m diameter PVC pipe with machine

slotted screens (0.5 mm) covered in filter cloth, and installed using either a 1 inch hand auger or a 3.5 inch portable solid-stem auger drill (Price 2005).

Volumetric moisture (VM) profiles were also collected along Transect C between 2001 and 2012 in the same locations where wells were installed (Figure 2.1), using either a model 501DR or 503DR Campbell Pacific Nuclear Corp. neutron probe. The probe contains a fast radioactive neutron source and a slow neutron detector. Fast neutrons are released from the source, which collide with nuclei of similar mass, predominantly hydrogen, slowing or thermalizing the neutrons. A 'cloud' of slow neutrons are generated within the soil near the source; the density of this cloud is sampled and translated to an estimate of VM. Other elements and hydrogen not associated with water may also cause some additional scattering of fast neutrons, however measurements are largely a function of soil moisture (Bell 1987). Measurements were taken every 15 cm to a depth of about 1.5 to 3 meters.

2.4.3 Push Tool Conductivity

A total of thirty-seven and sixteen PTC profiles were recorded for 2001 and 2004, respectively. Measurements were taken to approximately 5 meters below the surface with a sampling resolution of 1.64 cm. For areas which were easily accessible, near the crest of the dyke where vegetation was thin, a rig mounted hydraulic hammer was used to advance the PTC probe. In areas near the toe of the dyke which had more dense vegetation, the PTC probe was driven into the ground by hand using a 13.6 kg slide hammer (Komex 2004). PTC provides a relatively quick acquisition, high resolution vertical EC profile and was assumed, for this study, to be the most accurate representation of subsurface bulk EC. For this reason, PTC data was used to calibrate

EM and optimize ERT inversion; calibration and optimization procedures will be discussed in the following sections. A simple 5-point triangle smoothing filter was applied to raw PTC data to dampen high spatial frequency noise.

To calibrate EM data, which provides one integrated EC measurement of the subsurface, to PTC data, which provides bulk EC measurements with depth, PTC data was forward modeled to a simulated EM response using EM modeling software FreqEM (Loke 2006). This model is based off a 1-D layered earth, with a maximum of 8 layers, and is capable of both inversion and forward modeling of EM response of desired dipole orientation and geometry. It was therefore necessary to divide PTC profiles into distinct layers for which an EM response could be calculated through FreqEM. To achieve this with minimal bias over a large number of PTC profiles, a program was developed to automatically locate a desired number of layers from 1-D data (Appendix H). The program starts with a high number of layers and is primarily constrained by a layer variance threshold which is gradually increased until the model reaches the desired number of layers. Other constraints include a limit to minimum and maximum layer size which can be systematically increased with depth, and the percent change in mean values over a specified window size. This allowed the program to pick both more layers near the surface, within depths of high contribution to EM response, and layer boundaries at areas of high EC change. A user defined depth of investigation parameter also allowed constraints to be loosened with depth to improve model stability. Once layers were developed for the PTC profiles, the mean EC and thickness of the modeled PTC layers were implemented into the FreqEM package and forward modeled to a calculated EM EC

response. Examples of PTC profiles and their respective modeled layers may be found in Appendix A.

2.4.4 Electromagnetic Methods

Electromagnetic (EM) surveys were taken in the fall of 2001 and 2004. In 2001 surveys were taken over a large section in the northeast region of the SWSS dyke. In 2004 surveys were focused on only transects A and C. The Geonics EM-38 device was utilized in both cases and is particularly useful as a reconnaissance tool which can quickly map EC of the upper subsurface. In order to acquire data rapidly over a large area, the EM device was placed in a small sled designed to be pulled by an all terrain vehicle (ATV). In areas where vegetation, soil conditions, or instrumentation prevented the use of the ATV, the EM surveys were continued on foot. EM surveys were conducted with both horizontal and vertical dipole orientations allowing for nominal depths of exploration of 0.75 and 1.5 meters respectively. Only the data acquired in the vertical orientation are reported in this paper.

In both 2001 and 2004, EM surveys were conducted over several days under different moisture conditions due to rain. Consequently, large portions of EM data displayed differences in average EC, due to differences in average soil moisture on different days (Figure 3A). The largest discrepancies in EC existed along the upper parts of the bench and slopes where water tables are lower. Conversely at the toes of the slopes where water tables are high, the precipitation did not cause a large change in soil moisture and subsequently measured apparent EC. In order for the data to be used to make inferences on soil moisture and salinity, it was necessary to normalize the data so that the different spatial regions have similar statistical distributions of EC. A

normalization procedure was developed to shift the statistical distribution of measured EC in elevated zones of EM data, to a distribution of EC that was similar to surrounding EM data (Appendix G). A key component which made the normalization possible was that the SWSS dyke is an engineered structure which contains linear topographic features perpendicular to its aspect. Similarly, it was assumed that EC across the SWSS site should reflect this linearity, i.e., the EC statistics should display stationarity in space perpendicular to the dykes slope, given the same surface moisture conditions. Preliminary EM maps of non-elevated EC regions confirmed this assumption.

First, two zones of EM data which should display similar statistical distributions were selected; one of elevated EC and one of a reference EC. Data from the two zones were broken into 100 quantiles (percentiles) and the difference between the mean of the elevated data and the mean of the reference data at each respective quantile was calculated. Following, a piecewise linear function was developed consecutively connecting the calculated mean difference at each quantile. This created a continuous, polygonal curve in which the difference between the elevated and reference region could then be estimated for each data point in the elevated region. The data in the elevated region were then adjusted by the appropriate estimated difference from the polygonal curve, creating a normalized elevated region which statistically matched the reference region. This was done in several iterations until elevated EC regions displayed similar EC statistics to that of the non-elevated data region in space perpendicular to the dyke aspect. Elevated zones were defined by selecting regions which exhibited elevated EM EC of about 50 – 70 mS/m (uncalibrated conductivity) along the upper parts of the slopes and benches. Reference zones were selected in areas that show display statistical stationarity

to elevated zones. Elevated and reference zones were also selected to contain areas including the toes of the slopes where measured EC was high. As mentioned previously there was little discrepancy in measured EC between the elevated and reference zones in these areas due to already high water tables. Incorporating this high EC and statistically stationary area in the normalization procedure allowed the higher EC values in the total EC distribution to be well defined and provided a greater range of EC, which overall improved the normalization procedure results. Figure 2.3 displays contoured data and histograms for one normalization procedure of the 2001 EM data. Summary statistics for the normalization example of Figure 2.3 can be found in Table 2.1. Sections in the normalization example are labeled X, Y, & Z for comparison to histograms and summary statistics.

Following normalization, it was possible to calibrate the EM data to the calculated EM response from PTC data as discussed previously. The inverse distance interpolation method was used to estimate EM EC at the location of each PTC survey for 2001 and 2004. The resulting collocated EM EC data and calculated EM EC data were cross-plotted. A linear regression model with the y-intercept forced through zero was used to calibrate raw EM data in both 2001 and 2004 (Figure 2.4).

2.4.5 Electrical Resistivity Tomography

Electrical resistivity tomography surveys were conducted on the SWSS dyke in the fall of 2001, 2004 and 2008. Surveys were conducted using the Wenner array, one meter electrode spacing with a maximum a-spacing of 24 meters, and a total length varying from 600 to 800 meters. Data was inverted using finite difference resistivity inversion package Res2Dinv (Loke and Barker 1996). Inversion parameters within

Res2Dinv were optimized manually by finding the highest correlation coefficient between inverted ERT data and coincidental PTC data averaged across the inversion mesh. The correlation coefficient, as opposed to the sum square error (SSE) as utilized in Hayley et al. (2009), was deemed to be the strongest indicator of the best inverse model because the relationship between ERT EC and PTC EC did not seem to follow a '1 to 1' relationship, where error metrics would be most suitable. The cause of this may be a result of temporal discrepancies in PTC and ERT surveying and/or PTC calibration. Inversion parameters which had the greatest influence on the inversion results were data and model norms, vertical to horizontal flatness filter, vertical dampening, and mesh discretization. Table 2.2 outlines and provides values for these inversion parameters. Many other inversion parameters were tested yet inversion results were largely insensitive to parameters outside the ones listed.

Once inversion parameters were optimized, all ERT data were inverted under the same parameters and cross-plotted with PTC for calibration in a similar fashion as with EM methods. It should be noted that resistivity inversion techniques are fundamentally ill-posed problems which provide non-unique answers. Subsequently, calibration plots are subject to this non-uniqueness and should be considered as such. Confidence in calibration models follows from correlation strength between inverted ERT data and PTC data. However, due to smoothing of inverted ERT models, inversion procedures are often incapable of resolving sharp boundaries which were typically observed in PTC data at the SWSS. With regard to this, some scatter from the calibration model is expected and overall does not detract from confidence in the calibration. Furthermore, sharp EC contrasts were usually observed from low to high EC with depth, creating a scenario of

underestimating EC of ERT models in low ERT EC ranges. This can readily be observed in calibration plots, especially for 2004. Figure 2.5 displays cross-plots and calibrations between ERT and PTC data.

2.5 Results

EC maps were generated from EM-38 data for 2001 and 2004 overlying the study transects. Figure 2.6 and Figure 2.7 display normalized and calibrated EC contours for 2001 and 2004 respectively. EC values for both images are similar in magnitude despite having vastly different calibration models (Figure 2.4). This lends confidence to the normalization and calibration methods outlined previously. The terraced slope topography of the SWSS dyke creates a general scenario of high water tables in benches and deeper water tables along slopes (Figure 2.2). This is highlighted by distinctive high EC bands running in the northwest / southeast direction which can be observed in both 2001 and 2004 EM surveys. To better depict how topography influences groundwater and, subsequently, EC at the SWSS, EM EC for Transect A collected in 2004 was plotted along a topographic cross-section in Figure 2.8. As expected, it can be seen that high EC is found in the benches while lower EC is found on slopes.

Inverted ERT cross-sections were generated for 2004 and 2008 along Transect C (Figures 2.9 A and B). A difference or time-lapse plot between the two years was also generated (Figure 2.9 C). Furthermore, coincidental water level measurements are superimposed on inverted ERT cross-sections. It can be seen that water level measurements follow closely along low to high EC transitions. However, below the water table very little variation in EC is observed. The ERT difference plot shows most change around the location of the expected water table and in the near subsurface where

soil moisture conditions are variable. These differences are likely due to small changes in the water table between the two years. For the most part however, very little change in EC is observed between 2004 and 2008; a mean absolute difference of 4.3 mS/m was found. The remaining ERT inverted models and difference plots for other transects and years, not shown in this chapter, may be found in Appendix C.

Several locations along Transect C in 2004 had coincidental measurements of PTC, calibrated ERT, volumetric moisture (VM), and water levels. Figure 2.10 displays two locations with each of these measurements plotted. It can be seen that EC from both PTC and ERT follow closely to the general trend of the VM profile and transition to high EC near and below the water table. Smoothing within the ERT inversion routine can be observed as well. The ERT EC begins the transition to high EC near the location of the water table however, doesn't reach a maximum EC until, in some cases, several meters below the water table. This detail is important when using inverted ERT sections to locate the water table. Furthermore, elevated EC and VM are observed in both cases within the upper 1 m of the subsurface which is representative of the clay till and peat reclamation material placed on the dyke following construction. In part the elevated EC is due to elevated soil moisture, however additionally the presence of clay minerals is known to contribute to bulk EC, ultimately which lead to the development of bulk EC petrophysical models outside Archie's Law, as discussed previously in Chapter 1. Some variation in PTC EC below the water table can also be observed in Figure 2.10. Bulk EC below the water table was found to have a mean 68.4 and a standard deviation of 12.8. This variation is likely due to spatially variable porosity, and thus a spatially variable formation factor from Archie's Law. This indicates the tailings material which forms the

dam does contain some heterogeneity, likely due to the construction methods used to build the dyke, in which beached tailings are collected, placed, and compacted using large tractors (D9 Caterpillar).

Porosity was determined by the average of VM measurements from the fully saturated zone, below the water table, and found to be 26.9% with a standard deviation of 1.1%. VM data was transformed to saturation by dividing by porosity. Further analysis of the relationship between EC and soil moisture is shown in Figure 2.11, which contains a cross-plot of PTC EC and saturation. In Figure 2.11, data taken from the reclamation material zone was separated from data taken from underlying tailings sand material. A linear regression of the log transformed bulk EC and saturation was then used to describe the relationship in the tailings sand material following Archie's Law (Equation 2). A linear regression of reclamation material zone data was not performed as the soil contains clays and organics which may contribute to bulk EC, not defined by Archie's Law. Data were separated into reclamation material and tailings sand zones based on analysis of PTC profiles. For example, in Figure 2.10 a distinct shape in PTC profiles can be observed; higher EC (20 to 30 mS/m) near the surface (0 to 1 m), followed by low EC (0 to 10 mS/m) which transitions to high EC (>50 mS/m) near the location of the water table. The initial layer of higher EC (20 to 30 mS/m) reflects the contribution of moisture, clays, and organics found in the reclamation material. Following this assumption, data were divided accordingly into reclamation material and tailings sand zones, and statistically analyzed separately.

Relationships between bulk EC from geophysical measurements and collocated fluid EC measurements from groundwater sampling were also investigated. Figure 2.12

shows two cross-plots; PTC bulk EC versus fluid EC, and ERT bulk EC versus fluid EC. Linear regression with a y-intercept of zero was used to form a linear relationship between PTC and fluid EC. The slope of this regression, 0.18, is an estimate of the formation factor in Archie's Law (equation 1). However, the R^2 value is only 0.26. Interestingly, empirical estimates of the formation factor for sands of similar porosity have been reported with values around 0.18, assuming a cementation exponent, *m*, of 1.3 and tortuosity, *a*, of 1 (Archie, 1942). Due to the smoothing in the ERT model, an empirical relationship between ERT derived EC and fluid EC would not be expected to go through zero. The regression yielded a slope of 0.86 with an intercept of 36.7 mS/m and an R^2=0.34. Both methods showed weak correlation between bulk EC as measured by geophysics and groundwater EC, and indicate estimates of groundwater salinity from the geophysical methods will have large uncertainty in the SWSS dyke setting.

2.6 Discussion

The electromagnetic survey results are consistent with the hydrogeologic conceptual model presented in Figure 2.2. EC maps in Figures 2.6 and 2.7 display linear EC bands running in the northwest to southeast direction. Bulk EC is mainly a function of soil moisture; in areas of high water tables, (i.e., at the toes of slopes near the intersection with benches of the SWSS dyke) higher EC is observed (Figure 2.8). The main drawback of EM surveying conducted with only one dipole geometry and height is that it does not provide information about variations of EC with depth. However EM is a useful reconnaissance tool for finding near surface soil moisture. This can be useful for geotechnical application, especially if a large area needs to be surveyed rapidly.

Electrical resistivity tomography surveys are capable of providing EC estimates at depth. In general, depth of investigation depends on acquisition arrays and spacing. EC estimates with depth are particularly useful for building petrophysical relationships with coincidental geophysical or hydrogeological data. ERT results seen in Figure 2.9 show a few interesting features. In the near subsurface, ERT EC is similar to that of EM surveys, i.e. high EC in the benches and low EC along slopes. Also in the near subsurface, a layer with slightly higher EC (10 to 20 mS/m) relative to underlying unsaturated tailings sand is observed that correlates with the reclamation material layer. This can most easily be seen in ERT and PTC vertical profiles presented Figure 2.10. The reclamation material layer appears to be thicker near the toe of the dyke and is very thin or non-existent near the crest. This is consistent with field observations and denser vegetation found near the toe. A rapid transition from low to high EC and VM, which represents the top of the capillary fringe and generally rises about 50 cm above the water table, can also be observed in PTC and VM data. This capillary rise is consistent with the finer grained and compacted sand which forms the SWSS dyke (Heath 1983).

ERT data also display this transition, although smoothed by the inversion routine. The top of the capillary fringe coincides with the near-beginning of the smoothed ERT transition from low to high EC (Figure 2.10). The water table can subsequently be found about 50 cm below the beginning of this transition around a bulk EC of 5 to 25 mS/m at this site. ERT surveys from other studies also show that sharp conductivity boundaries are located near the beginning of the EC transition zone (e.g. Meads et al., 2003; Hirsch et al., 2008). There is some variation in the location of the water table within this transition that is related to depth. Deeper water tables coincide with smoother transitions

in ERT EC and more variation of the location of the water table within the EC transition. This is a result of reduced resolution with depth that is inherently associated with surface based ERT methods. Inversion damping parameters which are generally increased with depth, as well as increased model cell size with depth help to deal with this reduced resolution and stabilize the inversion procedure. Regardless, ERT images provided a reasonable estimate for the water table over a much larger spatial extent than traditional point measurements. Additional direct measurements are recommended to ensure the estimated water level from inverted ERT models, which again may exhibit smoothed features, accurately represents the water table. The continuous estimate of the water table location has a strong potential for improving the calibration of groundwater flow models at the SWSS and other similar sites.

The bulk EC in the SWSS dyke is most strongly correlated with soil moisture. Images from EM and ERT surveys show an EC structure that is consistent the hydrogeologic conceptual model of SWSS soil moisture (Figure 2.2). To further explore this relationship, PTC bulk EC data were cross-plotted with saturation from VM data in Figure 2.11. The tailings sand which forms the SWSS dyke is hypothesized to follow Archie's Law petrophysical model because it is assumed to be a clean (i.e., clay free) sand. The reclamation material zone displays a non-Archie Law relationship due to higher clay and organic content. For this reason, soil zone measurements were excluded from the linear regression shown in Figure 2.11. The regression relationship in Figure 11 yields an R^2 of 0.90 indicating that Archie's Law is a reasonable representation of the data. The linear regression slope in Figure 2.11 yields an empirical estimate of the saturation exponent of n = 3.8 for the SWSS tailings dyke material. The saturation

exponent models the dependency of non-conductive fluids within the pore space and is primarily a function of wettability. Many studies have investigated the range of the saturation exponent and its relationship with wettability to improve resistivity well log interpretations (Donaldson and Siddiqui 1989). Morgan and Pirson (1964) found a range of n from 2.5 to 25.2 for strongly water-wet to oil-wet packs of glass beads. Sweeney and Jennings (1960) found a range of n of 1.6 to 5.7 for carbonate rocks. Donaldson and Siddiqui (1989) examined several sandstone outcrops and found a range of n from <2 to 8. The value found in this study is slightly higher than commonly used value of $n = 2.0$ for unconsolidated, clean sands; however it is not outside reasonable ranges found from other field and laboratory based studies, especially when considering the potential of hydrocarbons in the form of residual bitumen in the SWSS tailings sand material

A previous groundwater flow and transport study was conducted at the SWSS site by Price (2005) utilizing the same hydrogeological data used for this study. Price characterized hydraulic head and salt distributions within the dyke with the use of field observations and groundwater numerical modeling. In part, the motivation for this study was to investigate the potential use of geophysical methods to constrain soil moisture and fluid salinity distributions in order to calibrate and validate groundwater flow and transport modeling. The soil moisture distribution and the water table location was estimated reasonably well by the ERT inversion results and will be useful in calibrating hydraulic heads during groundwater modeling efforts. However, fluid salinity was poorly estimated with the methods outlined in this paper as illustrated by large scatter in Figure 12 cross-plots. Consequently, the geophysical results will not contribute to constraining

the measured distribution of the salinity. Several factors likely contribute to this latter point.

First, in ERT inversion procedures, the overparameterization of the inverse models requires a smoothing constraint to facilitate convergence of the inverse solution. This smoothing adds uncertainty, especially in areas with large EC transitions. Again, this can be seen in calibration cross-plots shown in Figure 2.5, as well as in direct comparisons between ERT and PTC profiles in Figure 10. ERT resolution also varies spatially, inherently decreasing with increased distance from electrodes, i.e. with increased depth in surface based surveys. Additionally, sample support size must be considered when making direct comparisons between fluid EC measurements and calculated EC from ERT models. Groundwater samples were collected using a low flow method at a maximum rate of 125 mL/min for 3 to 4 minutes yielding a maximum volume of water sampled at about 500 mL, which, assuming a porosity of 26.9%, equates to a cube approximately 12.5 cm on each side. ERT methods cannot resolve features at this scale, and this size is smaller than the smallest model block used in the ERT inverse modeling. These reasons have previously been shown to pose difficulty when attempting to quantify fluid EC from ERT models through Archie Law petrophysical relationships (Singha and Gorelick 2006). Another potential source of uncertainty is the assumption that the tailings pond dyke consists of homogenous clean sand, which is not physically realistic. Although this is a reasonable assumption, in reality the tailings dyke, which was constructed and compacted with large tractors from beached tailings material, contains variable porosities contributing to Archie's formation factor and subsequently measured bulk EC.

This paper explores the geotechnical application for geophysical methods at tailings ponds. Although geotechnical and dam safety concerns were not a major motivator for this study, the high correlation of geophysical bulk EC data and soil moisture allows for dyke soil moisture to be investigated over large areas in a non-invasive manner. Unfortunately due to low confidence in bulk and fluid EC relationships, fluid salinity could not be reasonably quantified from geophysical methods and limits the environmental applications towards reclamation monitoring. The 2004 survey year, which provided the bulk of interpretations made in this report, was specifically designed as an integrated geophysical and hydrogeological study, however data from previous and following surveys were collected semi-independently and posed some difficulty due to temporal discrepancies in acquisition. Designing geophysical and hydrogeological surveys which specifically target the relationship between bulk and fluid EC by increasing the number of coincidental measurements, collecting data at similar times, and being mindful of support size, would likely improve confidence and allow for greater quantitative capability. Furthermore, although several temperature profiles were recorded, they were not sufficient to develop a complete subsurface temperature model due to the complexity of the temperature distribution within the SWSS dyke observed from these data. Incorporating a more detailed investigation of subsurface temperature, as well as a flow and heat transport model, is recommended to adequately characterize temperature at this site and other tailings sites, so temperature corrections on measured EC may be conducted (Hayley et al. 2007). This will improve the overall quantitative capability of future geophysical studies at the SWSS site and other tailings dykes.

2.7 Conclusions

A geophysical characterization of an undrained tailings pond dyke was performed at Syncrude's Southwest Sand Storage (SWSS) Facility. Geophysical methods which measure subsurface bulk EC can be greatly augmented with use of direct measurement techniques such as push tool EC and groundwater sampling. The normalization and calibration of geophysical data improves interpretive capabilities and allows for petrophysical relationships to be constructed across varying geophysical methods. It was found that geophysical measures of bulk EC are highly correlated with soil moisture at the SWSS. Electrical resistivity tomography (ERT) methods were capable of clearly identifying the location of the water table due to high dependence of EC on soil moisture. Some variation in bulk EC was observed below the water table that can be attributed to variable porosity and compaction of the tailings material in the dyke. Together this provides both geotechnical and hydrological applications for geophysical methods and furthermore, allows for inexpensive data acquisition over a larger spatial extent than traditional methods. Analysis of coincident bulk EC and fluid EC measurements displayed similar results to previous literature, however the relationship was not strong enough to support interpretations of fluid salinity from geophysical methods. Limited chemistry data, smoothing and resolution issues in ERT inversion procedures, a strong dependence of bulk EC on soil moisture, and heterogeneity in the tailings material are thought to be the primary causes of poor bulk and fluid EC comparison. Insights gained from this research may be applied to future studies and monitoring efforts at the SWSS site as well as at other tailings dykes.

2.8 References

Alberta's Energy Industry. An Overview. 2012. Alberta Energy Resources Conservation Board. http://www.energy.alberta.ca/org/pdfs/Alberta_Energy_Overview.pdf

Archie, G. 1942. The electrical resistivity log as an aid in determining some reservoir characteristics. T. Am. I. Min. Met. Eng., Vol. 146. 54 – 62.

Bell, J. 1987. Neutron probe practice. 3rd edition. Inst. of Hydrol., Rep. 19. 1 – 63.

Berkowitz, N. and Speight, J. 1975. The oil sands of Alberta. Fuel. Vol. 54. 138 – 149.

Booterbaugh, A. 2014. Geophysical characterization of an undrained oil sands tailings pond Alberta, Canada. (Master's Thesis).

Chalaturnyk, R., Scott, D., Özüm, B. 2002. Management of oil sand tailings. Petroleum Science and Technology. Vol. 20. Nos. 9 & 10. 1025 – 1046.

Clark, K. 1929. The separation of the bitumen from Alberta bituminous sands. Can. Inst. Min. Metall. Bull. Vol. 22. 1385 – 1395.

Donaldson, E. and Siddiqui, T. 1989. Relationship between the Archie saturation exponent and wettability. SPE Form. Eval. 359 – 362.

Dusseault, M. and Scott, J. 1983. Tailings pond behavior and characterization of oil sand tailings sludge. Particulate Science and Technology. Vol. 1. 295 – 309.

Hayley, K., Bentley, L, Gharibi, M., Nightingale, M. 2007. Low temperature dependence of electrical resistivity: Implications for near surface geophysical monitoring. Geophys. Res. Lett. Vol. 34. 1 – 5.

Hayley, K., Bentley, L., Gharibi, M. 2009. Time-lapse electrical resistivity monitoring of salt-affected soil and groundwater. Water. Resour. Res. Vol. 45. 1 – 14.

Heath, R.C., 1983, Basic Ground-water Hydrology: U.S. Geological Survey, 16.

Hirsch, M., Bentley, L.R., Dietrich, P. 2008. A comparison of electrical resistivity, ground penetrating radar and seismic refraction results at a river terrace site. J. Env.and Eng. Geophys., Vol. 13. 325-333.

Hoare, B. 1972. The disposal of mine tailings material. (Doctoral dissertation). University of Waterloo. 1-210.

Kasperski, K. and Mikula, R. 2011. Waste Streams of Mined Oil Sands: Characteristics and remediation. Elements. Vol. 7. 387 – 392.

Komex International Ltd. 2005. 2004 Geophysical Investigation of Southwest Sand Storage Facility. Syncrude Canada Ltd., Fort McMurray, Alberta.

Loke, M. 2006. 1-D frequency domain EM modeling. 115, Cangakay Minden Jalan 5, 11700 Penang, Malaysia. PugSoft Inc.

Loke, M., and Barker, R. 1996. Rapid least-squares inversion of apparent resistivity pseudosections by a quasi-Newton method. Geophys. Prospect. Vol. 44. 131-152.

Martínez-Pagán, P., Faz Cano, A., Aracil, E., Arocena, J. 2009. Electrical resistivity imaging revealed the spatial properties of mine tailing ponds in Sierra Minera of southeast Spain. J. Environ. Eng. Geoph. Vol. 14, 2. 63 – 76.

Masliyah, J., Zhou, Z., Xu, Z., Czarnecki, J., Hamza, H. 2004. Understanding water-based bitumen extraction from Athabasca Oil Sands. Can. J. Chem. Eng. Vol. 82. 628 – 654.

Meads, L.N., Bentley, L.R., Mendoza, C.A. 2003. Application of electrical resistivity imaging to the development of a geologic model for a proposed Edmonton landfill site. Can. Geotech. J. Vol. 40. 551-558.

Morgan, W. and Pirson, S. 1964. The effect of fractional wettability on the Archie saturation exponent. SPWLA 5th Annual Logging Symposium. 1 – 13.

Naeth, M., Chanasyk, D., Burgers, T. 2011. Vegetation and soil water interactions on a tailings sand storage facility in the Athabasca oil sands region of Alberta Canada. Phys. Chem. Earth. Vol. 36. 19-30.

Price, A. 2005. Evaluation of groundwater flow and salt transport within an undrained tailings sand dam (Master's Thesis). University of Alberta, Department of Earth and Atmospheric Sciences.

Roy, A., Apparao, A. 1971. Depth of investigation in direct current methods. Geophysics. Vol. 36, No. 5. 943 -959.

Singha, K., Gorelick, S. 2006. Effects of spatially variable resolution on field-scale estimates of tracer concentration from electrical inversions using Archies's law. Geophysics. Vol. 71, No. 3. G83 – G91.

Sjödahl, P., Dahlin, T., Johansson, S. 2005. Using resistivity measurements for dam safety evaluation at Ememossen tailings dam in southern Sweden. Environ. Geol. Vol. 49. 267 – 273.

Sweeney, S. and Jennings, H. 1960. Effect of wettability on the electrical resistivity of carbonate rock from a petroleum reservoir. J. Phys. Chem. Vol. 64. No. 5. 551 – 553.

Syncrude Canada Ltd.. 2008. Public Disclosure Document: South west sand storage Conversion.

Tóth, J. 1963. A theoretical analysis of groundwater flow in small drainage basins. J. Geophys. Res. Vol. 68, No. 16. 4795 – 4812.

Yuval, D. and Oldenburg, W. 1996. DC resistivity and IP methods in acid mind drainage problems: results from the Copper Cliff mine tailings impoundments. J. Appl. Geophys. Vol. 34. 187 – 198.

Table 2.1. Summary statistics for normalization example displayed in Figure 2.3. EM regions are labeled in the same fashion (regions X, Y, & Z) as seen in Figure 2.3.

	Elevated Region		
	Pre-normalization (X)	Post-normalization (Y)	Reference Region (Z)
Max	452	444.99	440
Min	137	67.74	59
Mean	224.13	162.98	162.99
Median	213	133.27	133
Variance	2608.09	4721.76	4736.25

Table 2.2. Manually optimized inversion parameters selected for ERT modeling.

Parameter	Value
Data norm	L1
Model norm	L1
Vertical to horizontal flatness filter ratio	0.25
Initial damping factor	0.1
Minimum damping factor	0.04
Increase damping factor with depth	1.1
Model block width	0.5 m
Model first layer height	0.125 m
Rate of layer height increase with depth	1.05

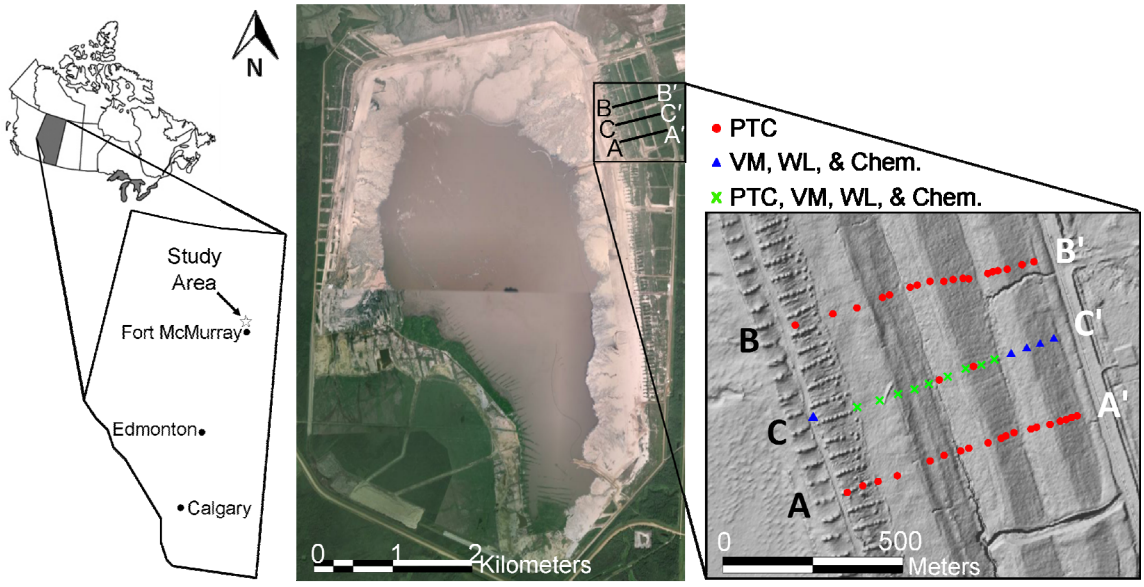

Figure 2.1. Syncrude's Southwest Sand Storage Facility (SWSS); located approximately 35 km northwest of Fort McMurray, Alberta, Canada. Study site was located in the northeast portion of the tailings dam and study transects are shown by solid black lines. Push tool conductivity (PTC), volumetric moisture (VM), water level (WL) and chemistry sampling locations are displayed on the shaded relief map (right). *Source:* "Syncrude Southwest Sand Storage Facility." 56º58′24.89″ N and 111º45′35.73″ W. **Google Earth.** July 21, 2010 and August 31, 2009.

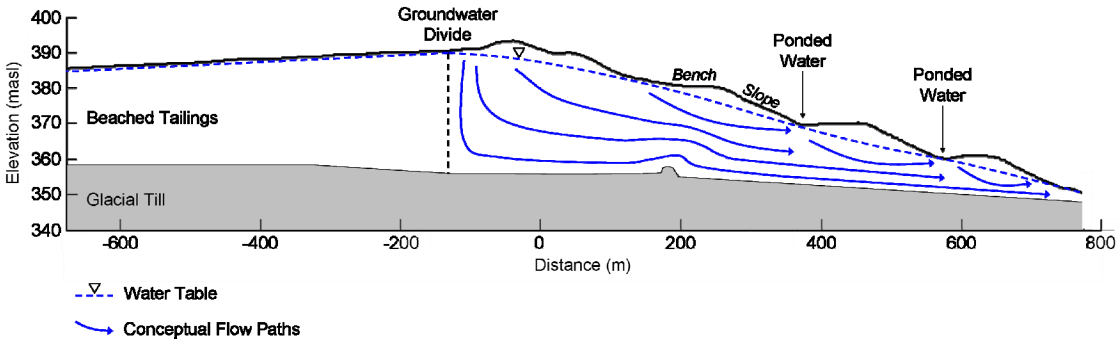

Figure 2.2. Cross-section of SWSS tailings dam and conceptual groundwater flow scenario. High water tables create reclamation and geotechnical concerns. Adapted from Price, 2005.

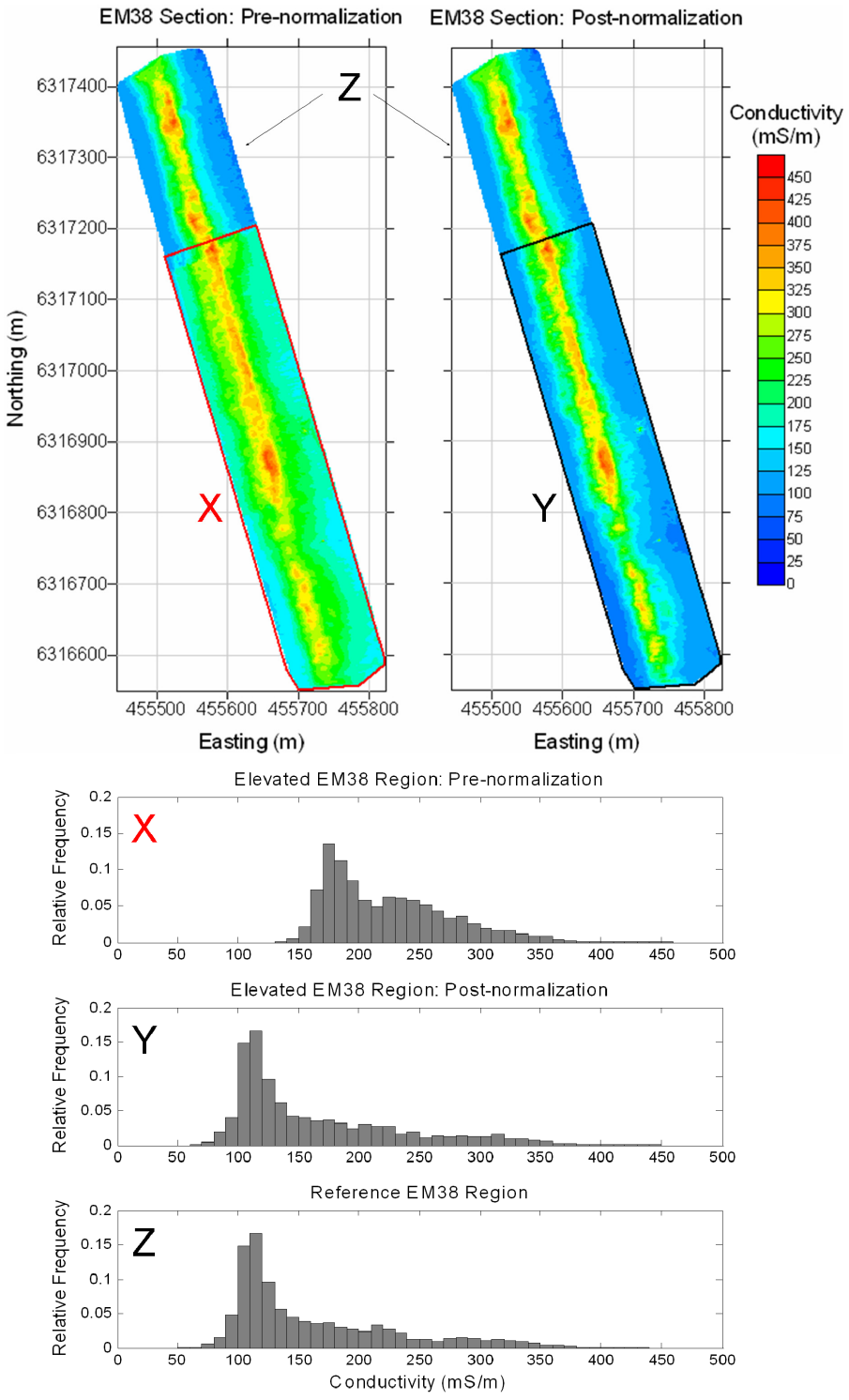

Figure 2.3. Contour and histograms of 2001 EM-38 data for one normalization procedure. The elevated EM region, outlined in red and labeled 'X' was shifted to the EM region outlined in black and labeled 'Y'. The reference region is labeled 'Z'. Note that EC values are un-calibrated in this example. UTM Zone: 12.

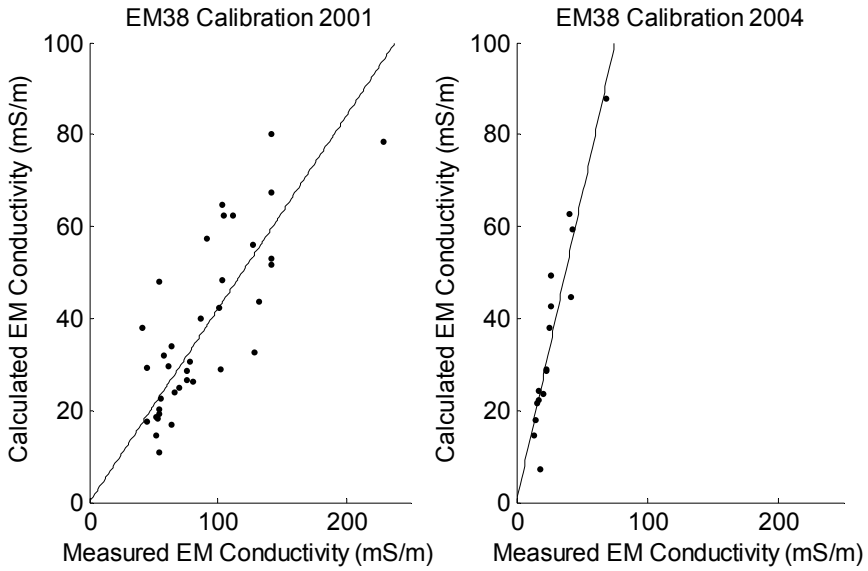

Figure 2.4. Calibration crossplots for EM-38 data from 2001 (left) and 2004 (right). Linear regression with y-intercept equal to zero was used to calibrate EM-38 EC measurements. Regression slopes varied significantly between 2001 and 2004; 0.420 and 1.33, respectively. R^2 values are 0.61 and 0.88 for 2001 and 2004, respectively. Note, regressions are site specific.

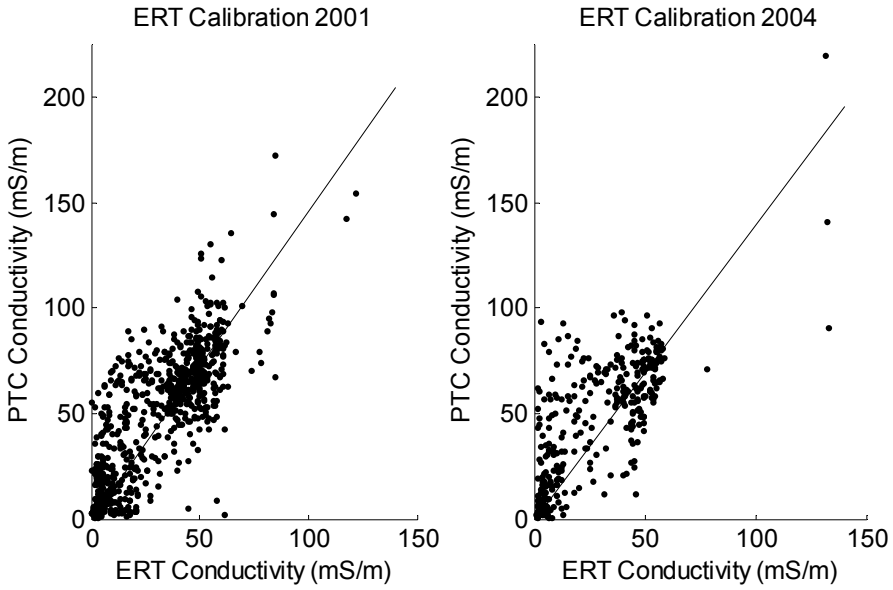

Figure 2.5. Calibration cross-plots for ERT data from 2001 (left) and 2004 (right). Linear regression with y-intercept equal to zero was used for the calibration model. Slopes for linear regression of 2001 and 2004 data are 1.46 and 1.40, respectively. R^2 values are 0.64 and 0.52 for 2001 and 2004, respectively. Note, regressions are site specific

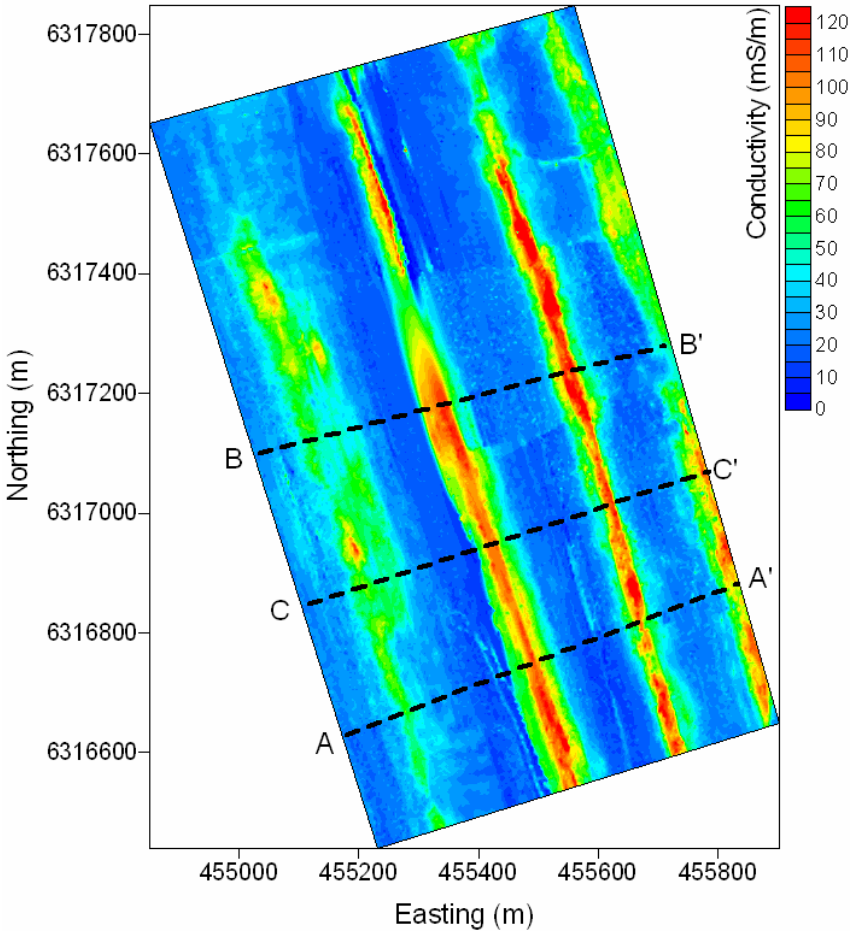

Figure 2.6. EM-38 normalized and calibrated EC image collected in the fall of 2001. EM-38 was collected over a large area of the SWSS tailings dam. Study transects are shown by black dashed lines. UTM Zone: 12.

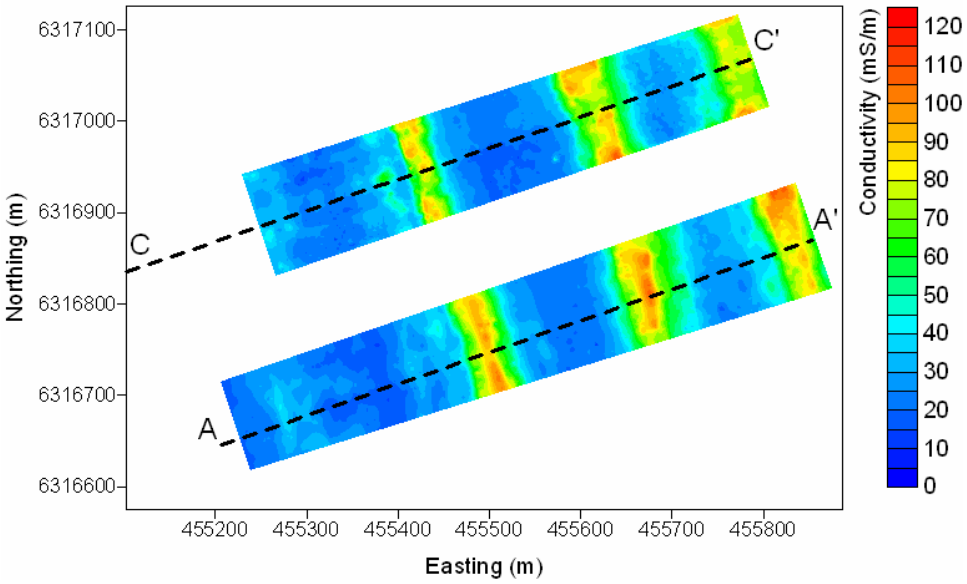

Figure 2.7. EM-38 normalized and calibrated EC image collected in the fall of 2004. EM-38 was only implemented in a small vicinity of study transects A and C, shown by black dashed lines. UTM Zone: 12.

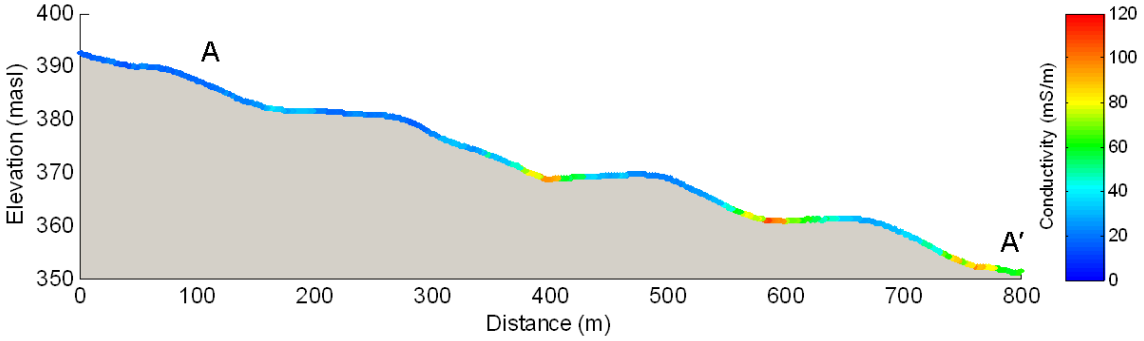

Figure 2.8. EM-38 normalized and calibrated EC data from fall of 2004 plotted along a cross-section of transect A to A′.

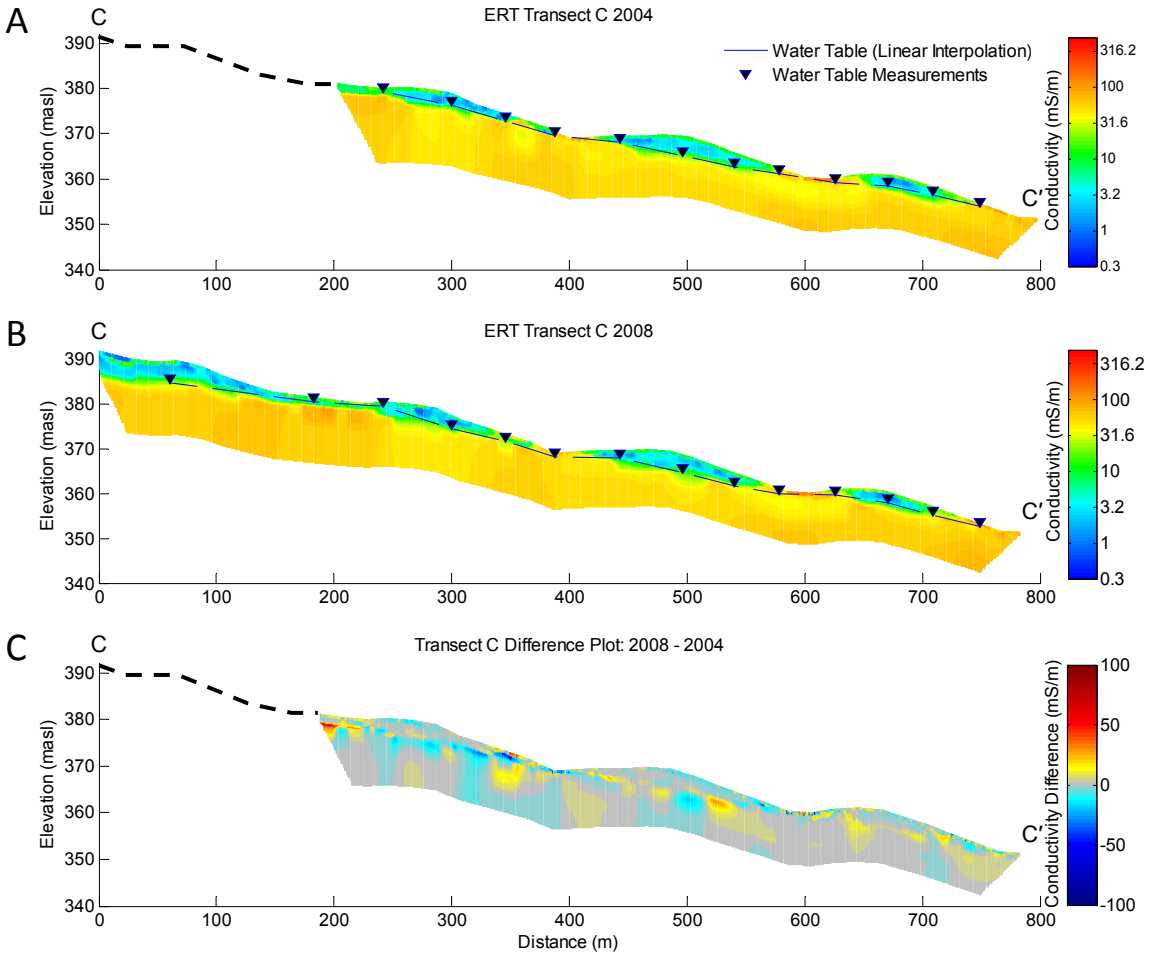

Figure 2.9. Electrical resistivity tomography for transect C from fall 2004 (A) and fall of 2008 (B). Coincidental water level measurements are superimposed. A difference plot is also shown (C) for 2008 minus 2004; mean absolute difference of 4.3 mS/m was found.

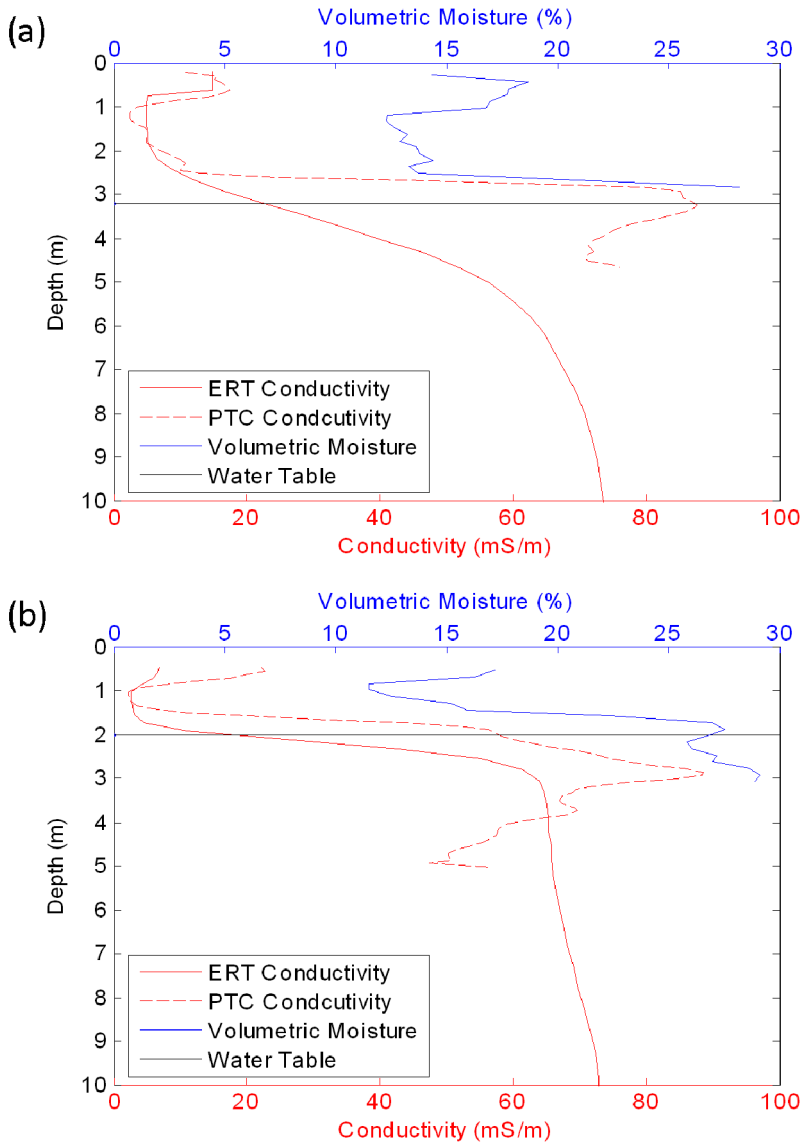

Figure 2.10. Composite plots of ERT profiles, PTC profiles, VM profiles, and water level measurements for two separate locations along Transect C during the fall of 2004.

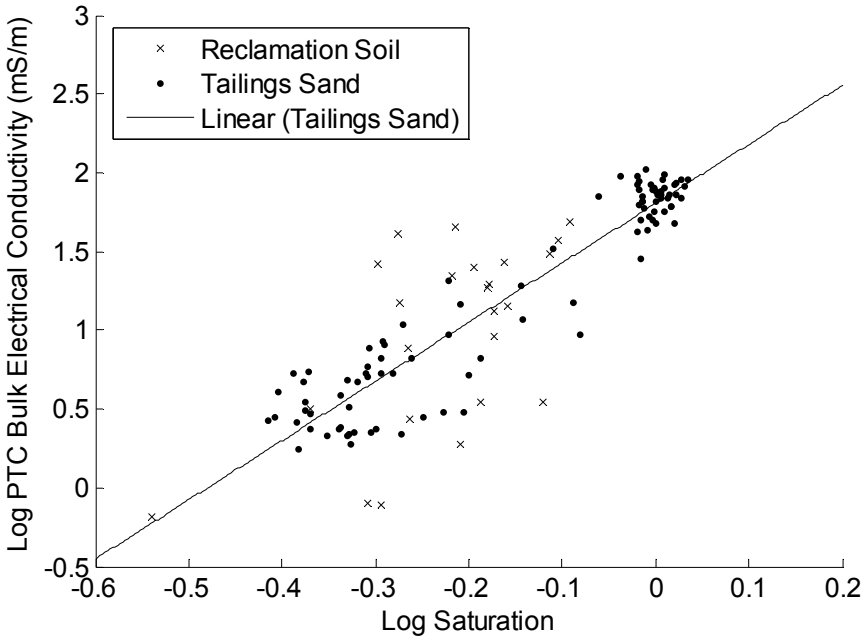

Figure 2.11. Saturation versus EC measurements from PTC. Linear regression of log transformed values was used to describe the relationship for the tailings sand zone only (black line). Regression was found to be [$log(\sigma_b) = 3.76 \cdot log(S_w) + 1.8$] with an R^2 value is 0.90. Note, regression is site specific.

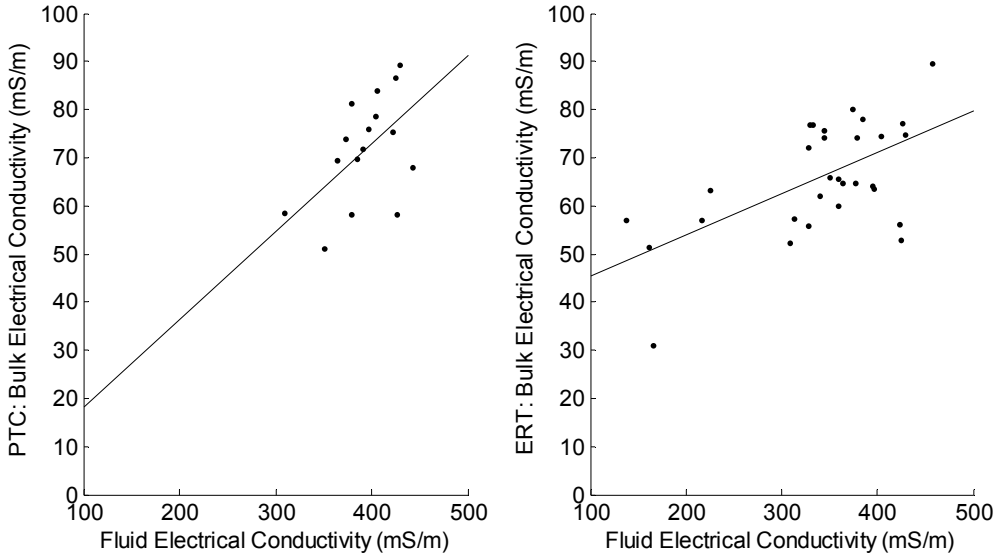

Figure 2.12. Fluid EC from groundwater sampling versus bulk EC measurements from PTC (left) and bulk EC estimates from ERT (right). Linear regression with y-intercept of zero for PTC vs. fluid EC yielded a slope of 0.18 and an R^2 of 0.26. Standard linear regression is shown for ERT vs. fluid EC (right); the regression equation is [$\sigma_b = 0.086 \cdot \sigma_f + 36.7$] with an R^2 value of 0.34. Note, regressions are site specific.

Chapter 3: Summary and Conclusions

3.1 Summary

The production of surface mined bitumen from oil sand deposits results in large tailings ponds which must be properly monitored to ensure safety, mitigate environmental damage, and improve reclamation efforts. In this study, past hydrogeological and geophysical data collected on a large tailings dyke in northern Alberta, the SWSS facility, were integrated to characterize soil moisture and salt distribution, and to observe any temporal variation. The methods and data utilized for this study included push tool conductivity (PTC), EM-38 electromagnetic (EM) profiles, electrical resistivity tomography (ERT), volumetric moisture (VM), water level, and fluid electrical conductivity (EC).

Throughout the study, PTC is assumed to be the most accurate representation of subsurface bulk EC. Under this assumption, EM-38 data was calibrated to a forwarded modeled EM response from PTC data, and ERT inversion parameters were selected to maximize correlation with PTC profiles. Large portions of EM-38 data displayed elevated background EC due to relatively high moisture content from precipitation events. In order to build a consistent EC map from EM-38 data, these portions of elevated EC were normalized based on a method developed for this study (Appendix G). This was done prior to calibration. The normalization and calibration of EM-38 data, as well as the optimization of ERT inversion parameters based on PTC data allowed for a consistent geophysical characterization of the SWSS dyke from which petrophysical relationships could be built.

The Archie's Law petrophysical model was used in this study and relates bulk EC, fluid EC, and soil-moisture in a clay-free porous medium. Through the relationship with bulk EC and VM, as well as bulk EC and fluid EC, it was possible to provide estimates for Archie's saturation exponent (n = 3.8) and formation factor respectively (F = 0.18). To complete this model, a porosity of 26.9% was estimated as the average VM from the fully saturated zone, and a cementation factor (m = 1.3) was assumed based on literature. Bulk EC and VM relationships displayed a strong correlation (R^2 = 0.90). Conversely, bulk and fluid EC relationships displayed relatively weak correlations with a R^2 of 0.26 for PTC versus fluid EC, and a R^2 of 0.34 for ERT versus fluid EC; although in general agreed with previous literature for formation factor estimates. Limited chemistry data, sample support discrepancies, ERT resolution issues, a strong dependence of bulk EC on soil-moisture, and heterogeneity in the tailings material which forms the dyke are thought to be the cause of weak correlation between bulk and fluid EC.

3.2 Conclusions

The results of this research show a strong correlation between bulk EC and soil-moisture at the SWSS dyke. Geophysical methods utilized in this study, which provide measurements of bulk EC, can therefore provide soil-moisture estimates in a non-intrusive manner over a much larger spatial extent than traditional invasive measurement techniques. This relationship has geotechnical and environmental relevance, especially at tailings sites similar to the SWSS facility where high water tables present both safety and reclamation concerns. The normalization and calibration of the EM-38 data, as well as the optimization of ERT inversion parameters using the correlation to PTC profiles is a valuable step to ensure each technique displays similar magnitudes and distributions of

bulk EC. This allows for consistent petrophysical relationships to be constructed across varying geophysical methods.

ERT methods clearly identified the location of the water table within the SWSS dyke, due to a high dependence of measured bulk EC on soil moisture. This is significant as it allows for a spatially exhaustive water level measurement in a much more rapid and non-invasive manner than the installation of water level monitoring wells. The installation of several water level wells may be useful for defining a precise water level location within the smoothed tomogram produced through ERT inversion. Regardless, ERT should be considered a very useful tool in this setting for not only geotechnical application, but also for use in calibrating groundwater flow models.

Geophysical methods, namely PTC and ERT, were incapable of resolving salinity changes or providing any reasonable quantitative estimates of fluid EC at the SWSS facility. The ability to resolve salinity was limited by insufficient coincidental bulk and fluid EC data, especially in PTC based relationships, as well as ERT smoothing, resolution, heterogeneity in the tailings material, and sample support issues. Furthermore, the strong dependence of bulk EC on soil moisture may have masked salinity variations within the SWSS dyke. That being said, bulk versus fluid EC relationships which were formed, albeit with weak correlation, displayed estimates for the Archie Law formation factor which were similar to literature values. To improve upon the correlation between bulk and fluid EC, future studies should be designed to greatly increase the number of coincidental measurements of these two parameters. Furthermore, detailed temperature profiling is vital for quantitative interpretations to be made from electrical geophysical techniques. A flow and heat transport model as well as a dense temperature measurement

program are recommended to adequately characterize the complex nature of the temperature distribution at this site.

3.3 Future Work

In 2009, the design of the SWSS dyke was altered to a centerline dyke construction method which includes internal drainage. These changes most likely had large impacts on the groundwater flow regime and salt transport within the structure. With this said, the research conducted in this study, and previously, present both the applicability and limitations of various integrated methods in characterizing soil moisture and salinity within oil sand tailings dams. The insights gained from this process may be applied to improve not only future monitoring at the SWSS facility, but also other tailings dams of similar nature. The high dependence of measured bulk EC on soil moisture in the SWSS presents the opportunity to use geophysical methods to calibrate and validate future groundwater flow models at the SWSS and other tailings dams. Future work which uses geophysical data for this purpose is highly recommended. Furthermore, future research should be conducted to better understand and define bulk versus fluid EC relationships in tailings pond dykes. Such information could be used to improve upon future transport modeling and overall enhance the management and reclamation of tailings ponds.

Appendix A: Push Tool Conductivity Figures & Data

Data for PTC data may be found in the attached material, in folder 'Appendix A'. Data files are separated by year, and the transect location is included in the file name; e.g. 'PTCA2001.txt' represents PTC data from Transect A in 2001.

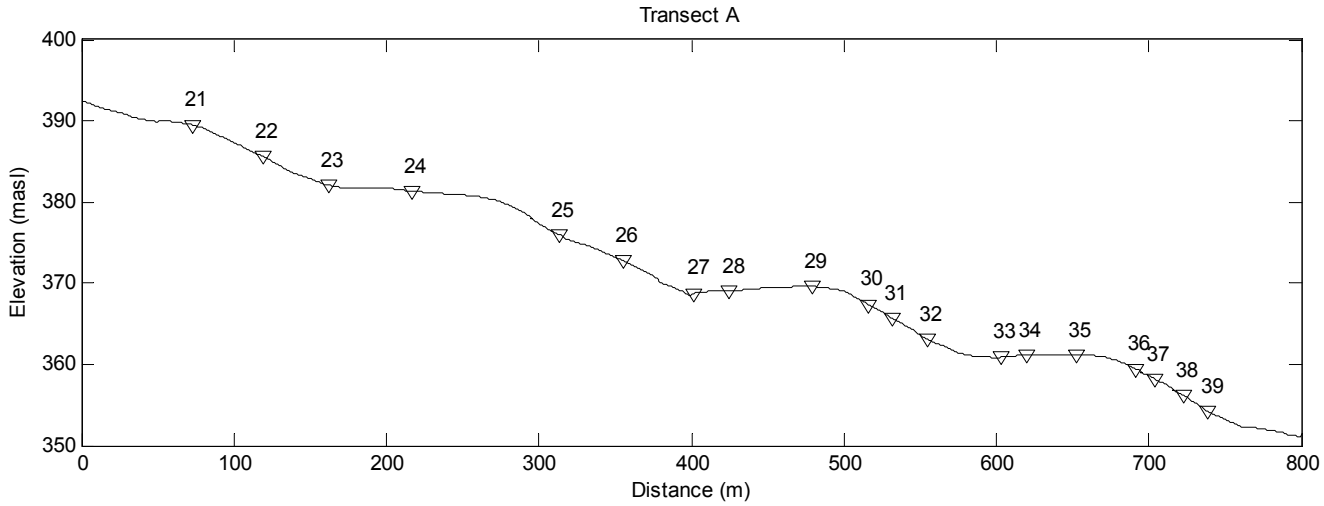

Figure A1. PTC locations and identification along Transect A.

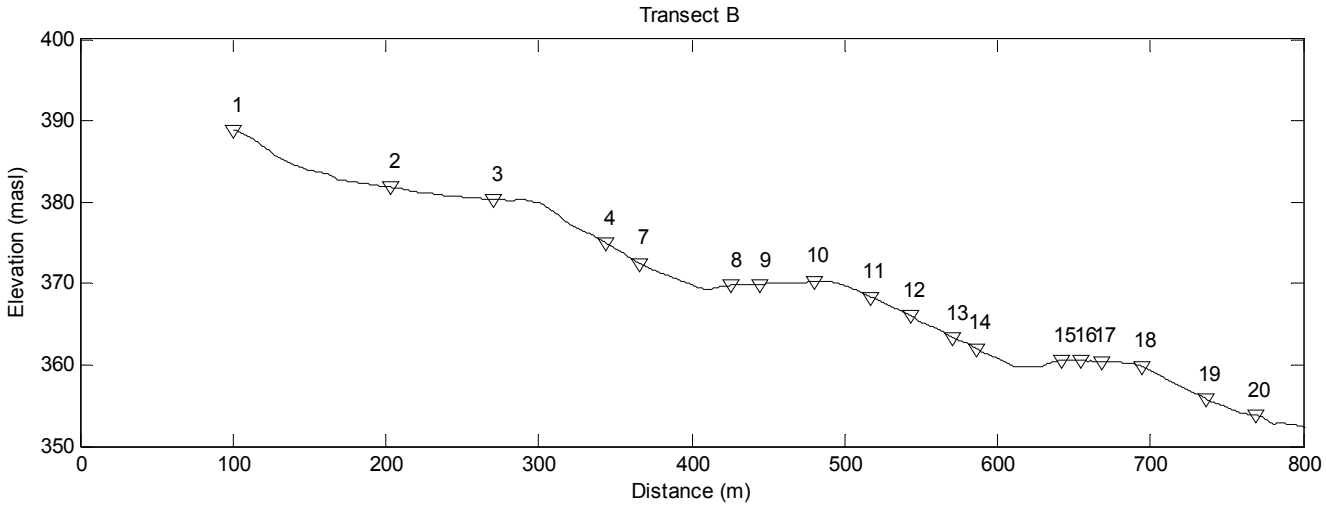

Figure A2. PTC locations and identification along Transect B.

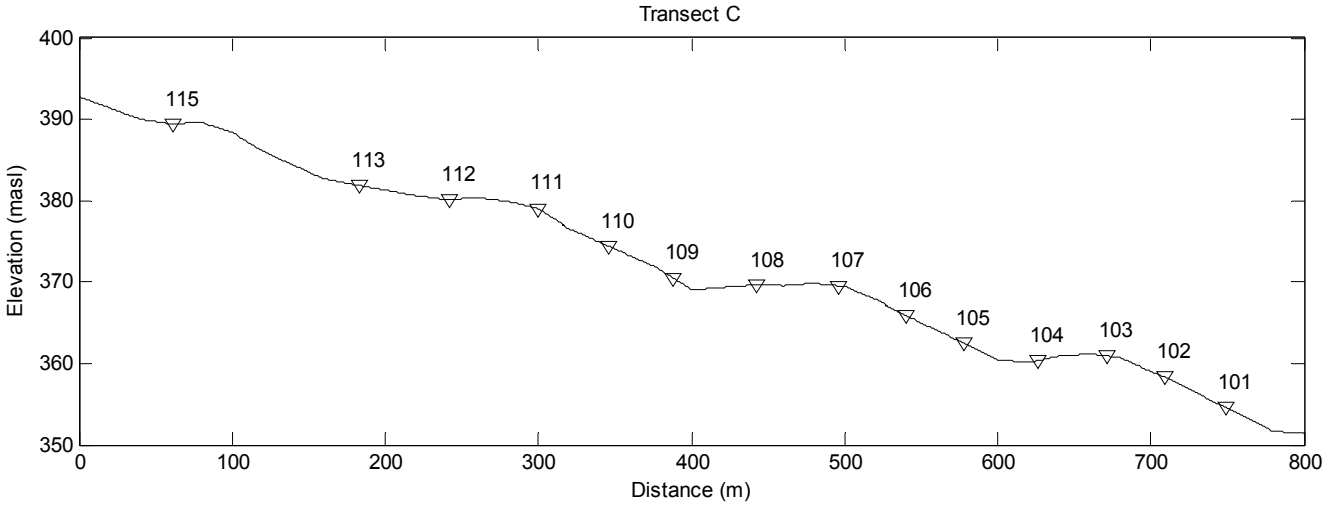

Figure A3. PTC and groundwater well locations, and identification along Transect C.

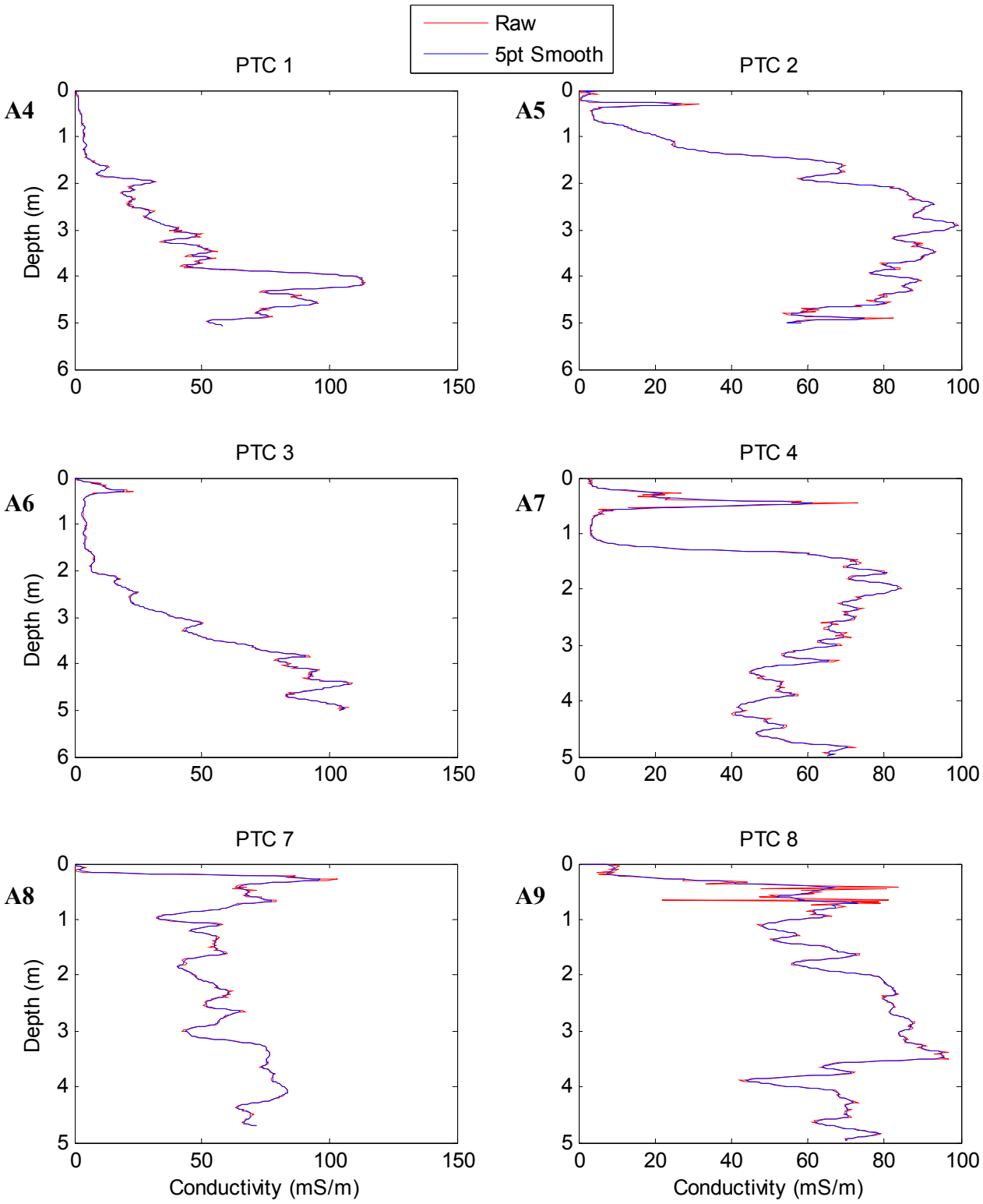
Raw
5pt Smooth
PTC 1
PTC 2
PTC 3
PTC 4
PTC 7
PTC 8
A4
A5
A6
A7
A8
A9
Depth (m)
Conductivity (mS/m)

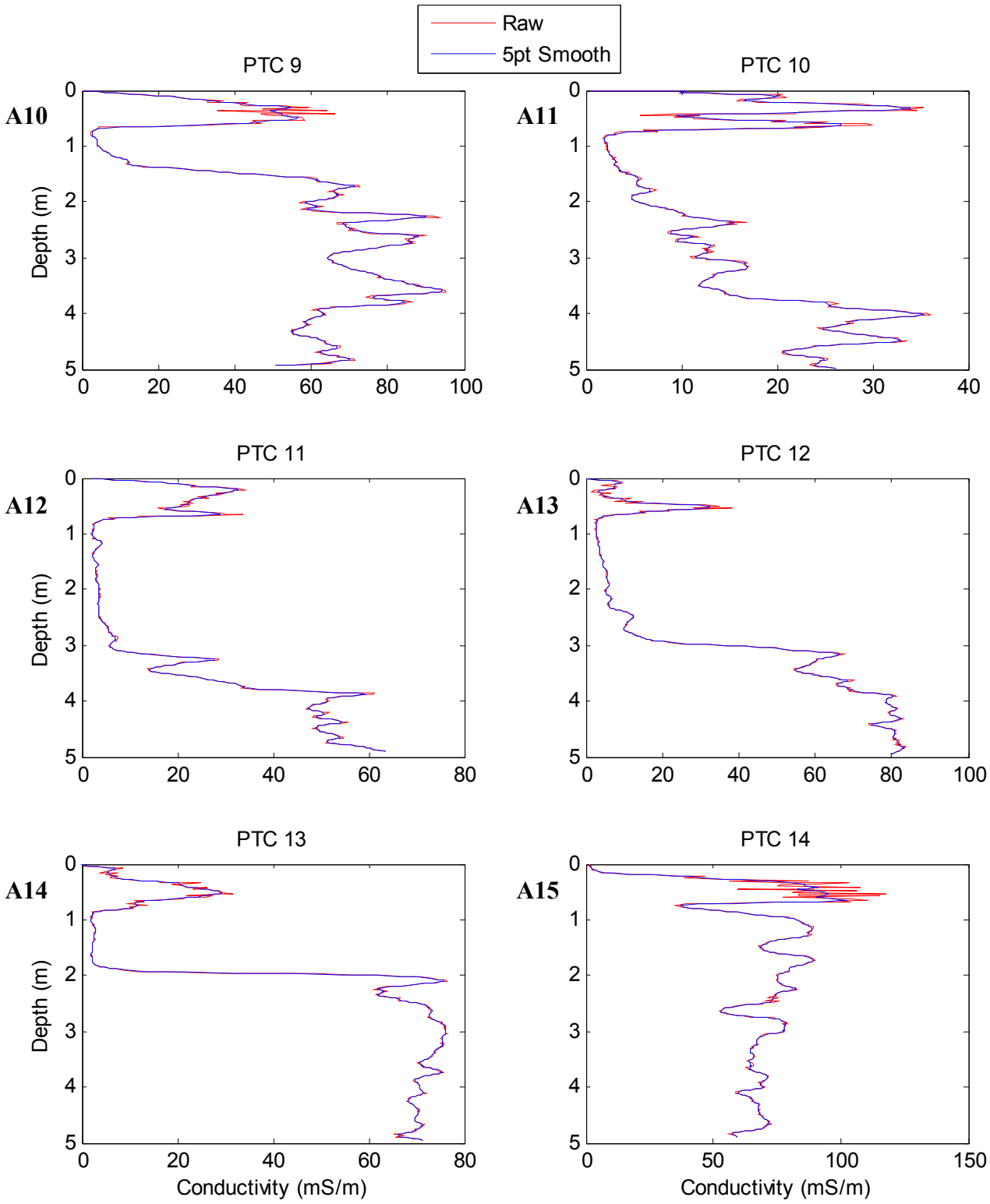
Raw
5pt Smooth
PTC 9
PTC 10
PTC 11
PTC 12
PTC 13
PTC 14
A10
A11
A12
A13
A14
A15
Depth (m)
Conductivity (mS/m)

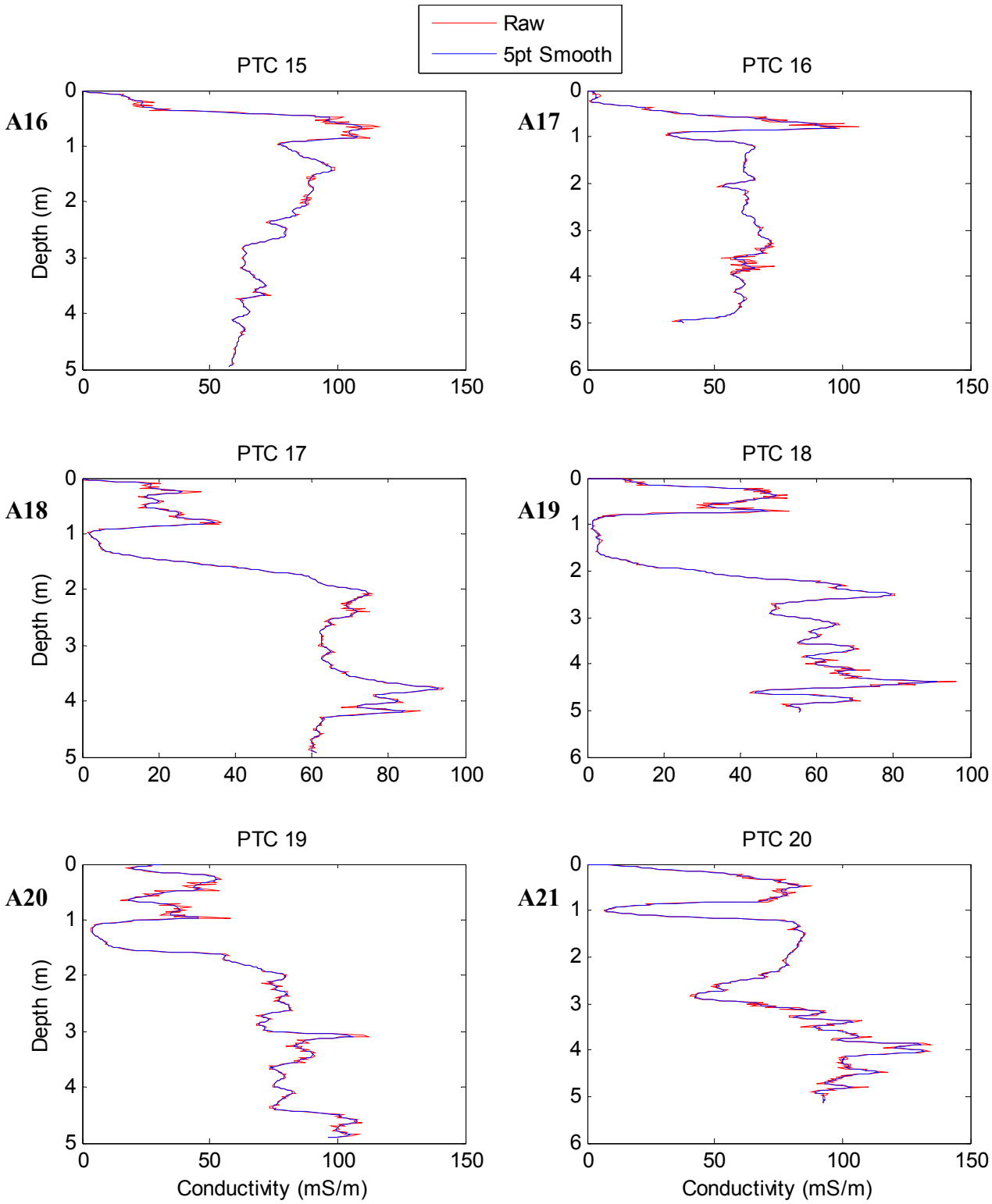
Raw
5pt Smooth
PTC 15
A16
PTC 16
A17
PTC 17
A18
PTC 18
A19
PTC 19
A20
PTC 20
A21
Depth (m)
Conductivity (mS/m)

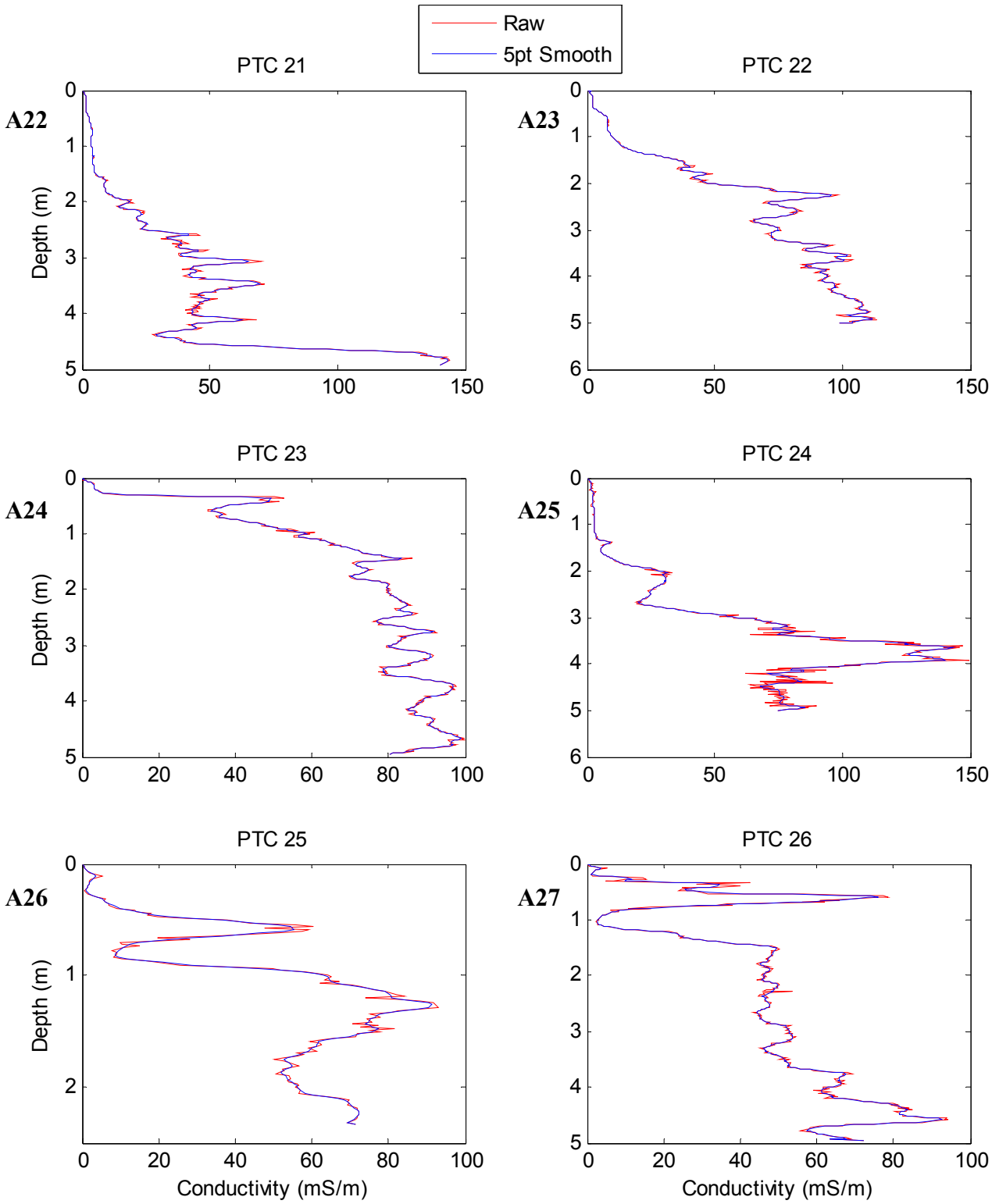
Raw
5pt Smooth
PTC 21
A22
PTC 22
A23
PTC 23
A24
PTC 24
A25
PTC 25
A26
PTC 26
A27
Depth (m)
Conductivity (mS/m)

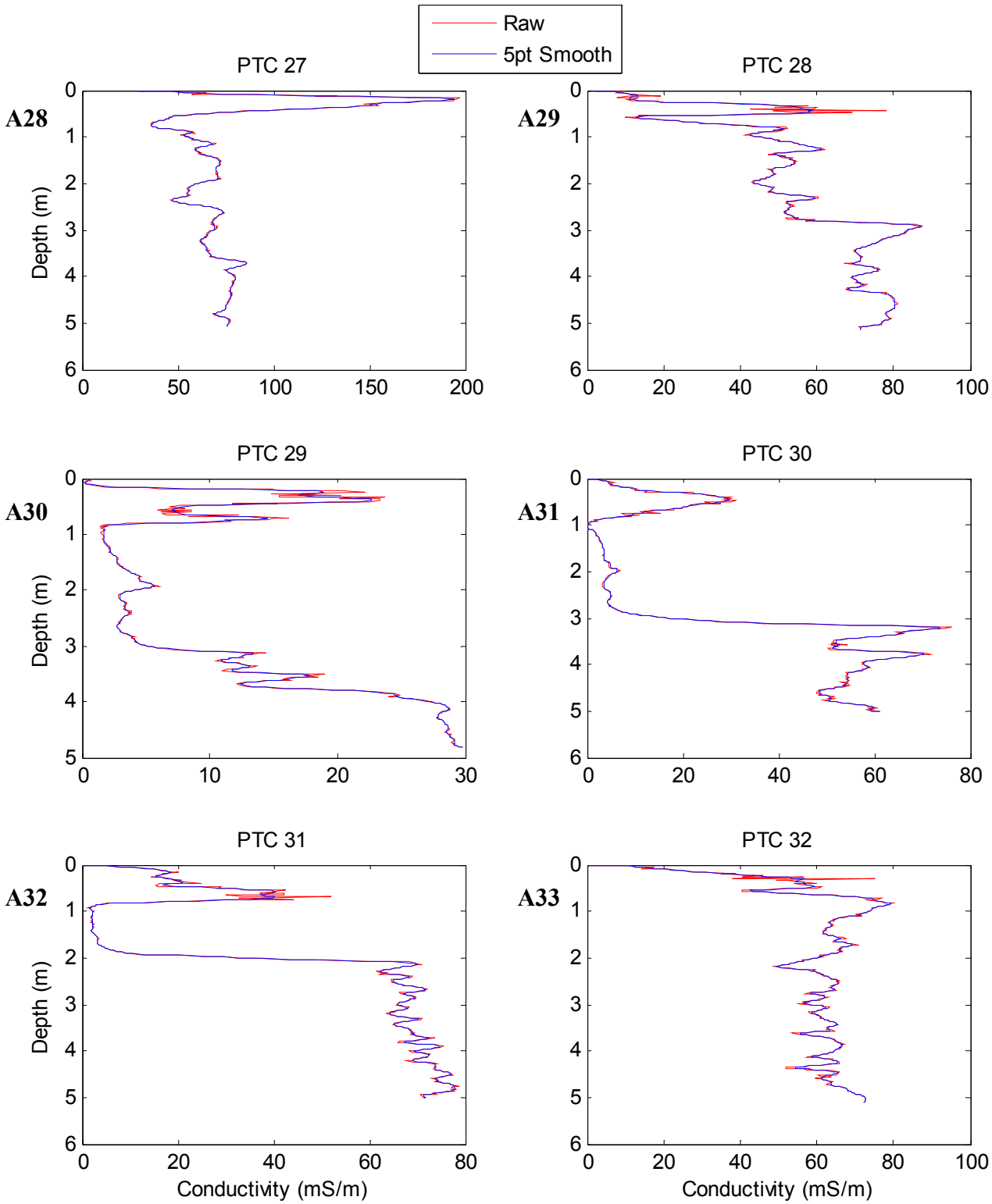
Raw
5pt Smooth
PTC 27
A28
PTC 28
A29
PTC 29
A30
PTC 30
A31
PTC 31
A32
PTC 32
A33
Depth (m)
Conductivity (mS/m)

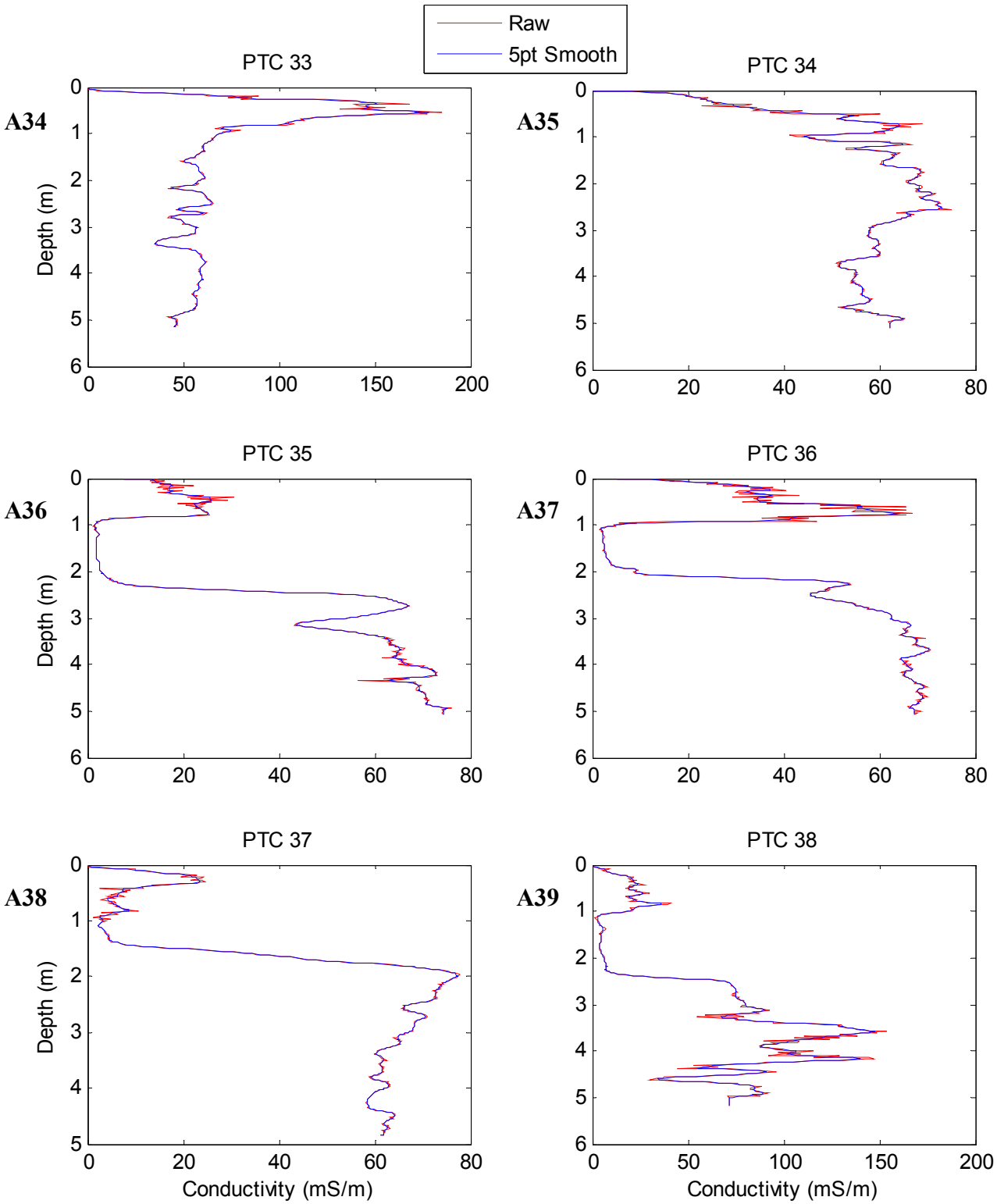
Raw
5pt Smooth
PTC 33
PTC 34
PTC 35
PTC 36
PTC 37
PTC 38
A34
A35
A36
A37
A38
A39
Depth (m)
Conductivity (mS/m)

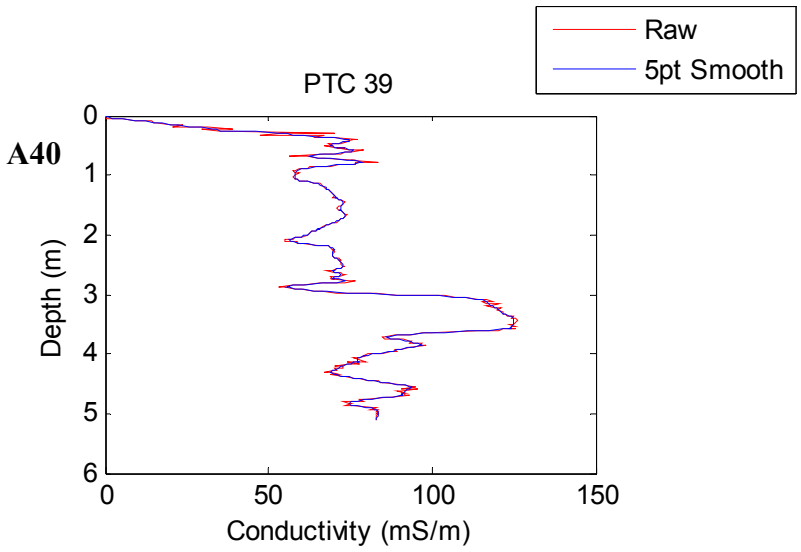

Figure A4 – A40. Raw and smoothed PTC data for 2001. A 5-pt triangle smoothing filter was utilized.

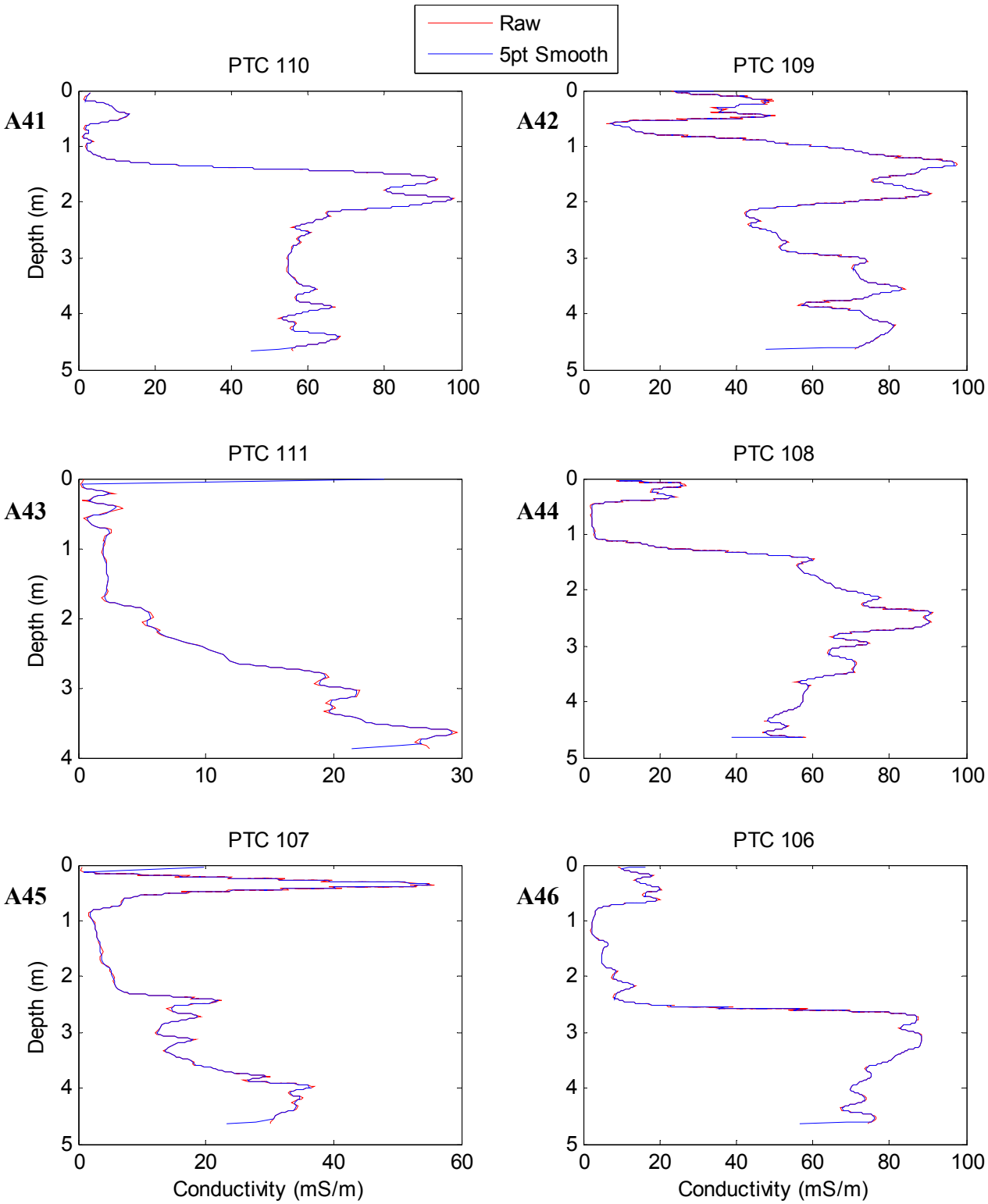
Raw
5pt Smooth
PTC 110
PTC 109
PTC 111
PTC 108
PTC 107
PTC 106
A41
A42
A43
A44
A45
A46
Depth (m)
Conductivity (mS/m)

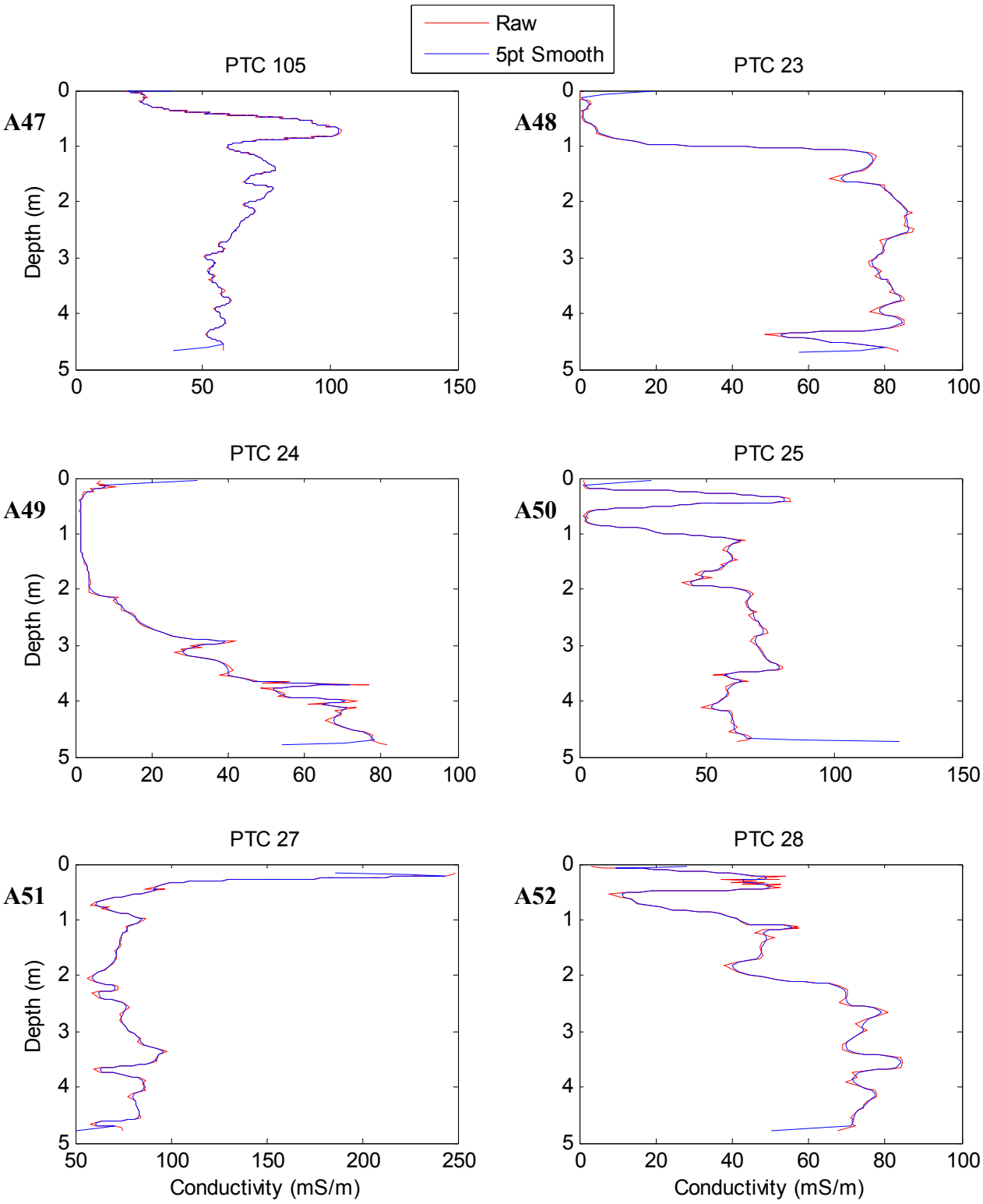
Raw
5pt Smooth
PTC 105
A47
PTC 23
A48
PTC 24
A49
PTC 25
A50
PTC 27
A51
PTC 28
A52
Depth (m)
Conductivity (mS/m)

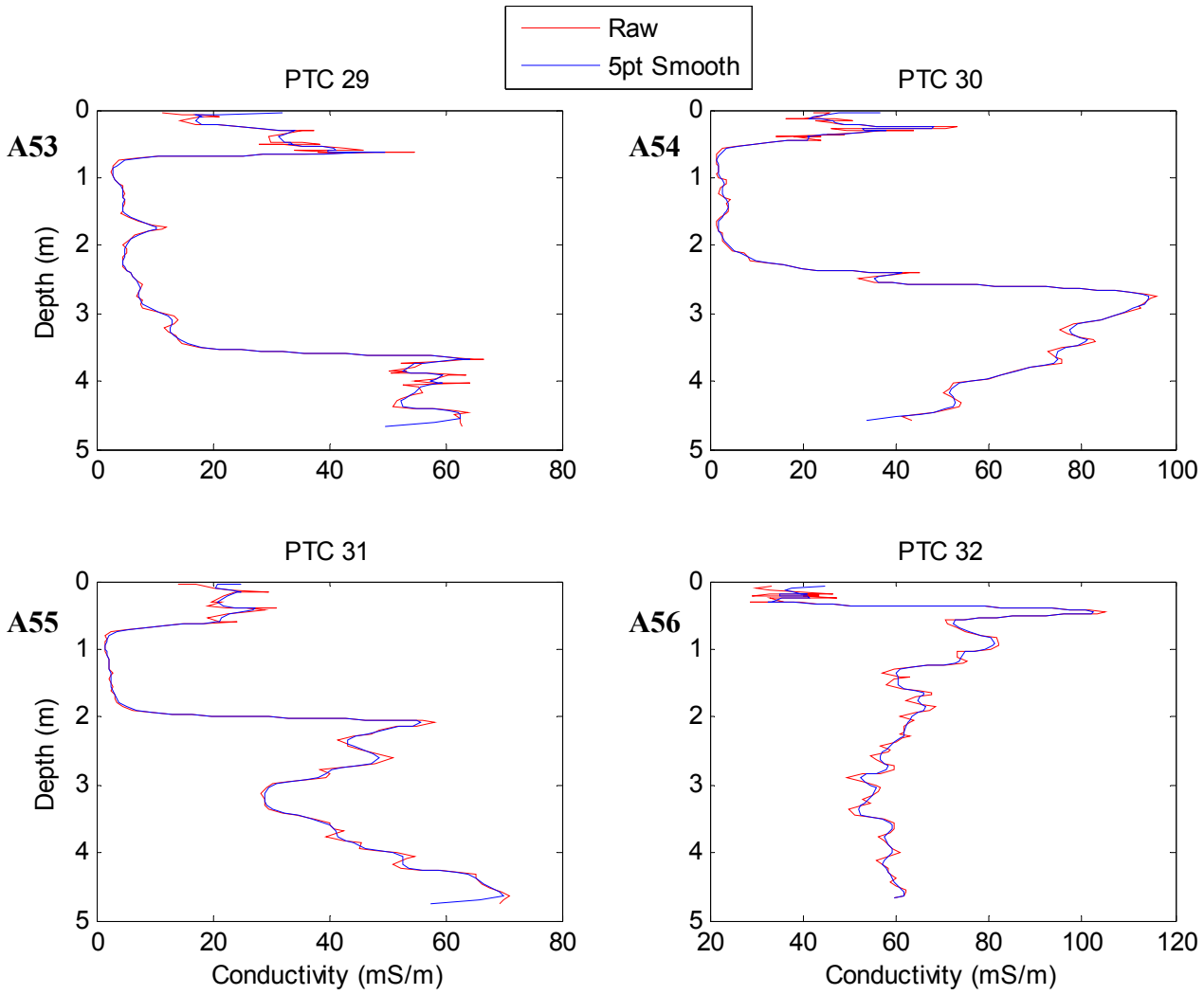

Figure A41 – A56. Raw and smoothed PTC data for 2004. A 5-pt triangle smoothing filter was utilized.

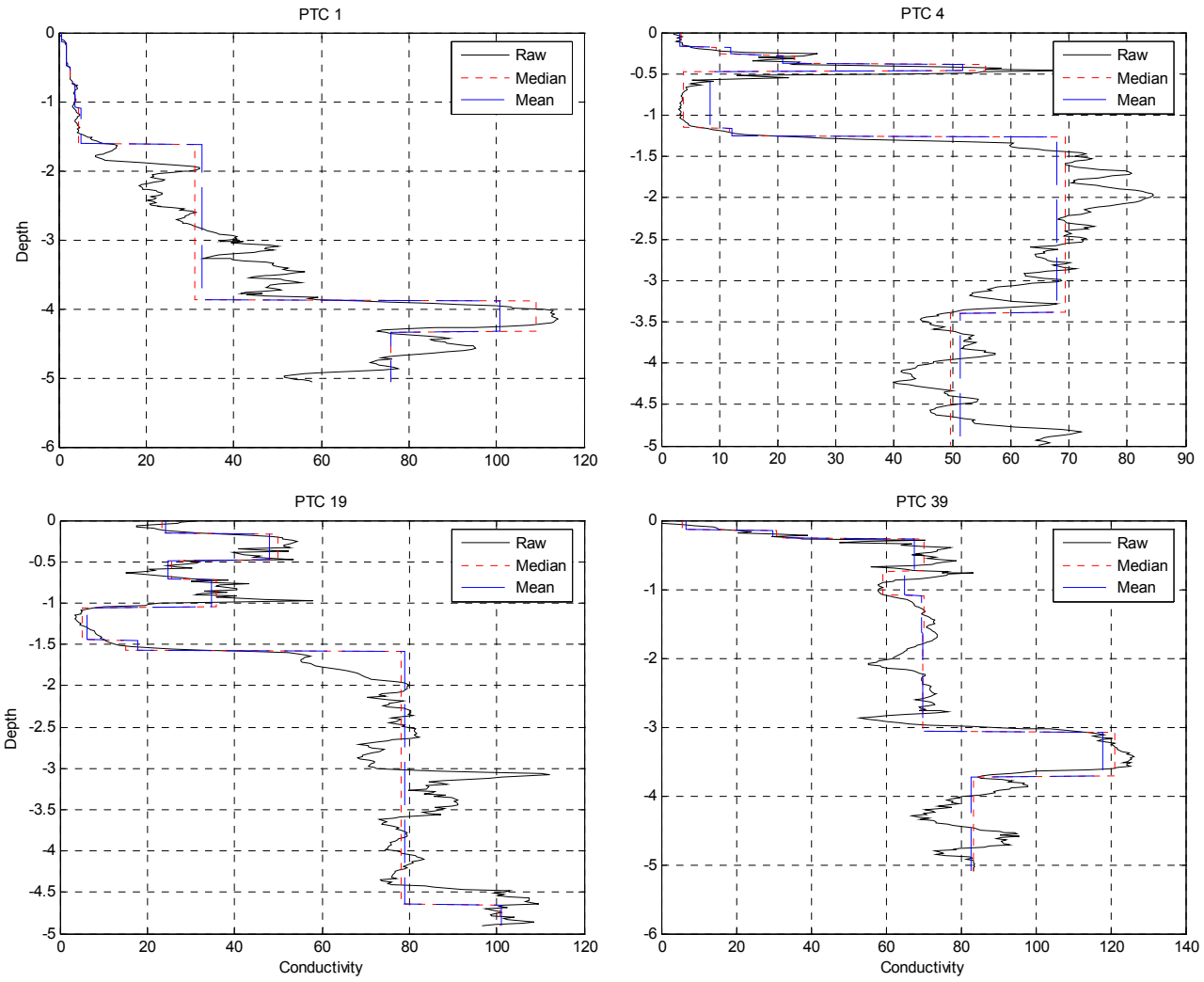

Figure Ax. Examples of automated layer modeling as described in Chapter 2.4.3. Vertical mean and median lines in the images above represent continuous layers which were modeled. Horizontal mean and median lines delineate layers. Conductivity and depth are in units of milisiemens per meter and meters respectively. The MATLAB program is shown in Appendix H.

Appendix B: EM-38 Data

The raw, normalized, and calibrated EM-38 data may be found in the attached material, in folder 'Appendix B'. The data is organized by survey year. Only data collected in the vertical dipole mode are given, as horizontal data was not reported in this study and not collected in 2004.

Appendix C: Electrical Resistivity Tomography Figures & Data

Raw and inverted ERT data may be found in attached material, in folder 'Appendix C'. Raw data is formatted for Res2DInv and includes complete topography from a 1 meter DEM. Inverted data is given as a four column matrix with distance (m), elevation (masl), resistivity (Ohm.m), and conductivity (S/m) respectively. Files are labeled with transect and year, e.g. 'Raw ERTA 2001.txt' represents raw ERT data from Transect A, surveyed during 2001.

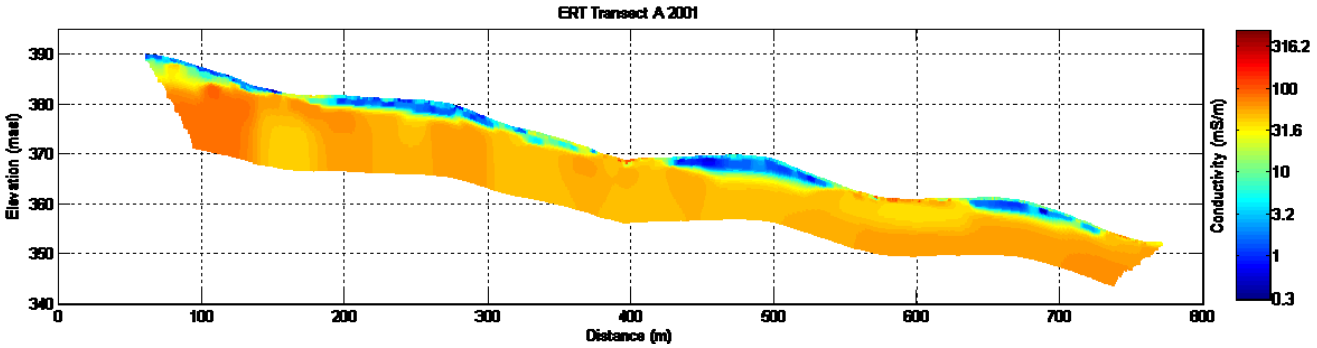

Figure C1. Inverted ERT cross-section for Transect A; data collected in 2001.

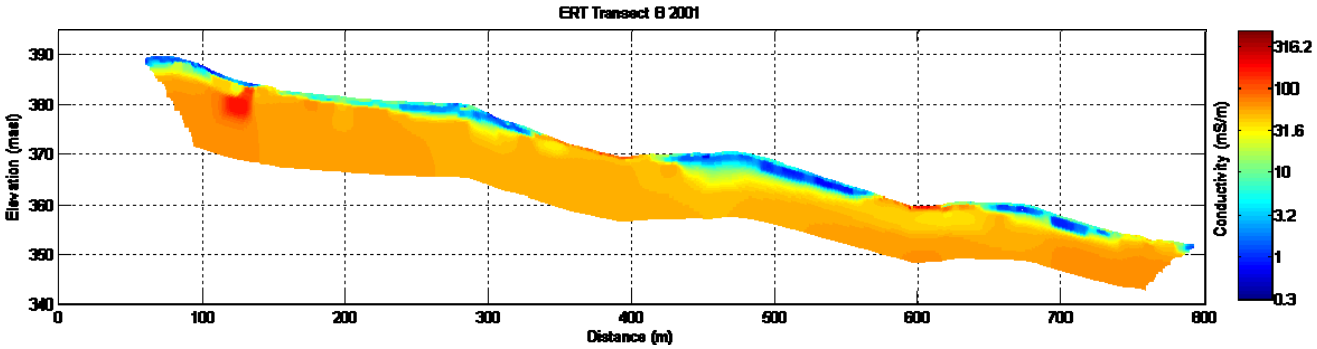

Figure C2. Inverted ERT cross-section for Transect B; data collected in 2001.

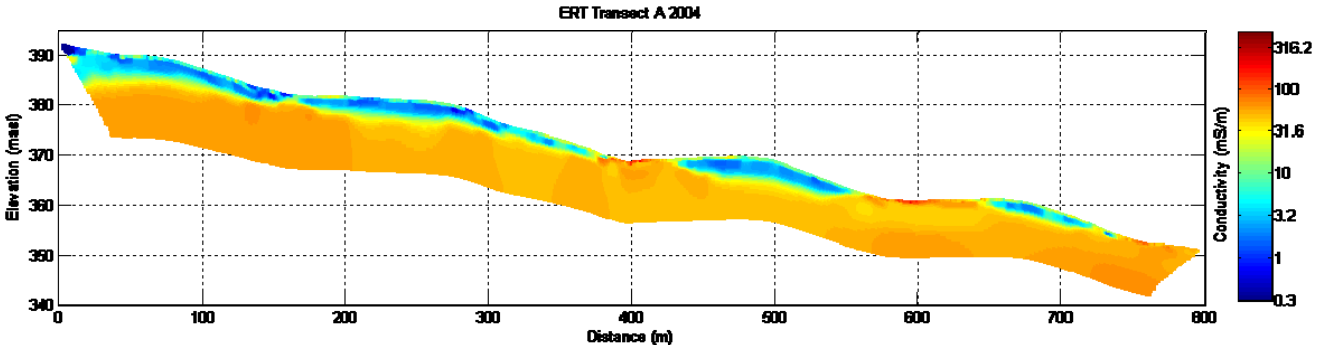

Figure C3. Inverted ERT cross-section for Transect A; data collected in 2004.

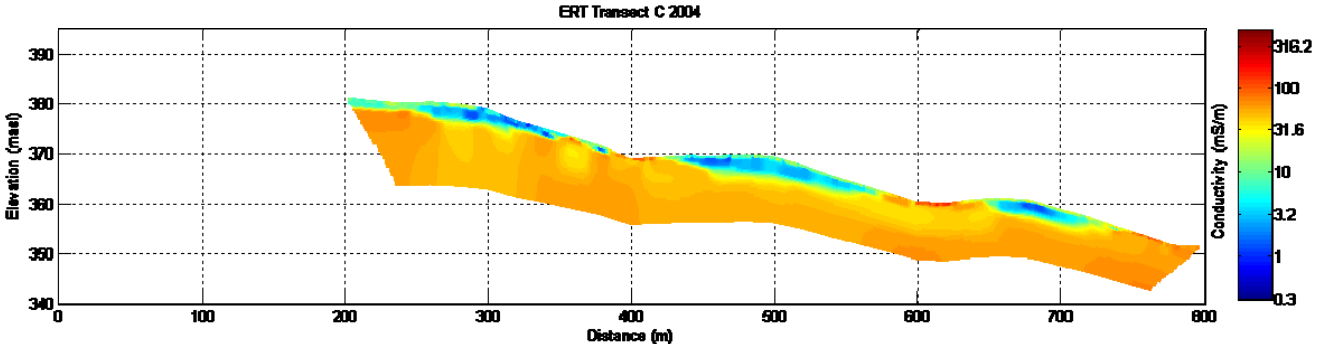

Figure C4. Inverted ERT cross-section for Transect C; data collected in 2004.

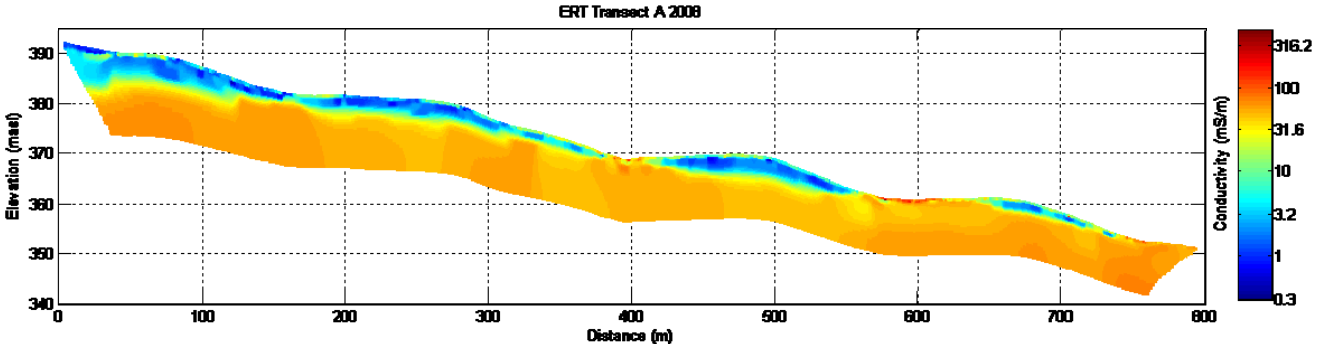

Figure C5. Inverted ERT cross-section for Transect A; data collected in 2008.

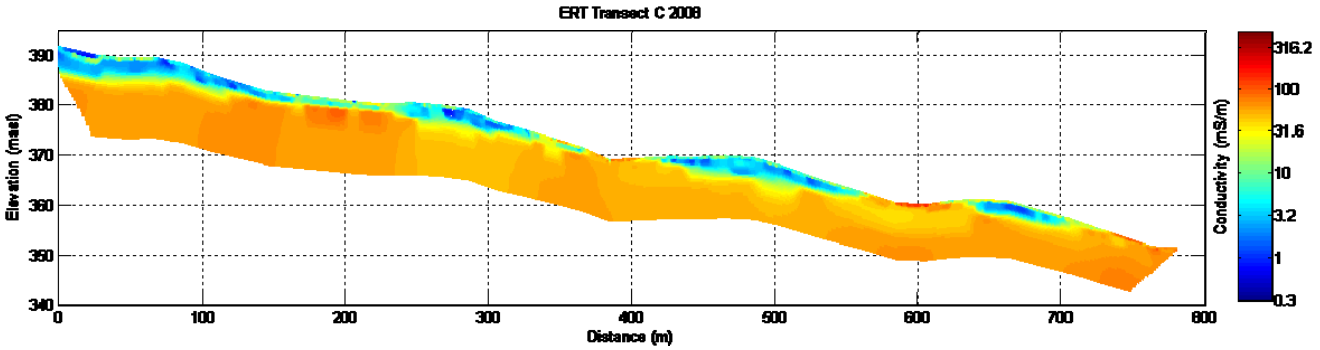

Figure C6. Inverted ERT cross-section for Transect C; data collected in 2008.

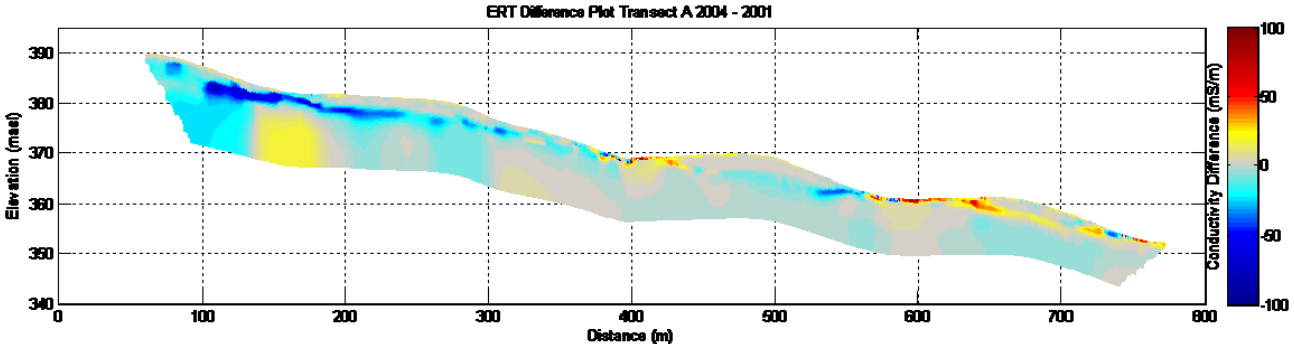

Figure C7. ERT difference plot for 2004 minus 2001 along Transect A.

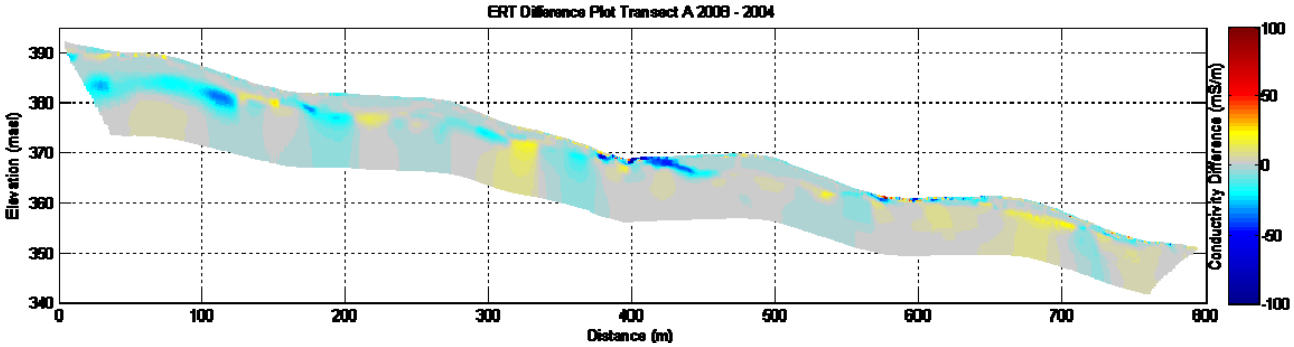

Figure C8. ERT difference plot for 2008 minus 2004 along Transect A.

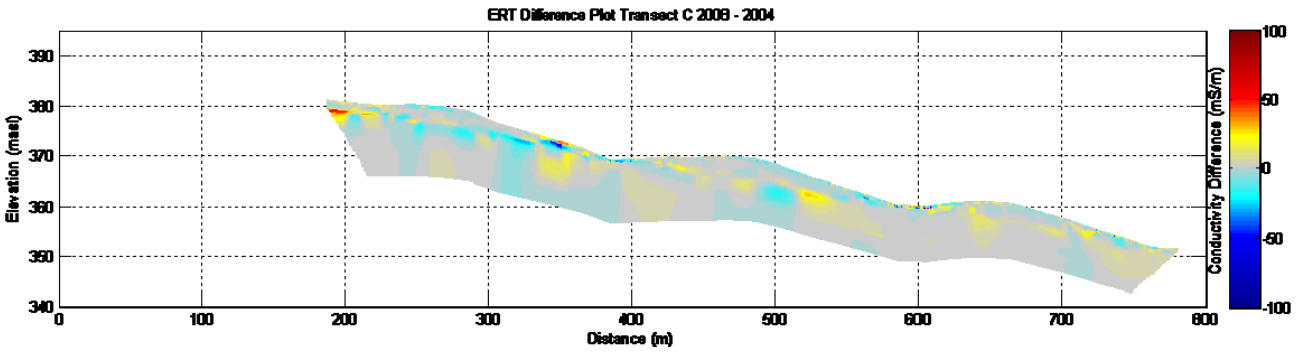

Figure C9. ERT difference plot for 2008 minus 2004 along Transect C.

Appendix D: Volumetric Moisture from Neutron Probe Figures & Data

Volumetric moisture data can be found in attached material, in folder 'Appendix D'. Data files are labeled by survey location, e.g. 'gw1.txt'. The first row displays the date of each survey at a given location in Julian days; the underlining column represents the volumetric moisture data for a given Julian date. The first column represents depth, measured in centimeters.

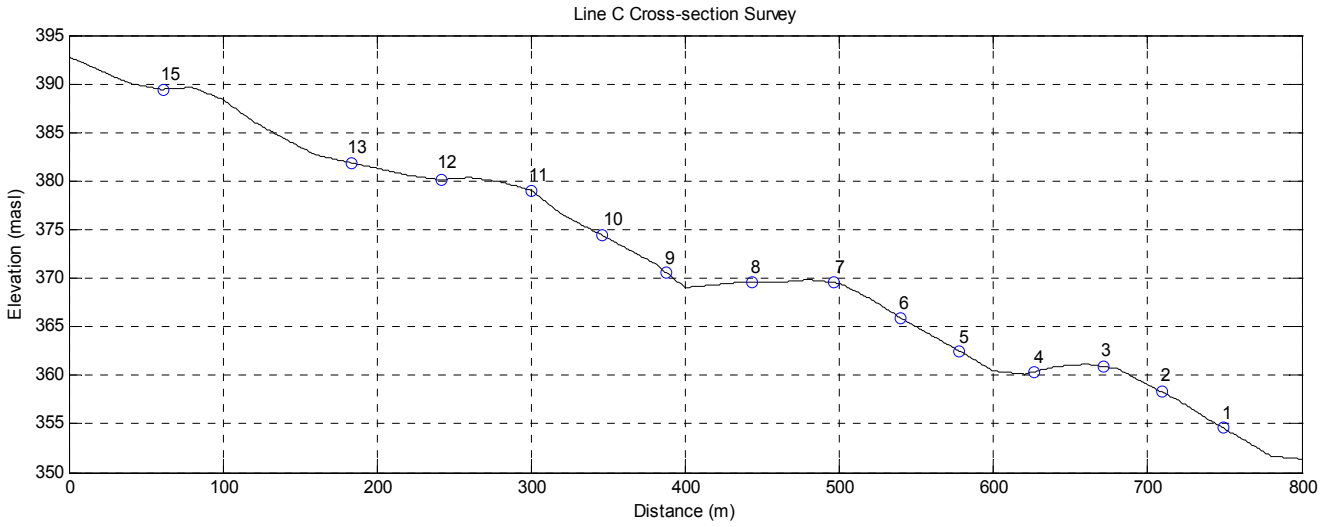

Figure D1. Location of groundwater sampling wells (GW) and neutron probe access tubes along Transect C. (Note: Appendix A utilized different identification numbers to prevent confusion with PTC data from other transects.)

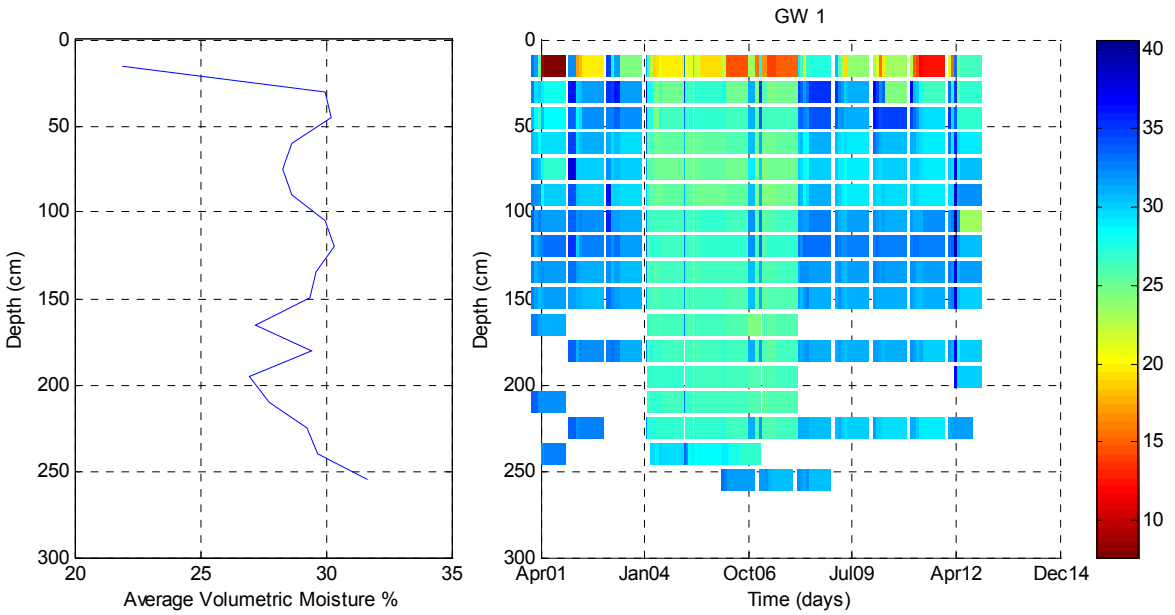

Figure D2. Volumetric moisture from neutron probe data from GW1. The average volumetric moisture for all profiles taken at the specified location is shown on the left. The image on the right displays volumetric moisture profiles through time with hot colors indicating low moisture and cool colors indicating high moisture.

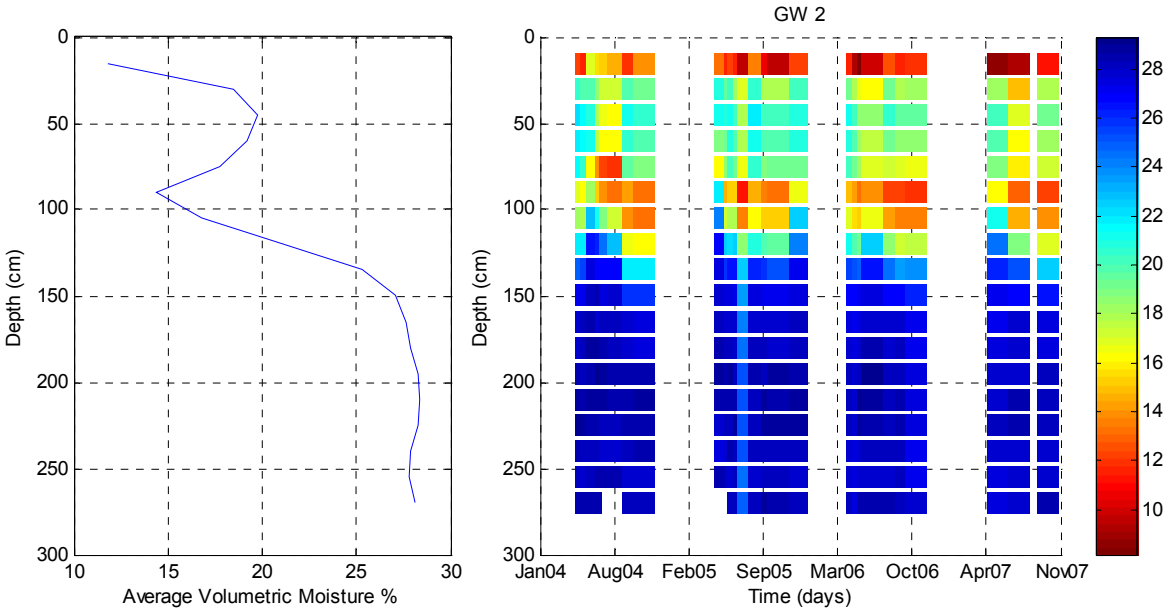

Figure D3. Volumetric moisture from neutron probe data from GW2. The average volumetric moisture for all profiles taken at the specified location is shown on the left. The image on the right displays volumetric moisture profiles through time with hot colors indicating low moisture and cool colors indicating high moisture.

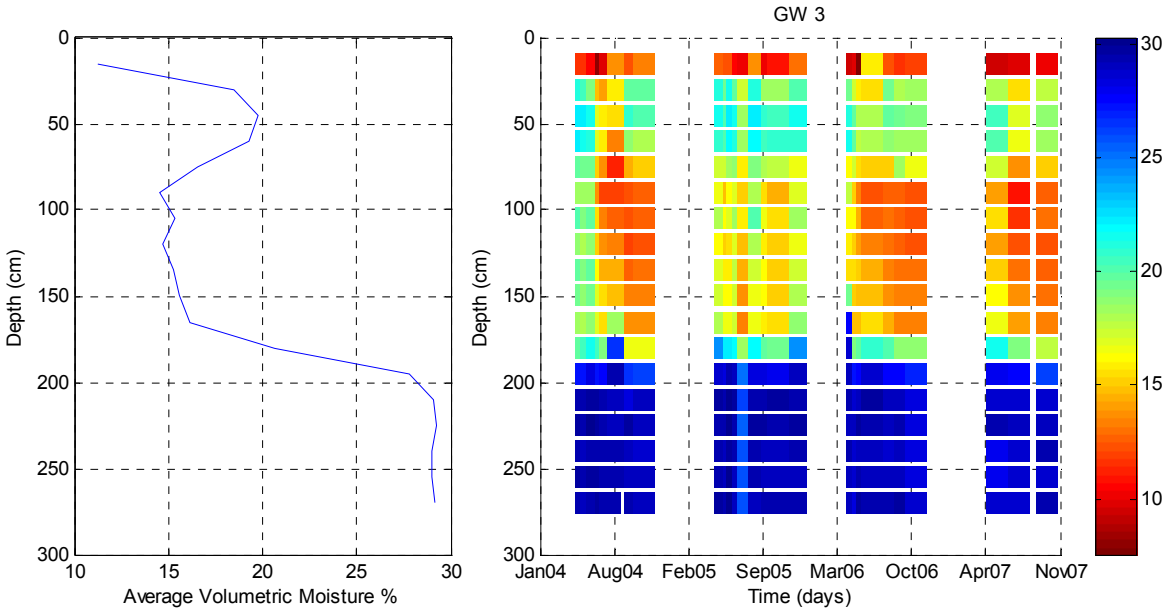

Figure D**4**. Volumetric moisture from neutron probe data from GW**3**. The average volumetric moisture for all profiles taken at the specified location is shown on the left. The image on the right displays volumetric moisture profiles through time with hot colors indicating low moisture and cool colors indicating high moisture.

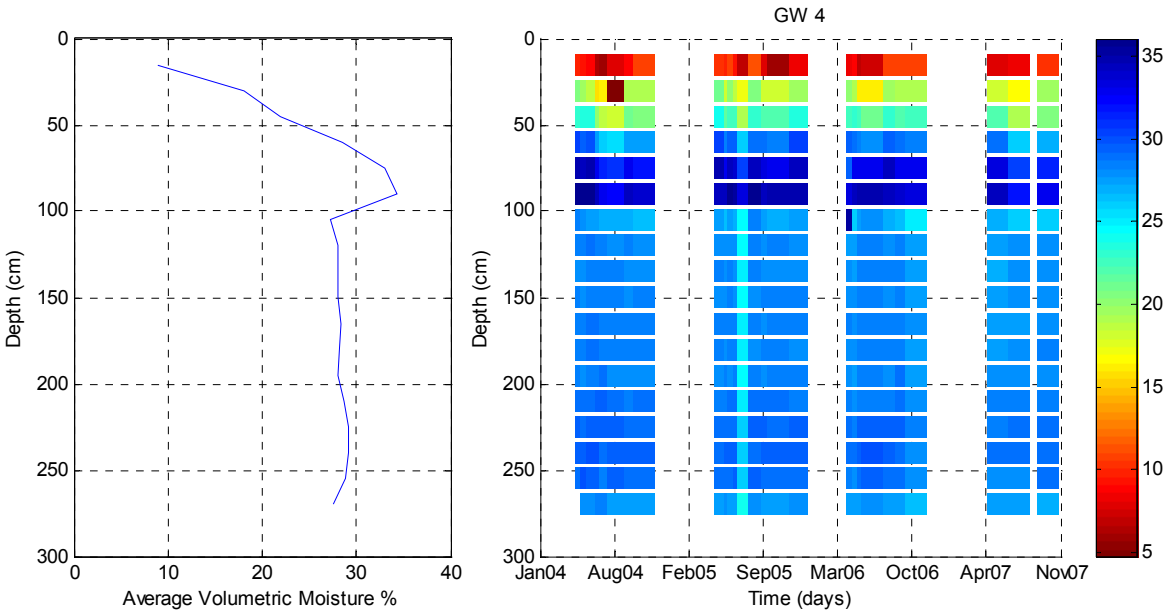

Figure D5. Volumetric moisture from neutron probe data from GW4. The average volumetric moisture for all profiles taken at the specified location is shown on the left. The image on the right displays volumetric moisture profiles through time with hot colors indicating low moisture and cool colors indicating high moisture.

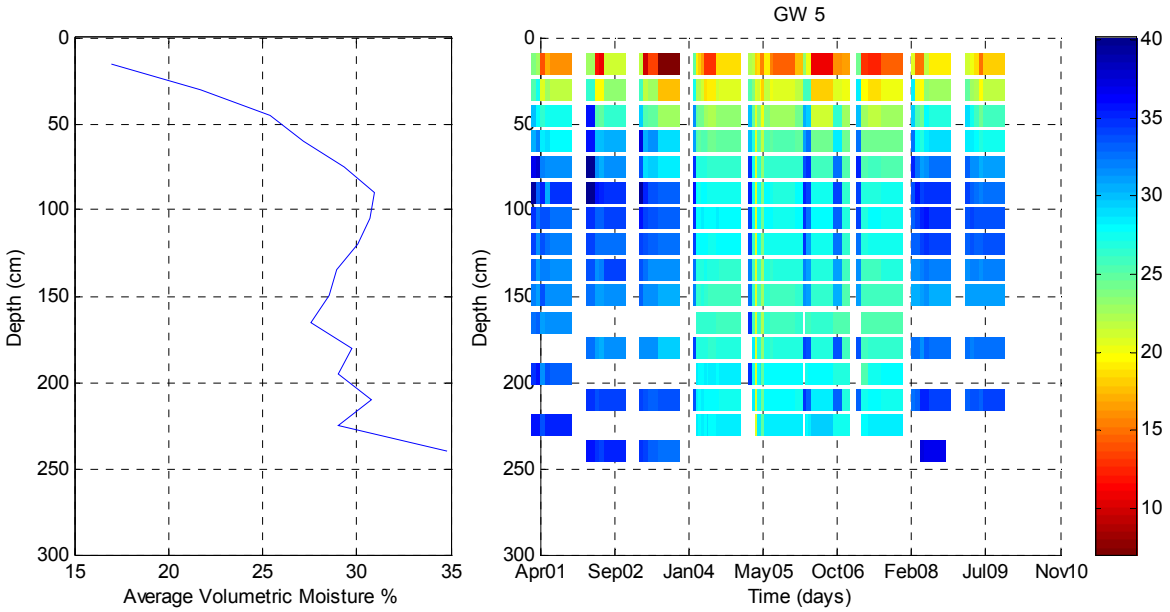

Figure D6. Volumetric moisture from neutron probe data from GW5. The average volumetric moisture for all profiles taken at the specified location is shown on the left. The image on the right displays volumetric moisture profiles through time with hot colors indicating low moisture and cool colors indicating high moisture.

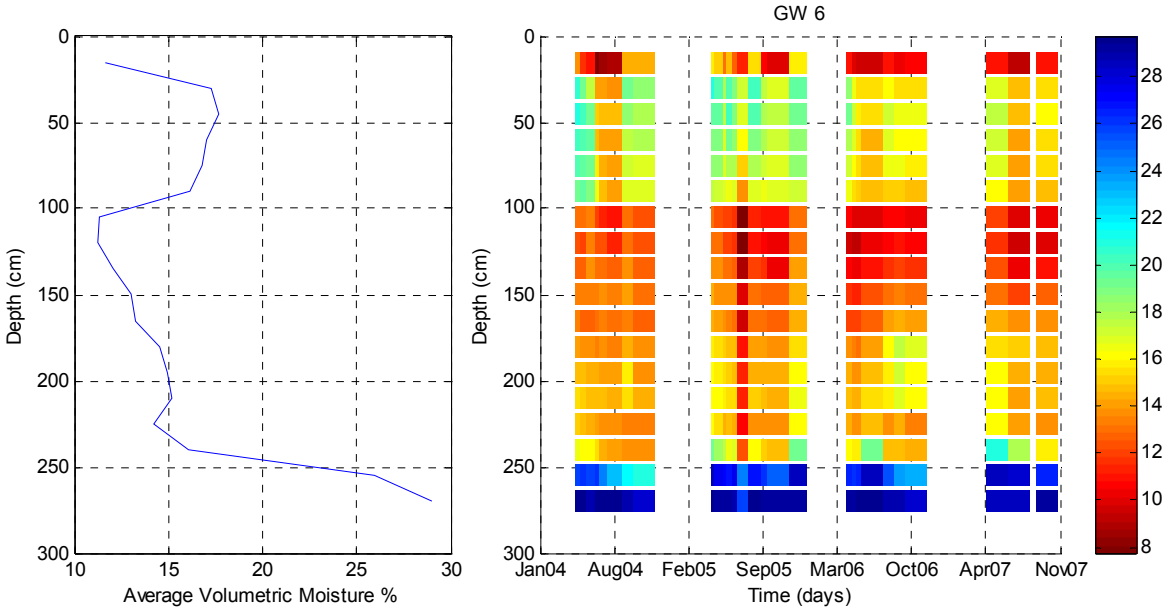

Figure D7. Volumetric moisture from neutron probe data from GW6. The average volumetric moisture for all profiles taken at the specified location is shown on the left. The image on the right displays volumetric moisture profiles through time with hot colors indicating low moisture and cool colors indicating high moisture.

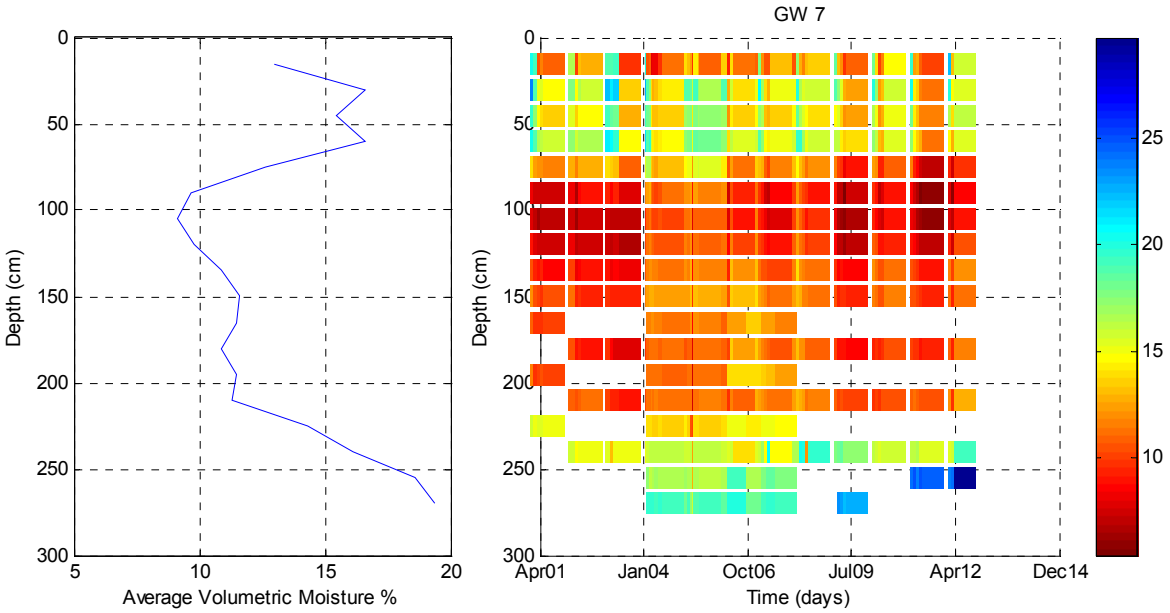

Figure D8. Volumetric moisture from neutron probe data from GW7. The average volumetric moisture for all profiles taken at the specified location is shown on the left. The image on the right displays volumetric moisture profiles through time with hot colors indicating low moisture and cool colors indicating high moisture.

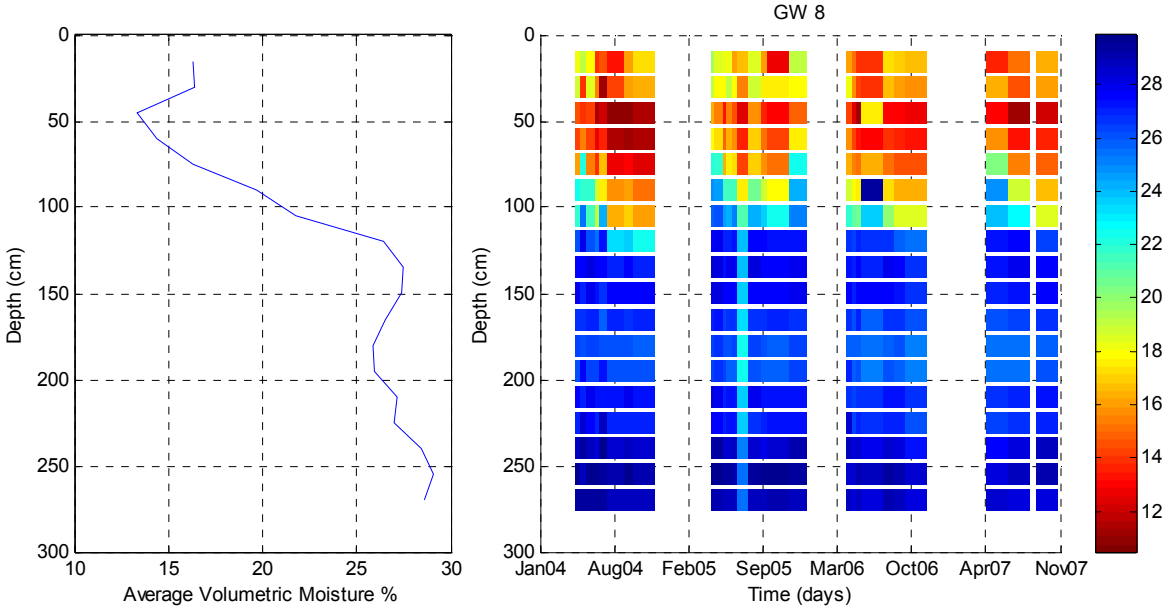

Figure D9. Volumetric moisture from neutron probe data from GW8. The average volumetric moisture for all profiles taken at the specified location is shown on the left. The image on the right displays volumetric moisture profiles through time with hot colors indicating low moisture and cool colors indicating high moisture.

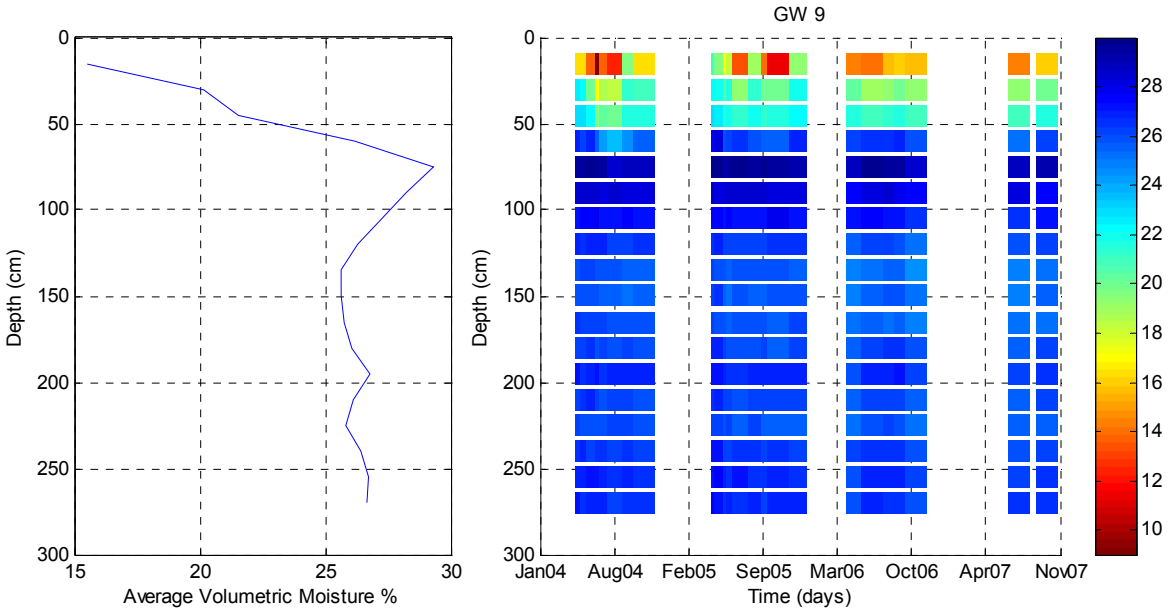

Figure D10. Volumetric moisture from neutron probe data from GW9. The average volumetric moisture for all profiles taken at the specified location is shown on the left. The image on the right displays volumetric moisture profiles through time with hot colors indicating low moisture and cool colors indicating high moisture.

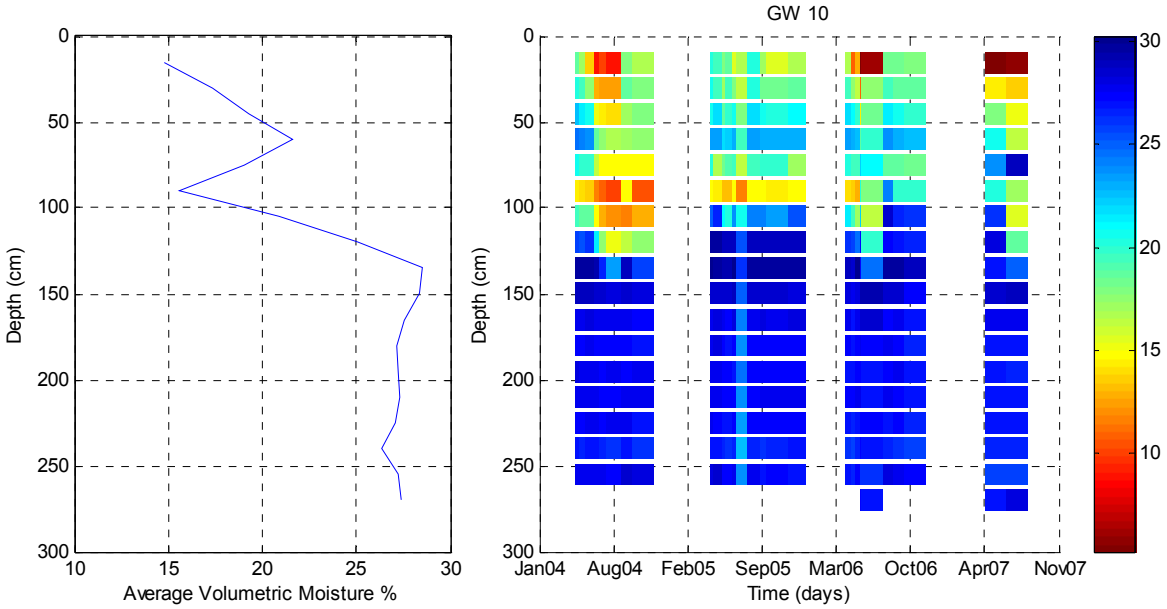

Figure D11. Volumetric moisture from neutron probe data from GW10. The average volumetric moisture for all profiles taken at the specified location is shown on the left. The image on the right displays volumetric moisture profiles through time with hot colors indicating low moisture and cool colors indicating high moisture.

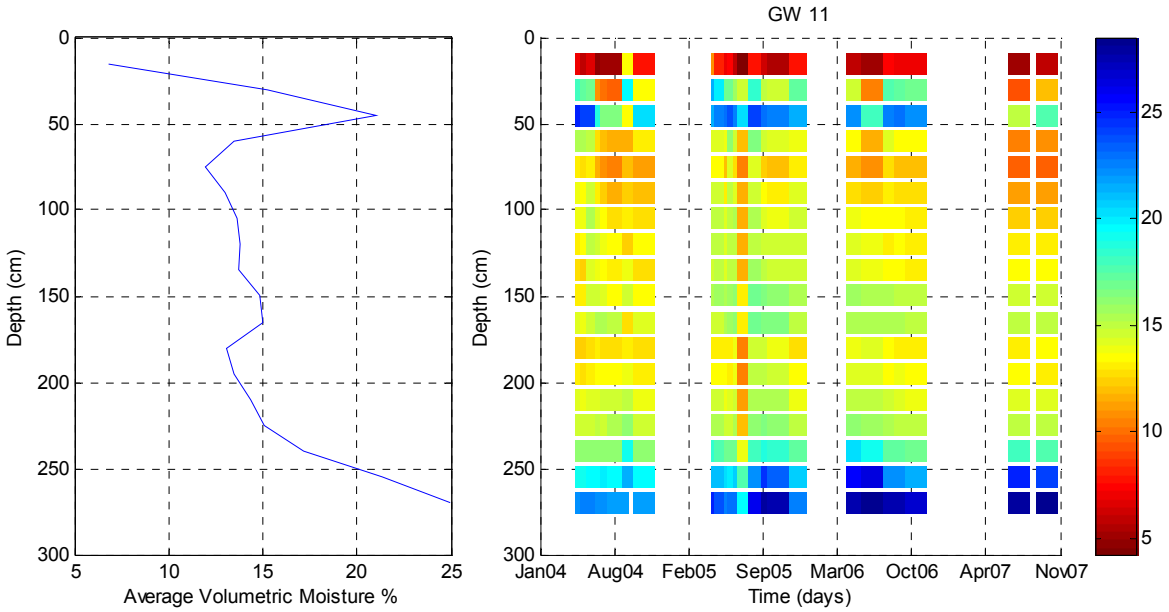

Figure D12. Volumetric moisture from neutron probe data from GW11. The average volumetric moisture for all profiles taken at the specified location is shown on the left. The image on the right displays volumetric moisture profiles through time with hot colors indicating low moisture and cool colors indicating high moisture.

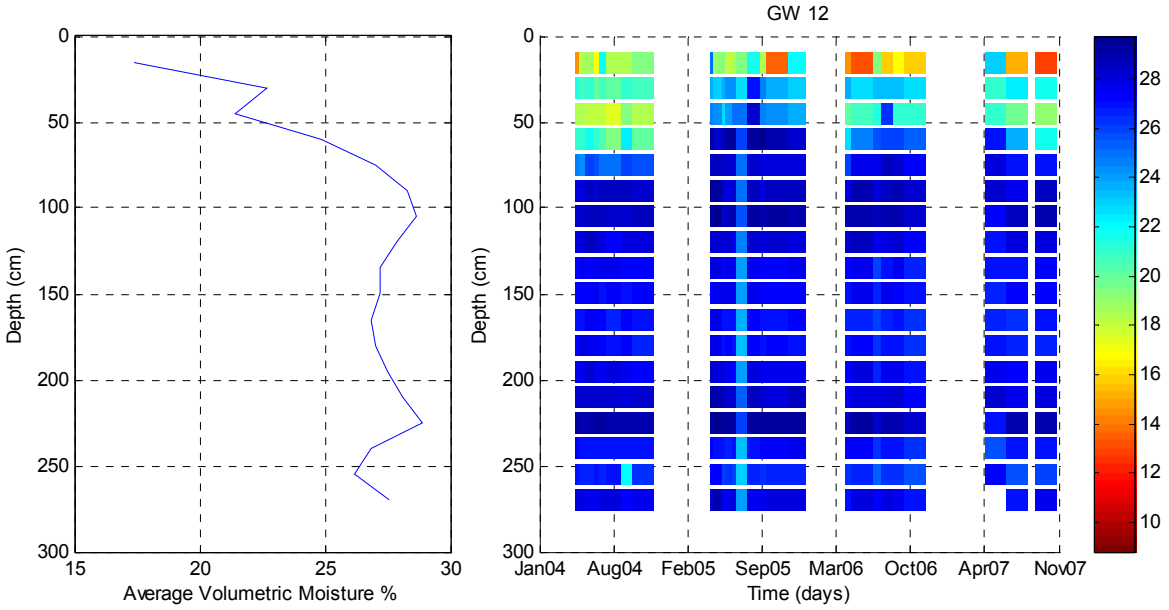

Figure D13. Volumetric moisture from neutron probe data from GW12. The average volumetric moisture for all profiles taken at the specified location is shown on the left. The image on the right displays volumetric moisture profiles through time with hot colors indicating low moisture and cool colors indicating high moisture.

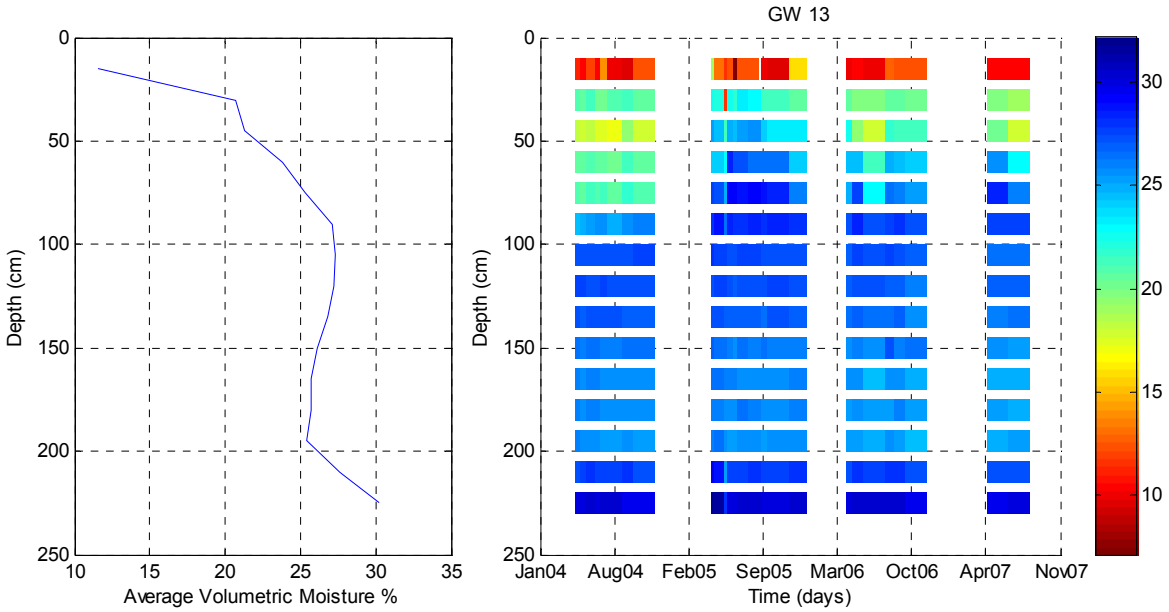

Figure D14. Volumetric moisture from neutron probe data from GW13. The average volumetric moisture for all profiles taken at the specified location is shown on the left. The image on the right displays volumetric moisture profiles through time with hot colors indicating low moisture and cool colors indicating high moisture.

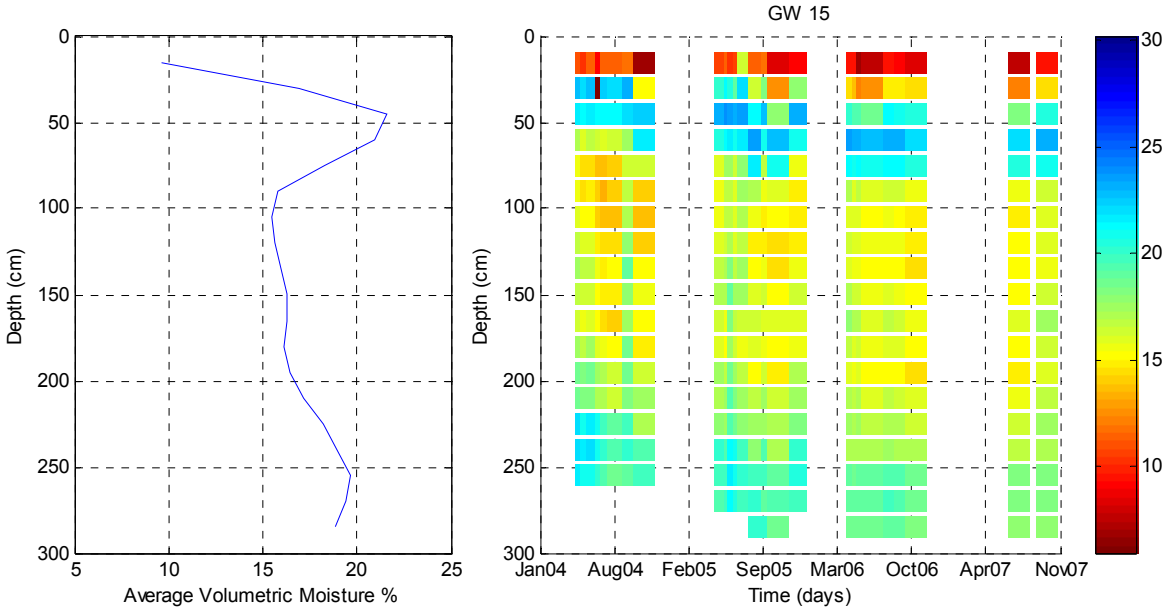

Figure D15. Volumetric moisture from neutron probe data from GW15. The average volumetric moisture for all profiles taken at the specified location is shown on the left. The image on the right displays volumetric moisture profiles through time with hot colors indicating low moisture and cool colors indicating high moisture.

Appendix E: Water Level Data

Water level measurements that were collected during similar times as geophysical data for 2004 and 2008 can be found in attached materials, in folder 'Appendix E'. The folder contains a .txt file which contains the water level data utilized in this study.

Appendix F: Fluid Electrical Conductivity Data

Fluid electrical conductivity data and other chemistry data collected along Transect C may be found in attached materials, in folder 'Appendix F'. The folder contains a .txt file that holds all chemistry data collected along Transect C and investigated in this study. For the results of this research, fluid EC was the primary parameter of concern. However, with the inability to resolve fluid EC from geophysics and build strong relationships between the two, many other parameters (TDS, major anion and cations, etc.) were excluded as they did not provide any further insight towards the study's objective.

Appendix G: EM-38 Normalization MATLAB Script

The following is the script for the EM-38 normalization procedure discussed in Chapter 2.4.4. The script is written in the MATLAB programming language. The user must input data for the elevated region as 'elef' and for the reference region as 'normf'. Furthermore, the user can set the number of desired quantiles in which to divide each data set into. This can be achieved by changing the assigned value of variable 'q' in line 8. A value of 100 was used in this study and found to produce reasonable results. The variable 'shift_ele' defined while running the script, represents the normalized elevated data set. The original elevated data 'elef' may be replaced with 'shift_ele' to produce a final normalized section.

EM-38 Normalization Script

```
%% Quantiles split

%normf - zone of reference or non-elevated EM data
%elef - zone of elevated EM data
%Both normf and elef must represent areas that should be statistically stationary for
%normalization process to work.

q = 100; % Number of desired quantiles
ne = length(elef);
nn = length(normf);
neq = ne/q; %number of data per elevated data quantile
nnq = nn/q; %number of data per reference data quantile
qele = 1;
qnorm = 1;
for i =1:(q-1);
   qele = [qele;(i*neq)]; %indexing in elevated data set
   qnorm = [qnorm;(i*nnq)]; %indexing in reference data set
end;

qele = round(qele);  %indexing in elevated data set, index must be integer
qnorm = round(qnorm);  %indexing in reference data se, index must be integer

for i =1:q;
   if i~=q;
      qele(i,2) = qele((i+1),1)-1; %indexing last data point for each quantile: elevated
      qnorm(i,2) = qnorm((i+1),1)-1;  %indexing last data point for each quantile: reference
   end;
   if i == q;
```

```
      qele(i,2) = length(elef);
      qnorm(i,2) = length(normf);
   end;
end;

qele(:,3)=qele(:,2)-qele(:,1);  %check each quantile is the same size: elevated
qnorm(:,3)=qnorm(:,2)-qnorm(:,1);  %%check each quantile is the same size: elevated

[z,i]=sort(elef(:,3)); %sort elevated data set
[z1,i1]=sort(normf(:,3));  %sort reference data set

elefs = elef(i,:); %sorted elevated data set
normfs = normf(i1,:); %sorted reference data set
clear z;clear i;clear z1;clear i1;

for i=1:q;
   meanele(i,1) = mean(elefs((qele(i,1):qele(i,2)),3)); %find mean of each quantile: elevated
   meannorm(i,1) = mean(normfs((qnorm(i,1):qnorm(i,2)),3));  %find mean of each quantile: ref
   shift(i,1) = meanele(i,1)-meannorm(i,1); %find difference between elevated and ref
end;

for i=1:q-4;
   smth_shift(i+2,1) = mean(shift((i:i+4),1)); %smoothening filter for quantile diference
%helps to eliminate any noise that causes error in quantile mean
end;

smth_shift(1:2,1)=smth_shift(3,1); %smoothening filter for quantile diference
smth_shift(q-1:q,1)=smth_shift(q-2,1); %smoothening filter for quantile diference

shift_ele = elefs; %create new variable for normalized elevated data
for i =1:q;
   shift_ele(qele(i,1):qele(i,2),3) = shift_ele(qele(i,1):qele(i,2),3)-smth_shift(i,1);
% applying quantile difference to elevated data set
end;

% The following limits the lowest data point in the now normalized elevated zone to the
% minimum of the reference region. (Prevents negative values)
min_norm = min(normfs(:,3));
bb = find(shift_ele(:,3)<min_norm);
shift_ele(bb,:)=[];

%%% !! Variable 'shift_ele' is the normalized elevated data set !! %%%%
% Elevated data set may be replaced with shift_ele to produce a normalized section
```

Appendix H: Automated Layer Modeling Program for 1D Data in MATLAB

The following MATLAB program was designed to automatically select layers for PTC profiles. This was performed so that a large number of PTC profiles could be broken into 8 distinct layers, in a non-biased fashion, for implementation into FreqEM to be forward modeled to a simulated EM-38 response. For a detailed description of the MATLAB program presented below and its specific uses in this study, refer to Chapter 2.4.3. It should be noted that the following program can be utilized for any 1D data and any desired number of layers. Input variable are described in detail in comments within the program.

Automated Layer Modeling for 1D

```
function[final]=laymodel(ptc,layn,mind,maxpcm,ws,name)
%
%[final]=laymodel(ptc,layn,mind,maxpcm,ws,name)
%
%Automated layer modeler for 1D data.  Parameters are described below.
%The input variable 'ptc' must be in the following nx4 matrix format.
%Multiple 1D profiles may be run as long as id number differs.
%
%1st col: PTC id number
%2nd col: PTC data elevation (masl)
%3rd col: PTC data (cond)
%4th col: PTC data depth (as positive)
%
%The variable 'layn' is the desired number of layers to be modeled.
%Sometimes the model will converge to a number lower than that of the
%desired number.  If this happens and is of concern, please enter the
%laymodel script and refine the var_step variable to a higher resolution.
%
%The 'name' variable should usually be the PTC id number but can be chosen
%as any non string or string input.  This input is used for the figure
%title.  If a non string (class double) is chosen, the resulting name will
%be "PTC (name)".
%
%EX. name = 5
%figure title will be 'PTC 5'
%
%Keep in mind that the modeling process is quite sensitive to the input
%parameters and constraints; the modeled layers produced are non-unique.
%Under "standard" input parameters the model performs well for many
%different tested profiles, however it may be necessary to alter input
%parameters slightly to obtain more favorable results.
```

```
%
%Standard inputs are as follows
%
%mind = 8;
%Minimum allowed number of data points per layer (exlcuding the last layer)
%
%maxpcm = 100;
%ws = 8;
%Maximum percent change in data mean (maxpcm) for designated window size (ws).
%If this constraint is breached, it will tell the model to create a new layer.
%This helps to isolate layers before and after large "jumps" in data.  Be
%careful not to over constrain the model with this parameter. A smaller
%window size will better model small spikes as unique layers.
%
% - - - - - - - - - - - - - - - - - - - - - - - - - - - - - - - - - - - - - -
%
%The following other parameters must be altered directly within the script.
%
%mdep1 = maxdep/(layn*2);
%Max thickness of 1st layer (can set as number or use "maxdep/(layn*2)")
%
%depch = 1.5;
%Rate at which maximum thickness of layer changes with depth based on
%mdep1*(depch^(n)), where n is the layer number
%
%mdoi = 1.75;
%Maximum depth of investigation (1.75m used for EM-38 FWD modeling).  Data
%below this level are no longer constrained by the maximum thickness or
%maximum percent change.  Powerful parameter which greatly improves the
%chances of generating a solution. Also useful to obtain higher resolution
%in data above the mdoi.  If you wish the model to be constrained
%throughout, set as a depth greater than the deepest data point.
%
%by: Aaron Booterbaugh

%%%%%%%%%%%%%%%%%%%%%%%%%%%%%%%%%%%%%%%%%%%%%%%%%%%%%%%%%%%%%%%%%%%%%%%
%%layn=8; %number of layers to model

%%% "Standard" input variables (these performed well with many different
%%% data profiles).
%%mind = 8; %minimum number of data points allowed in a layer
%%layn=8; %number of layers to model
%%maxpcm = 100; %max change in mean over a designated window size before and after current iteration
%%ws = 8; %window size
dep = ptc(2,4)-ptc(1,4);
maxdep = max(ptc(:,4));
depch = 1.5; %change of max thickness per layer allowed (usually 1.5 but depends on %data)
mdep1 = maxdep/(layn*2); %max thickness of 1st layer; (can set as number or use "maxdep/(layn*2)")
mdoi = 1.75; %max depth of interest (related to resolution of instrument if applicable)
%% the data below the mdoi are much more loosely constrained, this helps
%% the model to perform in a more robust manner (reduces the chances of not
```

```
%% producing a solution)
%%%%%%%%%%%%%%%%%%%%%%%%%%%%%%%%%%%%%%%%%%%%%%%%%%%%%%%%%%%%%%%%%%%%%%%%%%%%%%%%

m = mean(ptc(:,3)); %calculate mean
var = (1/length(ptc))*sum((ptc(:,3)-m).^2); %calculate variance
clear lay;
var_step = [5:2:var]; %iterative change in variance threshold
mdind = find(ptc(:,4)>mdoi); %index data below mdoi
mdind = min(mdind); %first data point below mdoi
for i =1:length(var_step); %variance threshold iterations
   h=1;
   n=0;
   f = 0;
   maxind2 = 1;
   minind2 = 1;
%The following works to define layers for each iterative variance threshold
      for k = h:length(ptc);
         m = mean(ptc(h:k,3));
         if k-h==0;continue;end;
         dvar = (1/(k-h))*sum((ptc(h:k,3)-m).^2);
         if k<=ws | k>=length(ptc)-ws;
            pcm = 0;
         else
             pcm = abs((((mean(ptc(k:k+ws,3)))-(mean(ptc(k-ws:k,3))))/(mean(ptc(k-ws:k,3))))*100);
         end;

         ind2 = find(ptc(:,4)>mdep1*(depch^(n)));
         minind2 = min(ind2);
         if k>=mdind;
            minind2 = length(ptc)+1;
            pcm = 0;
         end;

         if dvar > var_step(i) | pcm > maxpcm | k >= minind2;
            f=1;
            n=n+1;
            lay(h:k,i)=n;
            ind = find(lay(:,i)==n);
            if length(ind)<mind;
               n = n-1;
            end;
            h=k+1;
         end;
      end;

   if max(lay(:,i))<=layn-1; %Statement breaks loop if desired layer number is reached
      Modeled_Layers = max(lay(:,i))+1
      break;end;
end;

% The following selects final layer locations from the matrix generated previously
```

```
layp = lay(:,i);
layp(length(layp)+1:length(ptc),1)=0;
ind=find(layp==0);
layp(ind,1)=max(layp(:,1))+1;
ptc2 = ptc;
ptc2(:,5)=layp;

% Calculates statistics for final layered model
for i = 1:max(ptc2(:,5));
   ind = find(ptc2(:,5)==i);
   m = median(ptc2(ind,3));
   u = mean(ptc2(ind,3));
   var = (1/length(ind))*sum((ptc2(ind,3)-u).^2);
   cs = (3*(u-m))/(sqrt(var));
   ptc2(ind,6)=m;
   ptc2(ind,8)=var;
   ptc2(ind,7)=u;
   ptc2(ind,9)=cs;
end;

% Displays statistics for final layered model and plots
x = [1:Modeled_Layers]';
for i = 1:Modeled_Layers;
   ind=find(ptc2(:,5)==i);
   indmin = min(ind);
   indmax = max(ind);
   med(i,1) = ptc2(indmin,6);
   mea(i,1) = ptc2(indmin,7);
   var(i,1) = ptc2(indmin,8);
   cs(i,1) = ptc2(indmin,9);
   thick(i,1)=ptc2(indmax,4)-ptc2(indmin,4);
end;
disp('Layer, Median C, Mean C, Thickness, Variance, Pearson Coef Skew')
final = [x med mea thick var cs];
disp(final);

figure('name',num2str(name));
plot(ptc2(:,3),ptc2(:,4)*-1,'k','displayname','Raw');
hold on;
plot(ptc2(:,6),ptc2(:,4)*-1,'r:','displayname','Median');
plot(ptc2(:,7),ptc2(:,4)*-1,'b--','displayname','Mean');
grid on;
xlabel('Conductivity');
ylabel('Depth');
cl = class(name);
if cl=='double'
   a = 'PTC ';
   b = num2str(name);
   c = [a,b];
   title(c);
else
```

```
    title(name);
end;
```

legend toggle